Reprinted from the *Astronomical Journal*, 69, No. 1,
February, 1964

Technical Report No. 32-533

Symposium on Radar and Radiometric Observations of Venus during the 1962 Conjunction

edited by

F. T. Barath

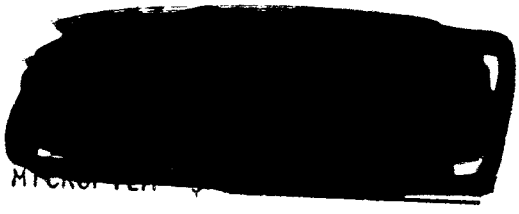

This paper presents the results of one phase of research carried out at the Jet Propulsion Laboratory, California Institute of Technology, under Contract No. NAS 7-100, sponsored by the National Aeronautics and Space Administration.

JET PROPULSION LABORATORY
CALIFORNIA INSTITUTE OF TECHNOLOGY
PASADENA, CALIFORNIA

February, 1964

CONTENTS

From the ASTRONOMICAL JOURNAL
69, No. 1, 1964, February—No. 1316
Printed in U. S. A.

Symposium on Radar and Radiometric Observations of Venus during the 1962 Conjunction

edited by
F. T. BARATH
Jet Propulsion Laboratory, California Institute of Technology, Pasadena, California

NEXT to the sun and the moon, the planet Venus is the most conspicuous object in the sky, and yet very little is known about its rotation rate, its temperature, its magneto-ionosphere, its atmosphere, and its surface. Radio waves provide perhaps the most powerful tool to study these characteristics; the unprecedented concentration of observations in the radio spectrum during the 1962 conjunction reported upon here has yielded a number of new results. These fourteen papers are believed to represent the total successful effort on Venus by U. S. observers during that period, with the exception only of two radiometric measurements by Copeland (1964), and Gibson and Corbett (1963). The following appear to be the most important conclusions that can be drawn from the observations; the full implications of all the details will have to await more thorough analysis.

Rotation Rate. Previous radio observations by U. S. and Soviet workers indicated substantial phase dependence of the data, providing partial evidence for a long rotation period. Some of the data indicated a retrograde rotation as well. The radar data reported here provide new and possibly conclusive evidence for a slow rotation rate of approximately 250 days and of retrograde direction. Both of these results are supported by the radiometric phase-dependence observations. In addition, only a rotation axis essentially perpendicular to the orbit plane is found to be consistent with all the conclusions. The improved radar experiments planned for the period of the 1964 conjunction should provide high-precision, and possibly final, values for the rotation rate and axis.

Temperature. A number of brightness temperature determinations were made at various wavelengths, with most of them falling in the well-known regions of the decimeter to millimeter transition curve. The two ground-based observations at 1.18 and 2.07 cm reported here and the two Mariner measurements, however, fall in the important but ill-defined transition region itself. Based upon the 1.18- and 2.07-cm data, it appears that the transition from the decimeter wavelength brightness temperature of about 600°K and the millimeter wavelength temperature of about 375°K lies mostly between 1.3 and 2.5 cm. The Mariner temperatures, taken as 400°K (1.35 cm) and 530°K (1.9 cm) averaged over the disk, also confirm this trend. Gibson's data at 1.35 cm, on the other hand, are completely at variance with the ones presented here, indicating the need for more observations before a firm conclusion can be drawn about the detailed shape of the transition curve. Observations would especially be of great value at and between 1.3 and 2.5 cm.

The NRAO data at 21.4 and 40 cm seem to indicate a trend toward decreasing temperatures at the longer decimeter wavelengths. This might well be accidental, since the observations were of short duration and confused by solar interference, but nevertheless an observation program in this region of the spectrum also should be carried out.

Atmosphere and Magneto-Ionosphere. No systematic temperature variations are evident from the data gathered at this conjunction as compared with the data of previous years. This remarkable constancy of emission, together with the definite phase effect of the Mariner 2 data and the lack of evidence of a substantial ionosphere in the radar data, strongly favors the atmospheric and aelospheric models of Venus. Both of these theories imply a high surface temperature, responsible for the high emission at long wavelengths, and an absorbing cloud progressively cooler as a function of altitude responsible for the lower emission measured at the shorter wavelengths. The transition characteristic undoubtedly holds the key to the atmosphere's dynamics and, to a certain extent, to its composition. Considerable

work will be necessary on this subject before a firm conclusion can be drawn.

Surface. Aside from the high temperatures thought to be characteristic of the Venusian surface, all our other information about its surface parameters are of essentially qualitative nature. It is found, for instance, that the mean slopes are small and that the material is likely to be sandy or rocky.

From the foregoing it is evident that as some characteristics of Venus are defined, new questions and the need for new and improved measurements arise. A few of these problems will undoubtedly be resolved during the next conjunction; others will have to wait longer, possibly until refined instrumentation can again be carried to the vicinity of the planet aboard a spacecraft.

REFERENCES

Copeland, J. 1964, *Astrophys. J.* (to be published).
Gibson, J. E., and Corbett, H. H. 1963, Report 5937, Office of Naval Research, Naval Research Laboratory, Washington, D. C.

From the ASTRONOMICAL JOURNAL
69, No. 1, 1964, February—No. 1316
Printed in U. S. A.

Further Venus Radar Depolarization Experiments*

G. S. Levy and D. Schuster†
Jet Propulsion Laboratory, California Institute of Technology, Pasadena, California

The antenna feed system employed during the 1962 Jet Propulsion Laboratory Venus radar experiment permitted the remote automatic selection of the sense of circularity independently for both transmitting and receiving. During most of the experiment, right-handed circularly polarized energy was transmitted and left-handed circularly polarized energy was received. (Specular reflection reverses the sense of circularly polarized energy.) Several times during the experiment, however, right-handed circularly polarized energy was both transmitted and received. The depolarized component was found to be approximately 11.5 dB below the matched component. An integrated spectrum of the depolarized component was compared with the matched return. Although the spectrum is extremely noisy, it appears that the depolarized echo-scattering law lies somewhere between Lambert and Lommel–Seeliger scattering, characteristic of a rough surface. The matched component has a very pronounced specular spike, which would be expected from a smooth reflector.

I. INTRODUCTION

THE polarization characteristics of a signal transmitted in a radar astronomical observation can be precisely controlled by the experimenter. A comparison of the polarization of the transmitted and received signals can be used to deduce certain characteristics of the reflecting body and the transmission medium. Levy and Schuster (1962) reported Venus radar depolarization experiments conducted during the inferior conjunction of Venus in 1961. This paper discusses subsequent depolarization measurements conducted during the Venus inferior conjunction of 1962.

In the 1962 experiment, conducted at the NASA/JPL Deep Space Instrumentation Facility at Goldstone, California, one 85-ft paraboloidal antenna was used for both transmission and reception. The necessity of time-sharing transmission and reception functions in the same microwave components resulted in a more complicated polarization system than required by the two-antenna technique employed in the 1961 experiment. A Cassegrainian feed was utilized to provide a low effective noise temperature, good aperture efficiency, and convenient configuration for mounting instrumentation (Potter 1962). Figure 1 illustrates the configuration employed. A dual-mode conical feed horn (Potter 1963) and nonoptical beam-shaping flange permitted a substantial improvement in performance of the antenna above that reported for the 1961 experiment (Schuster, Stelzried, and Levy 1962). Table I compares the antenna and microwave system of the 1961 and 1962 experiments.

The feed horn is supported by a 14-ft-long conical structure which also houses all of the microwave receiving components, as illustrated in Fig. 2. The transmitter klystron behind the paraboloid surface feeds into a mechanical waveguide transmit–receive switch. The signal next passes by way of a rectangular-to-rectangular-waveguide rotary joint to another mechanical waveguide switch which selects one of two ports of a turnstile junction.

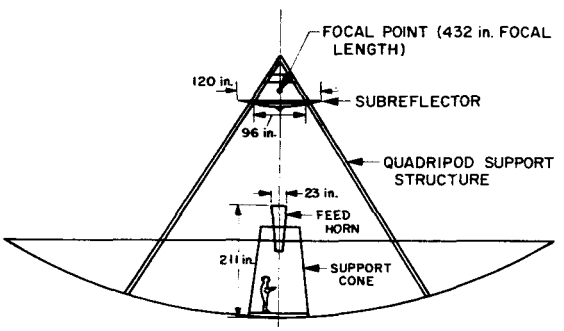

FIG. 1. *S*-band Cassegrain configuration.

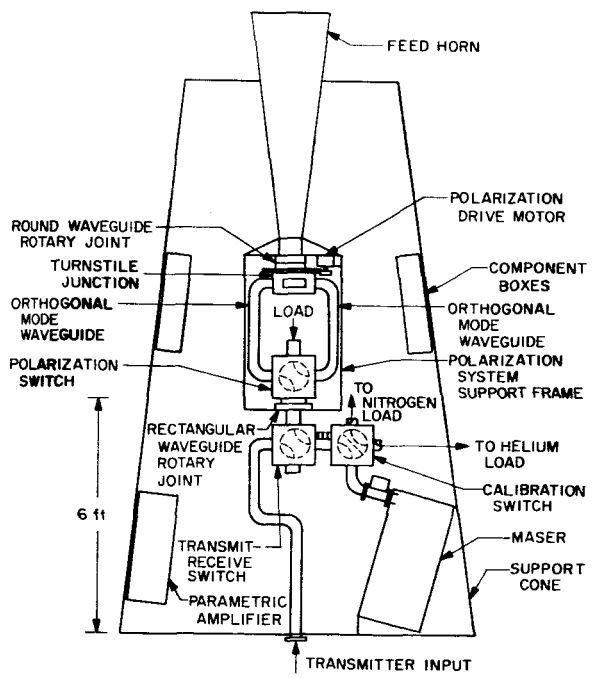

FIG. 2. Cassegrain cone installation.

* This paper presents the results of one phase of research carried out at the Jet Propulsion Laboratory, California Institute of Technology, under Contract NAS 7-100, sponsored by the National Aeronautics and Space Administration.

† Danver Shuster's sudden and tragic death occurred 9 October 1963, shortly after the completion of this paper which is dedicated to his memory.

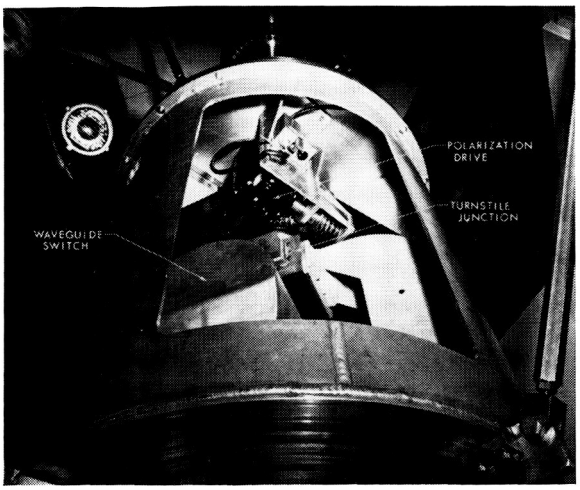

FIG. 3. Polarization system.

A turnstile junction can be used for simultaneous reception of any two orthogonally polarized elliptical components of an incident wave: the ellipticity accepted is determined by the length of the two shorted arms of the junction (Meyer and Goldberg 1955). The two limiting cases of elliptical polarization, circular and linear, are of most interest. For the linear case it is desirable to be able to rotate the plane of polarization, which must be done by mechanically rotating the feed system. The size of the feed horn makes physical rotation of this component impractical. Therefore, a circularly symmetrical horn configuration was chosen and only the turnstile junction and associated waveguide is rotated. A circular-waveguide rotary joint connects between the stationary horn and the rotatable turnstile.

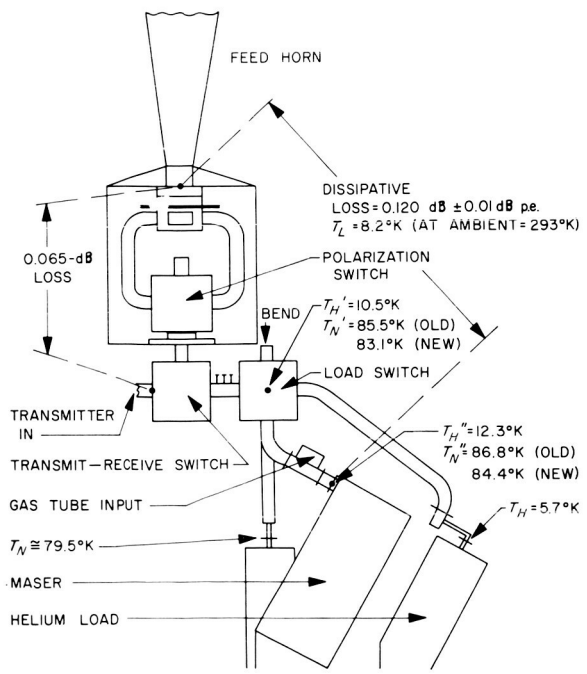

FIG. 4. Insertion loss and excess temperature diagram.

TABLE I. Comparison of the antenna and microwave system in the 1961 and 1962 experiments.

	1961	1962
Frequency	2388 Mc/sec	2388 Mc/sec
Optical equivalent	Gregorian (2 antennas)	Cassegrainian (1 antenna)
Gain at feed	53.6±1 dB	54.3±0.15 dB
Efficiency	55%±13%	60±2%
Antenna temperature at feed	15±4°K	11.0±1°K
Transmission-line temperature	14±3°K	8.2±0.7°K
Polarizer type	Quarter-wave plate	Turnstile junction

Two of the rectangular ports of the turnstile give orthogonally polarized output signals. The other two

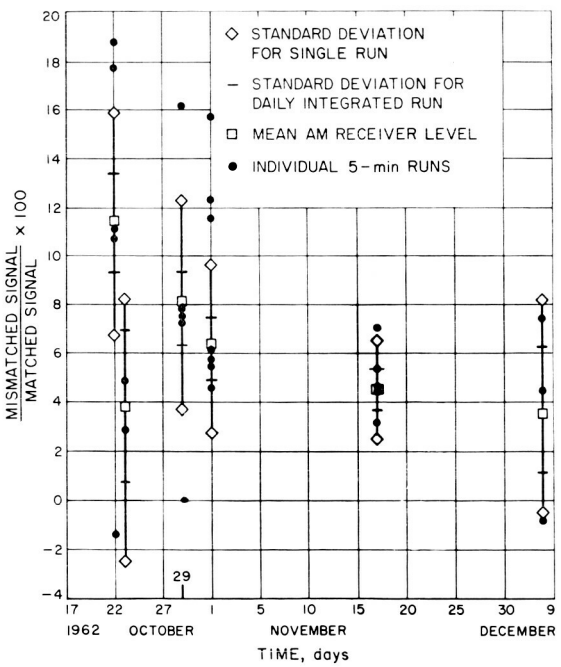

FIG. 5. Relative magnitude of depolarized signal from Venus.

rectangular ports are terminated in short circuits, one a quarter of a wavelength longer than the other; two sets of shorted waveguides which must be changed by hand allow selection of either circular or linear polarization. In the normal operating mode the signal will go into port 1 of the turnstile junction, which will convert the signal to right-handed circular polarization (RCP) and transmit it through circular waveguide to the conical horn (see Fig. 2). The normal received signal will be left-handed circular polarization (LCP), which will come out of port 2 of the turnstile junction. The received signal then passes through the polarization-selection waveguide switch, and the rectangular rotary joint to the transmit–receive (TR) switch. During

reception, the signal goes through the TR switch, the calibration switch, a cross-guide directional coupler and circulator to the cavity maser preamplifier. A partial view of the polarization system is seen in Fig. 3.

All of the components between the circular and rectangular rotary joints can be remotely rotated from the control room by use of an electric-drive motor and synchro readout.

II. CALIBRATION OF WAVEGUIDE SYSTEM

Impedance-matching of the system had to be performed in several steps. Initially the turnstile junction

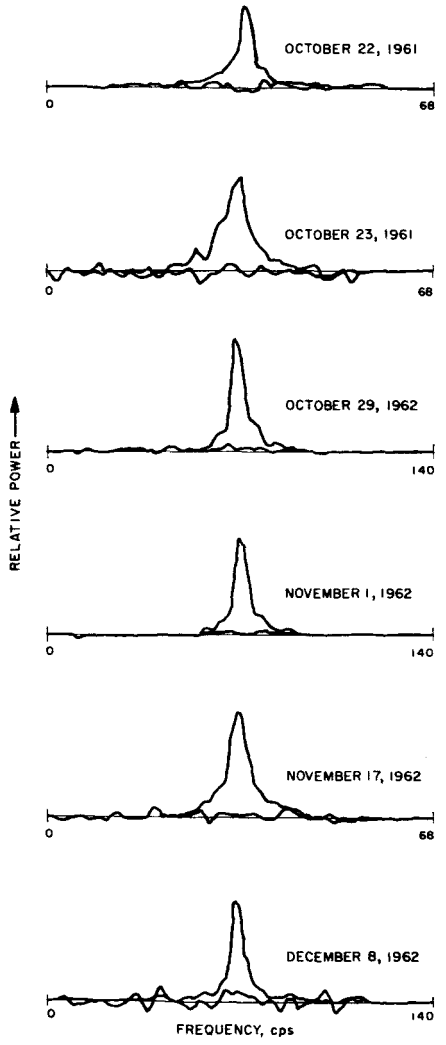

FIG. 6. Matched and mismatched polarized spectra AM receiver.

was tuned for best isolation between the two output ports and was matched with the feedhorn as a load. After installation of the horn on the antenna, reflected power into the horn from the two-reflector system was partially diverted and matched out by means of the vertex-matching cone mounted on the hyperboloid.

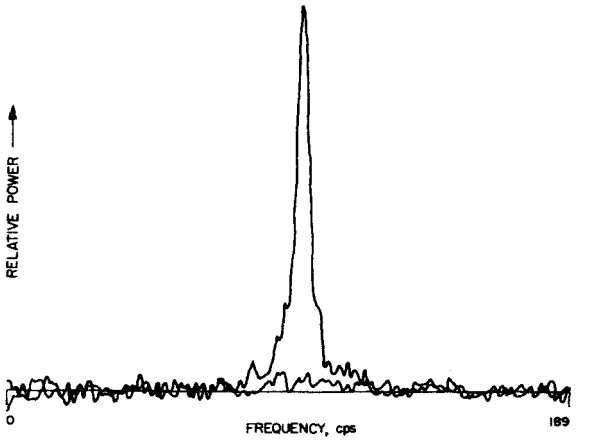

FIG. 7. Matched and mismatched polarized spectra CW receiver, 1 November 1962

The complete receiver feed system was matched at the input to the maser by means of a triple-stub waveguide tuner located between the transmit-receive and calibration switches. Slight mismatches in the helium and nitrogen load transmission lines were matched by a separate tuner in each line. The VSWR's of the system after tuning were 1.02 at the helium and nitrogen loads and 1.04 looking toward the antenna from the maser input.

The insertion losses of individual components of the waveguide system were measured wherever possible. Insertion losses of the complete system and of the lines to the helium and nitrogen loads of the calibration system were also measured. Figure 4 shows the important losses and the calculated excess temperatures of the reference loads at various points. The point for comparison of the reference loads and the gas tube is essentially at the input to the maser.

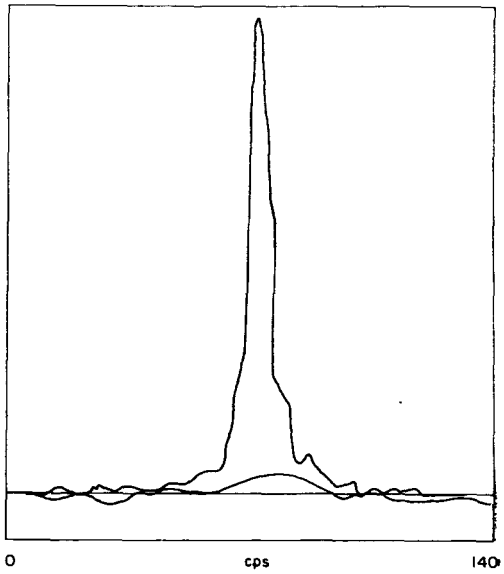

FIG. 8. Integrated matched and mismatched circularly polarized Venus echoes, 29 October, 1, 21, 30 November 1962, AM receiver.

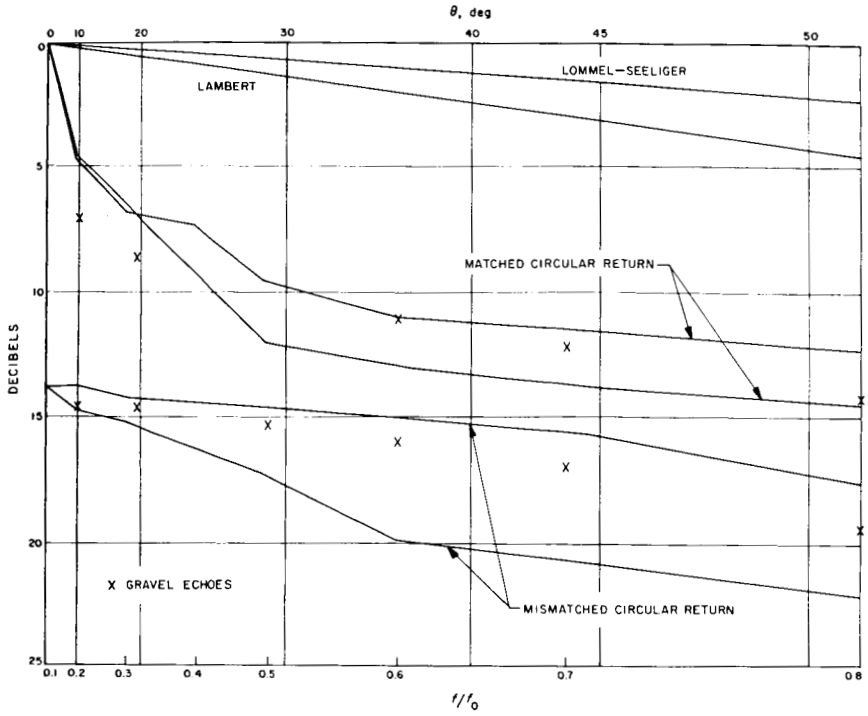

FIG. 9. Integrated matched and mismatched polarized signal on log-log $\cos\theta$ plot.

III. EXPERIMENTS

The polarization switching equipment permitted remote automatic selection of the sense of circularity independently for both transmit and receive. During most of the radar experiment the feed system on the 85-ft antenna was set so that RCP energy was transmitted and LCP energy was received. (Specular reflection reverses the sense of rotation of circularly polarized energy.) Several times during the experiment, however, RCP energy was both transmitted and received. If the reflection mechanism were purely specular, we would expect to get no depolarized return. The depolarized component was found to be approximately 11.5 dB below the matched component, a result confirming the measurements made during the 1961 Jet Propulsion Laboratory radar experiment (Victor, Stevens, and Golomb, 1961).

The axial ratio of the polarization ellipse was measured by rotating a linear antenna at the collimation tower about 1 mile away; the result was 0.45 dB for both RCP and LCP. An additional test of ellipticity was made by using a circularly polarized horn with 1-dB ellipticity at the collimation tower and measuring the isolation between the RCP and LCP outputs of the 85-ft antenna feed. The minimum isolation was found to be 22.5 dB, as compared to 21.2 dB calculated. In a later test the axial ratio of the illumination horn was improved to 0.25 dB and the minimum isolation was found to be 25.5 dB, as compared to 24.5 dB calculated.

Measurements were made of the strength and spectrum of the matched and mismatched polarization signals. The standard deviation of signal-to-noise ratio for a single mismatched polarization run for each day was computed. This deviation from the daily mean of mismatched polarization runs was plotted (Fig. 5). The ratio of mismatched to matched polarized signal was then plotted in percent for each run (approximately 5 min). It was found that about 65% of the points fell within the $1-\sigma$ limits of the daily mean. This indicates that the apparently highly variable data on a short-term basis may actually be the result of a low signal-to-noise ratio. The standard deviation of the daily mean is also indicated for each day. The variation of the daily mean indicates that the reverse polarized reflection coefficient is changing with time.

Spectral data were obtained from two modes of radar system operation: AM (Fig. 6) and CW (Fig. 7). The integrated matched and mismatched spectra are plotted on the same scale for each day. The mismatched mode has extremely low signal-to-noise ratio. In the matched mode a very narrow-band specular spike is the most marked feature. In the depolarized case the spike is not apparent.

A usable matched and mismatched polarized spectrum was obtained by algebraically summing the data from 9 October, 1, 21, and 30 November 1962. The resulting spectrum is presented in Fig. 8. The estimated limb-to-limb Doppler bandwidth for each day based on a 250-day retrograde orbit is, respectively, 46, 42, 39, and 42 cps. For the purposes of this date analysis it was assumed that the Doppler bandwidth was constant for all 4 days. R. Goldstein (1962) has shown that the frequency-backscattering function has an angular cosine series transform. The frequency-backscattering

function $P(f)$ is given by

$$P(f)=\left[\frac{2R^2}{f_0}\right]\left[a_1b_1\left(1-\frac{f^2}{f_0^2}\right)^{\frac{1}{2}}+a_2b_2\left(1-\frac{f^2}{f_0^2}\right)+a_3b_3\left(1-\frac{f^2}{f_0^2}\right)^{\frac{3}{2}}+a_nb_n\left(1-\frac{f^2}{f_0^2}\right)^{n/2}\right],$$

where f_0 is $\frac{1}{2}$ total limb-to-limb Doppler spread, and R is Venus radius. If only the first term in the series were present, the scattering would be Lommel–Seeliger scattering or that from a uniformly illuminated disk. If only the second term were present, it would be Lambert scattering, where the energy reflected per unit area is proportional to the cosine of the angle θ formed by the incident ray and the surface normal. The angular-scattering function may be represented by a cosine series:

$$F(\theta)=b_1\cos\theta+b_2\cos^2\theta+b_3\cos^3\theta+\cdots,$$

where the first and second terms have the same significance as in the $P(f)$ expression.

The matched and mismatched spectra have been replotted in Fig. 9 on log paper with the abscissa adjusted to produce a straight line for any integral power of

$$(1-f^2/f_0)^{\frac{1}{2}n},$$

where the slope of the line is a function of $\frac{1}{2}n$, the power of the term. Since both spectra were asymmetric, and the logarithmic plot folds the spectrum at its center, both sides of each spectrum are plotted.

The mismatched polarized signal appears to follow approximately a Lambert scattering law from 0 to 50 deg (although the spread in the data is such that a Lommel–Seeliger law should not be ruled out). The data are usable only to 50 deg, because the signal-to-noise ratio becomes too small at larger angles. The matched polarization signal appears to be composed of a specular as well as a diffuse component. The diffuse component seems to be somewhere between a Lommel–Seeliger and Lambert scattering law.

Taylor and Peake (private communication) of Ohio State University obtained the points indicated by X's in Fig. 9 by measuring the matched and mismatched backscattering cross section of gravel with an average diameter of $\frac{1}{3}$ of a wavelength and well-rounded edges. The relative magnitudes of the angular backscattering function and the amplitude difference between polarizations are presented.

The depolarization observed, although very weak, appears to be similar to what one would expect from a rough-surface scattering phenomenon. The integration of several days of data has made it necessary to assume a more or less uniform surface distribution. There are not sufficient data at this time to discuss surface irregularities.

ACKNOWLEDGMENTS

The authors wish to thank R. Stevens for making these experiments possible. The use of Dr. R. Goldstein's AM receiver, as well as his many helpful suggestions, is greatly appreciated. R. L. Carpenter reduced the CW spectra. Dr. E. Rechtin, W. K. Victor, and P. D. Potter are thanked for their valuable support during the experiments. D. L. Nixon and F. E. McCrea performed the installation of most of the microwave components. R. G. Petrie designed and fabricated the polarization switching controls.

REFERENCES

Goldstein, R. 1962, *Radar Exploration of Venus*, Tech. Rept. No. 32-280, Jet Propulsion Laboratory, Pasadena, California, May 25.

Levy, G. S., and Schuster, D. 1962, *Astron. J.* **67**, 5, 320.

Meyer, M. A. and Goldberg, H. B. 1955, *IRE Trans.* **MTT3**, 40.

Potter, P. D. 1962, *IRE Trans.* **PGSET Set-8**, 154.

Schuster, D., Stelzried, C. T., and Levy G. S. 1962, *IRE Trans.* **PGAP AP-10**, 3, 286.

Victor, W. K., Stevens, R., and Golomb, S. W., 1961, *Radar Exploration of Venus*, Tech. Rept. No. 32-132, Jet Propulsion Laboratory, Pasadena, California, August 1.

From the ASTRONOMICAL JOURNAL
69, No. 1, 1964, February—No. 1316
Printed in U. S. A.

Faraday Rotation of Venus Radar Echoes*

D. SCHUSTER† AND G. S. LEVY
Jet Propulsion Laboratory, California Institute of Technology, Pasadena, California

In November and December of 1962 some Venus radar experiments were conducted at the NASA/JPL Deep Space Instrumentation Facility at Goldstone, California. In these experiments, linear polarization was used for transmission and reception. The orientation of the linear transmitted polarization was kept constant with reference to the local vertical. A signal was transmitted for approximately 5 min (the time of two-way flight), after which the feed-polarization angle was rotated by a remotely controlled servo-drive system. After the feed was properly realigned, the receive cycle was started.

Power received was plotted as a function of receiving polarization angle. The null angle indicated the Faraday rotation and the null depth gave an indication of the surface depolarization.

The data, although quite noisy, can be explained completely by the earth's ionosphere. This implies that no extraterrestrial magneto-ionic interaction existed in a configuration to cause measurable Faraday rotation.

INTRODUCTION

A MEDIUM in which both charged particles and a magnetic field exist can be said to be "optically active" and can exhibit Faraday rotation. A linearly polarized electromagnetic signal will be split into two circularly polarized components. The refractive index and, therefore, the velocity of these two components will not be equal. Upon emerging from the magneto-ionic medium there will be a relative phase shift between the two circular components, resulting in an apparent rotation of the resulting linearly polarized signal.

I. C. Browne *et al.* (1956) first attributed slow lunar radar fading to Faraday rotation in the ionosphere. This effect was used by J. V. Evans (1956) and others to determine the total electron content of the ionosphere. A somewhat similar technique was employed by Yeh and Swenson (1961) using the Faraday rotation rate of two frequencies radiated from a satellite.

Bauer and Daniels (1959) show that the rotation Ω in radians for two-way propagation is

$$\Omega = 4.72\times10^{4} f^{-2}\int_{h1}^{h2} NB\cos\theta\sec\delta\, dh,$$

where f is frequency in cps, N is electron density (electrons/cm^3), B is the earth's magnetic field in gauss, δ is zenith angle, and θ is the angle between the magnetic field and the direction of propagation. The assumption is generally made that all Faraday rotation takes place within an altitude of 500 km of the earth. Yeh and Swenson (1961) found that using the values of B and θ at 350-km altitude gave a good fit to the integration:

$$\Omega = 4.72\times10^{4} f^{-2} B\cos\theta\sec\delta\int_{h1}^{h2} N dh.$$

On 20 November, 27 November, and 1 December 1962, Venus radar experiments were conducted using linear polarization for transmission and reception. In these experiments the orientation of the linear transmitted polarization was kept constant with reference to the local vertical. A signal was transmitted for approximately 5 min (the time of two-way flight), after which the linear rotatable feed was rotated by a remotely controlled feed-drive system, discussed in a companion paper in this issue. When the feed was properly aligned, the receive cycle started.

VENUS MEASUREMENTS

The actual measurements that were made are summarized in Tables I, II, and III for 20 and 27 November and 1 December 1962, respectively. In these tables, S/N is the computer output of the AM receiver and T°K is the system temperature. Unnormalized signal strength is the product of S/N and T°K. The first signal-strength level obtained from parallel transmitted and received polarization was used for normalization. The ratios were then converted into decibels. The transmitted and received polarizations, as well as the transmitter start time and elevation angle, are tabulated for each run.

If there were no surface depolarization, one would expect the returned-signal power to obey the following law:

$$P = \tfrac{1}{2}C[1+\cos 2(\psi-\Omega)] = C[\cos^2(\psi-\Omega)],$$

where ψ is the angle between transmitter and receiver polarization orientations and Ω is the angle of Faraday rotation. If, in addition to Faraday rotation, there was also surface depolarization, then,

$$P = [C_1 + C_2\cos 2(\psi-\Omega)].$$

In Figs. 1(a) through 1(f) the signal strength of 20 November has been plotted as a function of ψ, the angle between transmit and receive. The data have been broken up into consecutive time periods through the day. Figure 1(a) is very nearly a $\cos^2(\psi-\Omega)$ curve where

* This paper presents the results of one phase of research carried out at the Jet Propulsion Laboratory, California Institute of Technology, under Contract NAS 7-100, sponsored by the National Aeronautics and Space Administration.

† Danver Schuster's sudden and tragic death occurred 9 October 1963, shortly after the completion of this paper which is dedicated to his memory.

TABLE I. Polarization data, 20 November, 1962.

Run	S/N	T, °K	Signal strength	Normalization		Polarization, deg		Transmitter start time	El angle	
				Ratio	—dB	Receiver	Transmitter		Transmitter	Receiver
1	0.293676	51.8	15.212	1	0	0	0	14:12:33	7.1	7.78
2	0.005837	50.6	0.295352	0.019415	17.1	90	0	14:27:46	8.60	9.67
3	0.327853	48.4	15.86808	1.04313	(−)0.2	0	0	14:32:58	10.59	11.38
4	0.233424	48.0	11.20435	0.736546	1.3	30	0	14:42:07	12.19	12.95
5	0.070427	45.7	3.21851	0.211577	6.8	60	0	14:51:45	13.68	14.52
6	0.002677	44.4	0.118858	0.007813	21.0	90	0	15:01:16	15.34	16.15
7	0.085914	45.7	3.92627	0.258103	5.9	120	0	15:10:51	16.90	17.61
8	0.264246	49.5	13.08012	0.859855	0.7	150	0	15:20:31	18.44	19.13
9	0.362741	43.4	15.74296	1.0349	(−)0.2	180	0	15:30:15	19.83	20.65
10	0.004024	43.1	0.173434	0.011401	19.4	90	0	15:40:04	21.40	22.07
11	0.032881	42.9	1.410593	0.092729	10.3	100	0	15:49:42	22.81	23.46
12	0.010648	42.3	0.4505104	0.0296088	15.3	80	0	15:58:41	24.09	24.78
13	0.410922	41.3	16.97107	1.115636	(−)0.5	0	0	16:09:03	25.46	26.07
14	0.027379	41.3	1.130752	0.074333	11.3	90	0	16:18:30	26.64	27.22
15	0.030532	40.0	1.22128	0.080284	11.0	100	0	16:28:06	27.89	28.40
16	0.013395	42.0	0.56259	0.0369833	14.3	80	0	16:37:41	28.98	29.50
17	0.032438	40.8	1.32347	0.087001	10.6	70	0	16:47:17	30.01	30.49
18	0.077894	39.0	3.03786	0.1997015	7.0	60	0	16:56:49	30.99	31.43
19	0.012959	38.8	0.502809	0.033053	14.8	90	0	17:06:23	31.89	32.29
20	0.005640	36.3	0.204732	0.013458	18.7	85	0	17:16:03	32.71	33.09
21[a]	0.413986	36.3	15.02769	0.98788	0.05	0	0	17:25:38	33.47	33.81
22	0.014838	39.0	0.578401	0.038023	14.2	0	270	17:35:01	34.15	34.44
23	0.021714	39.6	0.859874	0.056526	12.5	0	260	17:44:30	34.73	34.98
24	0.023181	39.5	0.9156495	0.060142	12.2	0	265	17:54:12	35.23	35.43
25	0.030940	40.0	1.2376	0.0813568	10.9	0	280	18:03:49	35.63	—
26	0.043757	39.0	1.70652	0.112182	9.5	0	250	18:13:25	35.95	36.06
27	0.073866	38.8	2.86600	0.1884039	7.3	0	290	18:23:03	36.16	36.23
28	0.390638	40.3	15.7427	1.03488	(−)0.2	0	0	18:32:37	36.28	—
29	0.095809	36.9	3.53535	0.232405	6.3	0	60	18:42:00	36.31	—
30	0.139778	39.2	5.47929	0.360195	4.4	0	120	18:51:40	36.23	—
31	0.015378	39.3	0.604355	0.0397288	14.0	0	80	19:01:22	36.06	—
32	0.034071	40.3	1.373061	0.090261	10.5	0	100	19:11:01	35.79	35.63
33	0.017214	38.5	0.662739	0.043566	13.6	0	95	19:20:46	35.43	—
34	0.378994	37.9	14.36387	0.94424	0.3	0	0	19:30:27	34.96	—
35[b]	—	—	—	—	NEGATIVE	—	—	—	—	—
36[b]	—	—	—	—	NEGATIVE	—	—	—	—	—
37	0.375503	37.9	14.2315	0.935544	0.3	0	0	19:59:50	33.04	—
38	0.038385	37.6	1.443276	0.094877	10.2	60	0	20:08:42	32.25	—
39	0.102844	37.8	3.88750	0.255554	5.9	120	0	20:18:14	31.39	30.95
40[b]	—	—	—	—	NEGATIVE	—	—	—	—	—
41	0.013316	42.0	0.559272	0.036765	14.4	100	0	20:37:36	29.40	—
42	0.011556	42.0	0.485352	0.031905	15.0	85	0	20:47:16	28.29	—
43[b, c]	—	—	—	—	NEGATIVE	—	—	—	—	—
44	0.024994	40.75	1.018505	0.066954	11.8	50	0	21:07:02	25.86	—
45[b]	0.007355	42.2	0.310381	0.020403	16.9	—	0	21:16:40	—	—
46[b, c]	—	—	—	—	NEGATIVE	—	—	—	—	—
47[c]	0.000770	45.0	0.03465	—	—	—	—	—	—	—
48	0.346303	46.7	16.1723	1.06312	(−)0.3	0	0	22:05:52	17.28	—
49[b, c]	—	47.1	—	—	NEGATIVE	—	—	—	—	—
50	0.018172	47.75	0.86771	0.057041	12.4	60	0	22:25:01	14.14	—
51[b]	NEGATIVE	—	—	—	—	—	—	—	—	—
52[c]	0.015099	48.5[d]	0.73230	0.0481396	13.2	—	0	—	—	—
53[c]	—	—	—	—	—	—	—	—	—	—

[a]The computed signal strength for the run was −167 dbm.
[b]Bad data.
[c]Bad command.
[d]Estimated temperature.

$\Omega \approx 2$ deg. Very little depolarization is indicated because the null depth is between 16 and 21 dB. Figures 1(b) and 1(c) give approximately the same picture. In Fig. 1(d) the null appears to be only 13 dB deep. The data for Fig. 1(d) were taken near an angle (ψ) of 270 deg rather than 90 deg to test the symmetry of the antenna system. Figure 1(e) shows a rotation of approximately 5 deg. The data in Fig. 1(f) show a great deal of scatter

~~26~~ 9

TABLE II. Polarization data, 27 November 1962.

Run	S/N	T,°K	Signal strength	Normalization		Polarization, deg		Transmitter start time	El angle	
				Ratio	—dB	Receiver	Transmitter		Transmitter	Receiver
1	0.161	46.5	7.49	1.0	0	0	0	20:52:36	24.1	—
2	0.000309	46.5	0.0144	0.00191	27.2	90	0	21:02:29	22.6	—
3	0.0275	47.75	1.31	0.175	7.57	60	0	21:13:07	20.95	—
4	0.0508	49.25	2.50	0.334	4.78	120	0	21:23:31	19.22	—
6	0.0295	51.5	1.52	0.203	6.94	100	0	21:44:39	15.54	—
7	0.1488	52.2	7.77	1.03	+0.10	0	0	21:55:12	13.9	—
8	0.00306	55.9	0.171	0.0228	16.42	80	0	22:05:39	—	—

and, therefore, the rotation angle of 11 deg is assigned a much higher uncertainty than any of the other points.

The data for Fig. 2 were taken 27 November from 2052 to 2205 GMT; the rotation angle appears to be about 5 deg. Figures 3(a), (b), (c) represent data for 1 December. The period 1533 to 1843 had a 2-deg Faraday rotation. The last two runs had a 5-deg rotation. The very low signal-to-noise ratio in the null is illustrated in Fig. 3(c), which presents the one-standard-deviation limits. The standard deviation for the AM receiver is calculated from the following equation (private communication from R. Goldstein):

$$\sigma = 1/(TB)^{\frac{1}{2}},$$

where T is the two-way flight time in seconds and B is the filter bandwidth. (A 50-cps filter was used 20

TABLE III. Polarization Data, 1 December 1962.

Run	S/N	T,°K	Signal strength	Normalization		Polarization, deg		Transmitter start time	El angle	
				Ratio	—dB	Receiver	Transmitter		Transmitter	Receiver
1	0.134456	40.3	5.418	0.959	0.2	0	0	15:33:35	—	31.30
2	0.142812	40.3	5.75	1.017	+0.04	0	0	15:44:00	—	32.52
3	0.034338	40.3	1.38	0.244	6.12	60	0	15:54:25	—	33.67
4	0.012928	37.5	0.485	0.0858	10.65	80	0	16:26:22	—	36.7
5	0.160885	37.5	6.03	1.06	+0.2	0	0	16:37:28	—	37.5
6	0.000417	37.5	0.0156	0.00276	25.6	80	0	16:47:52	—	38.1
7	—	—	—	—	NEGATIVE	—	—	—	—	—
8	0.013007	39.0	0.507	0.0897	10.5	80	0	17:09:58	—	39.2
9	0.015950	39.0	0.622	0.110	9.6	85	0	17:20:56	—	39.5
10	—	—	—	—	NEGATIVE			—		
11	0.012895	38.5	0.496	0.0877	10.6	100	0	17:43:09	—	39.7
12	0.047132	37.6	1.77	0.313	5.0	120	0	17:54:09	—	39.6
13	—	—	—	—	NEGATIVE	—	—	—	—	—
14	0.022314	37.5	0.836	0.147	8.3	110	0	18:21:00	—	38.8
15	0.029059	38.3	1.11	0.196	7.1	67	0	18:31:58	—	38.3
16	0.164521	38.7	6.36	1.13	−0.5	0	0	18:43:03	—	37.7
17	0.154560	38.1	5.88	1.04	+0.1	90	90	18:56:31	—	36.7
18	0.054516	39.0	2.13	0.377	4.2	140	90	19:06:55	—	35.8
19	0.019197	38.1	0.732	0.130	8.8	155	90	19:17:41	—	34.8
20	0.004127	38.8	0.160	0.0283	15.5	170	90	19:28:24	—	34.3
21	—	—	—	—	NEGATIVE	—	—	—	—	—
22	0.012537	38.5	0.483	0.0854	10.7	190	90	19:49:08	—	32.0
23	—	—	—	—	NEGATIVE	—	—	—	—	—
24	0.015091	40.3	0.608	0.1076	9.7	190	90	20:11:00	—	29.2
25	0.002124	34.0	0.0826	0.0146	18.3	180	90	20:21:46	—	27.0
26	0.027516	41.3	1.14	0.202	7	200	90	20:32:44	—	25.4
27	—	41.6	—	—	NEGATIVE	—	—	—	—	—
28	0.065551	41.8	2.74	0.484	3.2	220	90	20:51:24	—	23.3
29	0.009989	41.8	0.418	0.0740	11.3	180	90	21:03:01	—	20.7
30	0.131749	42.7	5.63	0.996	0	270	90	21:15:07	—	18.7
31	0.042134	42.0	1.77	0.313	5.1	50	0	21:25:50	—	16.8
32	0.012282	44.6	0.548	0.0969	10.1	65	0	21:36:50	—	14.8
33	0.013876	44.6	0.619	0.110	9.6	110	0	21:47:50	—	13.9
34	0.054807	47.7	2.61	0.462	3.35	130	0	21:58:50	—	11.0
35	0.004866	52.7	0.257	0.0455	13.4	90	0	22:09:51	—	9.1
36	0.000789	34.2	0.0270	0.00477	23.2	Cold sky calibration runs	—	22:36:15	—	87.6
37	0.008702	34.8	0.303	0.0536	12.7		—	22:46:45	—	87.6
38	0.000865	34.8	0.0301	0.00533	22.7		—	23:02:21	—	87.6

~~27~~ 10

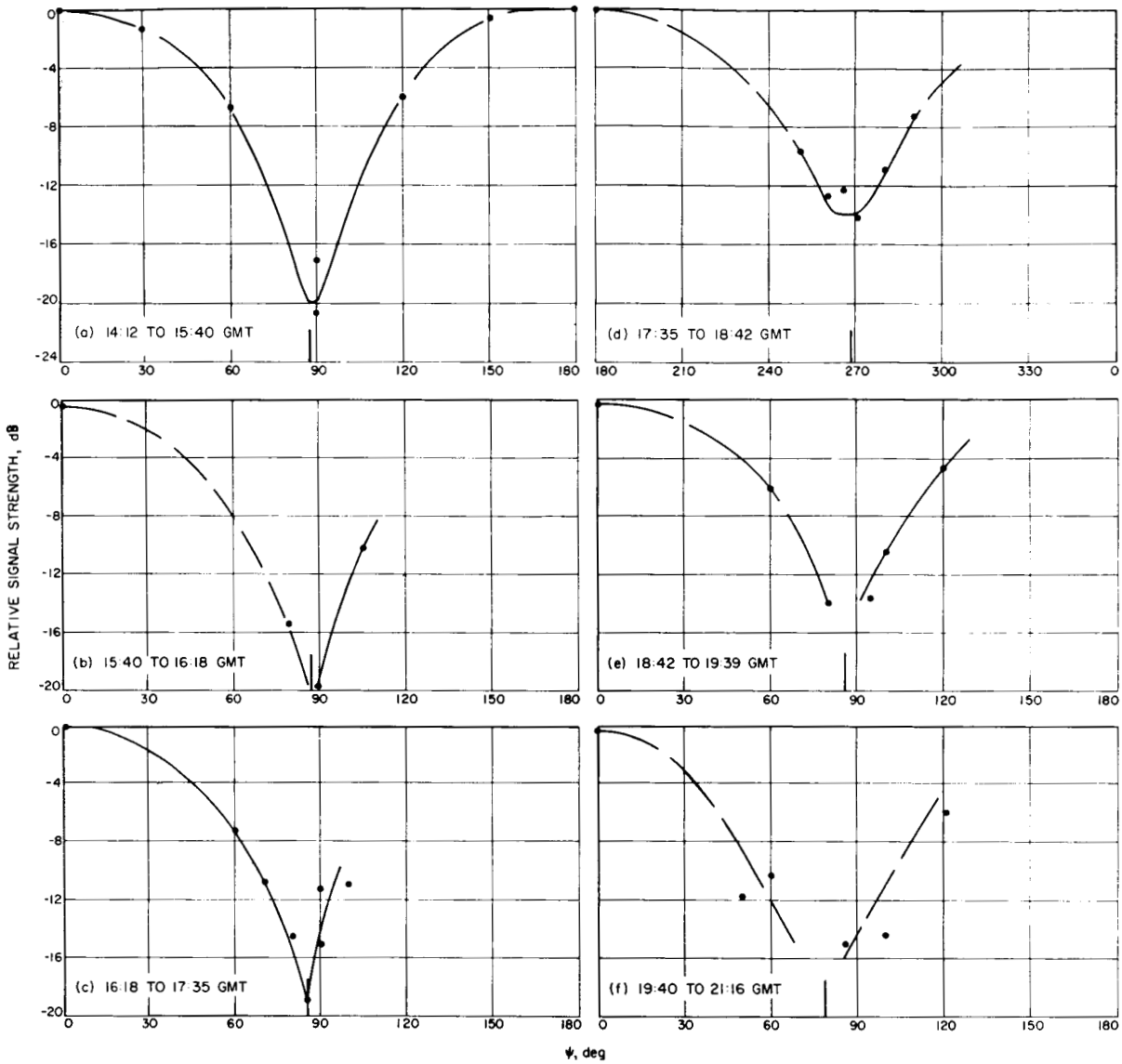

FIG. 1. Relative power vs rotation angle, 20 November 1962.

November, and a 100-cps filter was used 27 November and 1 December.) The received power at 90 deg was found to be down 13.4 dB from the parallel signal. However, the standard deviation was found to be 1.14 times greater than the power received at 90 deg.

Figure 4 presents all the Faraday rotation angles with their estimated uncertainties as a function of time after Venus rise. The computed value of Faraday rotation based solely on the earth's ionosphere is also presented. Calculations of the rotation expected from the earth's ionosphere were made using Yeh and Swenson's (1961) estimates of the integrated electron density for a period of minimum solar activity. The calculated rotation angle, shown in Fig. 4, has a maximum value occurring near 1400 h, the time of peak ionospheric electron content.

Preliminary data in the weekly report from the High Altitude Observatory at Boulder, Colorado, indicate that there was very little solar activity during this period. The following sunspot numbers were reported:

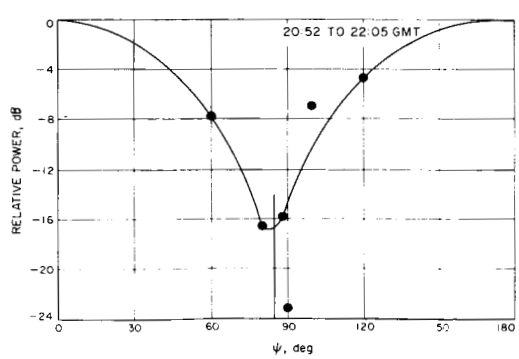

FIG. 2. Relative power vs rotation angle 27 November 1962.

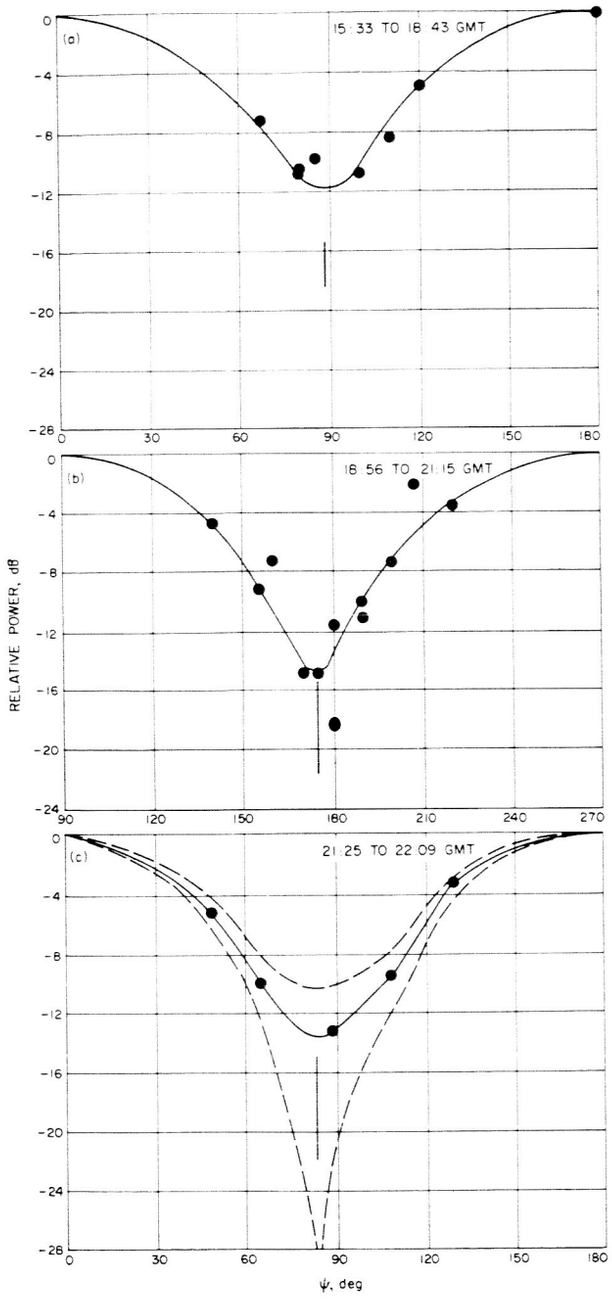

FIG. 3. Relative power vs rotation angle, 1 December 1962.

for 20 November—(11), for 1 December—(11), for 27 November—(25). The preliminary data from Mariner 2 also indicate no unusual magnetic or electron activity.

Considering the probable error assigned to the individual points and the uncertainties involved in the ionospheric parameters, it appears that all the rotation could be ascribed to the earth's ionosphere. Using preliminary Mariner data, it was estimated that interplanetary space would contribute less than 10^{-3} deg of rotation.

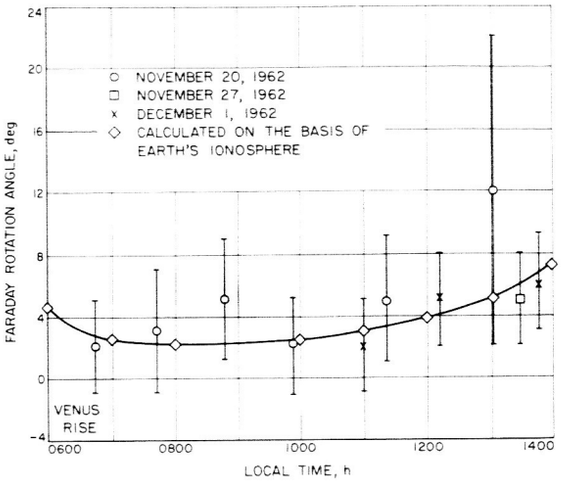

FIG. 4. Faraday rotation vs time of day.

LUNAR MEASUREMENTS

A series of lunar Faraday rotation measurements was run from 3 March to 29 March 1963 to check the measurement techniques and verify the assumptions used in the Venus calculations.

It was not possible to use the planetary radar system in its normal configuration for lunar polarization diversity experiments because of the short two-way time of flight between the earth and the moon. The time of flight (approximately $2\frac{1}{2}$ sec) was too short to permit the use of waveguide switches to switch between the transmitter and receiver or between orthogonal modes of polarization. Also, it was not possible to rotate the

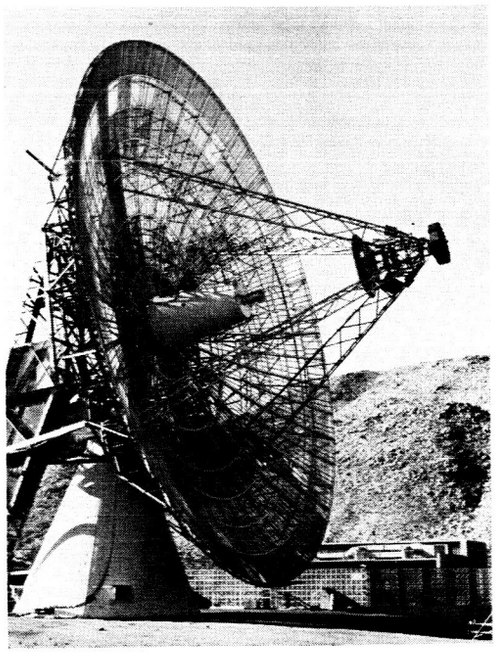

FIG. 5. 85-ft Cassegrain antenna with 6-ft tunnel dish on the apex.

12

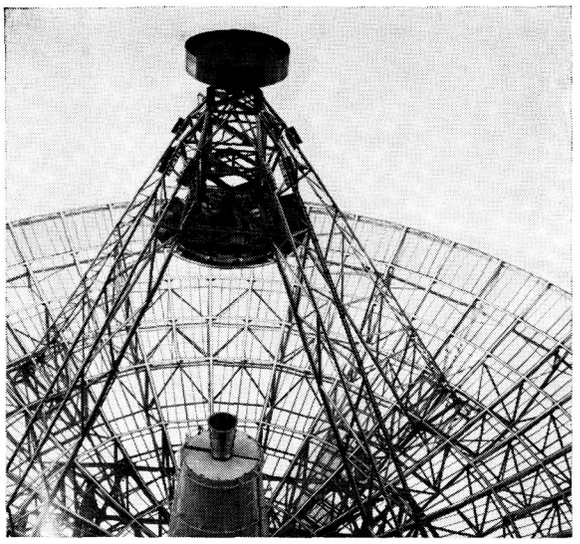

FIG. 6. Closeup of 6-ft tunnel dish on apex.

angle of linear polarization between the transmit and receive cycles.

To overcome these problems, a 6-ft-diameter parabolic antenna with a 12-in.-long cylindrical tunnel was installed on the apex of the 85-ft antenna at the Venus site at Goldstone, California (Figs. 5 and 6). The 6-ft-diameter parabolic antenna could be fed either by a Rantec Corporation circularly polarized feed or by an Andrew Corporation linearly polarized feed. A 7/8-in. coaxial transmission line connected the small antenna feed to a 1-kW klystron amplifier. The amplifier was

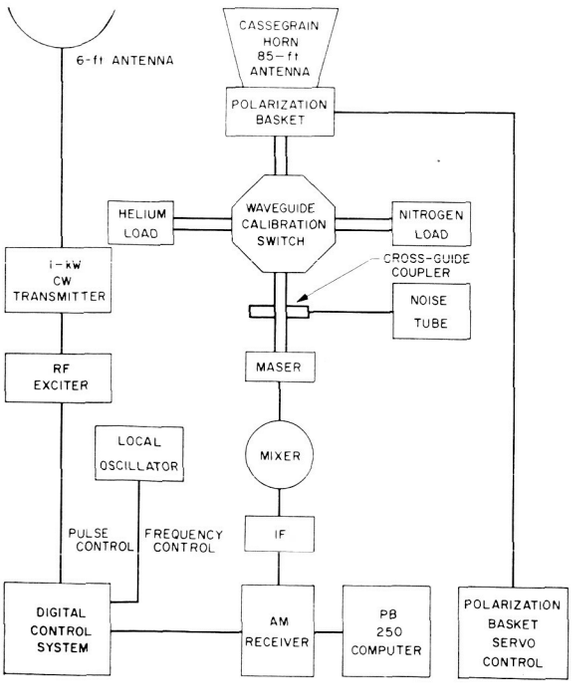

FIG. 7. Lunar radar system block diagram.

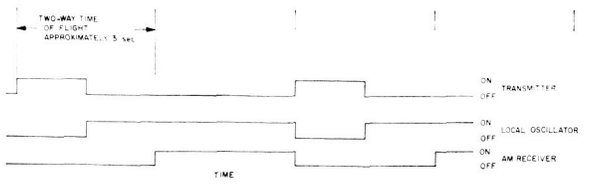

FIG. 8. Lunar echo-timing sequence.

mounted on the alidade of the 85-ft antenna; it was driven by the normal planetary radar-transmitter exciter. Figure 7 is a block diagram of the system.

Isolation between the transmitter and receiver was maintained in several ways. It was found that the isolation between the input to a vertically polarized linear feed in the 6-ft antenna and the output of the

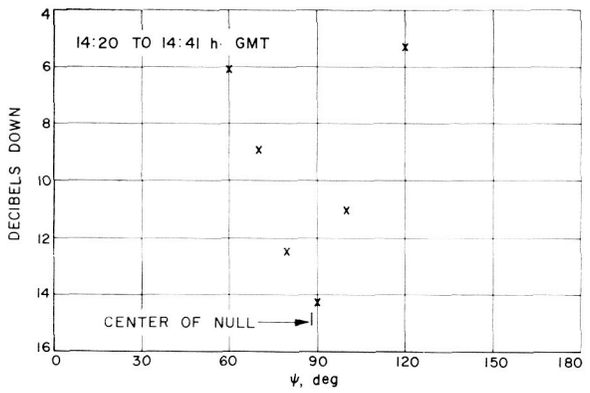

FIG. 9. Lunar Faraday rotation 2388 Mc/sec 21 March 1962; signal level vs angle ψ.

85-ft antenna with circularly polarized feed was approximately 90 dB. This was adequate to protect the maser, parametric amplifier, and the mixer during the transmit period. To protect the rest of the receiver circuitry, a digitally controlled programming sequence was employed. Figure 8 illustrates the keying scheme. The exciter is keyed for one-half the two-way time of flight. During the time that the transmission occurs, the local oscillator signal is removed from the mixer. At the end of the transmission time the digital controller removes the rf excitation from the klystron and reapplies local oscillator drive to the mixer. The receiver system is allowed to recover for one-half the two-way transit time. At the end of this time, the signal from the moon returns and the AM receiver is keyed on. For the first half of this cycle, signal and noise are received; for the second half, noise only is received. Since the transmitting and receiving feeds were independent, it was possible to vary them with respect to each other without any constraints based on the time of flight.

For the Faraday rotation experiments a vertically polarized linear feed was employed on the 6-ft antenna. This feed was found to have an ellipticity of approximately 35 dB. It was aligned by using a spirit level to orient the feed vertically. An illuminating antenna on

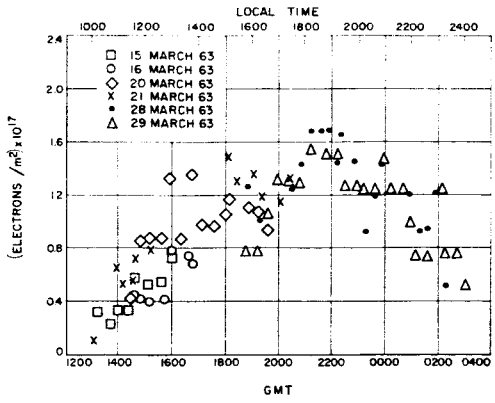

FIG. 10. Integrated electron density/m².

the collimation tower was rotated until the null position was reached. The 85-ft antenna polarization rotator was then used to rotate the turnstile junction (used with linear shorts) to the null position. The null of the turnstile junction was found to be in excess of 40 dB down.

The Faraday rotation suffered by 2388-Mc/sec energy reflected by the moon was obtained by measuring the received-signal level at the several polarization orientation angles in the following sequence: 0, 90, 80, 100, 70, 110, 60, and 120 deg. This sequence was chosen so that any system drift would not tend to bias the null position. After these signal levels were obtained, they were plotted as a function of orientation angle as shown in Fig. 9. The measured rotation was used to compute an integrated electron density for the ionosphere. The results of this are plotted in Fig. 10 where integrated electron content/m² is plotted against time.

The lunar Faraday measurements show good agreement with the zero sunspot number interpolation of Yeh and Swenson (1961). These results verify the models and techniques used for measuring the Venus Faraday rotation.

Muhleman (1963) has postulated an ionosphere on Venus with an integrated electron density of 10^6 electrons/cm² and has calculated that the Faraday rotation would be of the order of 6 deg for an average magnetic field of 100 γ. This would occur if the magnetic axis (assuming a dipole field) was properly aligned with the line of sight. These data then would imply that: (1) there is no magnetic field of the order of 10^{-3} G, or (2) the alignment of the field is in such a direction that it noes not give rise to Faraday rotation, or (3) the electron density is lower than postulated. Mariner 2 data agree with the first conclusion.

ACKNOWLEDGMENTS

The authors wish to thank R. Stevens for making these experiments possible. The use of Dr. W. Goldstein's AM receiver is gratefully appreciated. Dr E. Rechtin and W. K. Victor are thanked for their valuable support during the experiments. W. Wollenhaupt performed the digital computer programming. D. L. Nixon, F. E. McCrea and R. G. Petrie provided much valuable assistance in fabrication and testing of the microwave equipment.

REFERENCES

Browne, I. C., Evans, J. V., Hargreaves, J. D., and Murray, W. A. S. 1956, *Proc. Phys. Soc. (London)* **B69**, 901.
Daniels, F. B., and Bauer, S. J. 1959, *J. Franklin Inst.* **267**, 187.
Evans, J. V. 1956, *Proc. Phys. Soc. (London)* **B69**, 953.
Muhleman, D. O. 1963, *Icarus* **1**, 5, 6.
Yeh, K. C., and Swenson, G. W., Jr. 1961, *J. Geophys. Res.* **66**, 1061.

From the ASTRONOMICAL JOURNAL
69, No. 1, 1964, February—No. 1316
Printed in U. S. A.

Radar Scattering from Venus and the Moon*

D. O. MUHLEMAN
Jet Propulsion Laboratory, California Institute of Technology, Pasadena, California

A statistical theory for the radar backscatter function for a planetary surface will be derived. The physical basis of the theory involves combining two random variables which represent height variations and horizontal scattering lengths to form the probability distribution function for surface slopes. Two classes of distribution functions representing the two random variables are studied: those related to the normal distribution, and those related to the exponential distribution. These two classes result in slightly different distribution functions for slopes. Each of the slope functions contains a single parameter which is shown to be the expectation value of the slopes, i.e., the mean effective slope.

The probability density function of slopes is shown to be directly related to the radar backscatter function under the assumption of geometrical optics. These functions are applied to radar observations of the moon at wavelengths of 3.6, 10, 12.5, and 68 cm and it is shown that the exponential statistics yield slightly superior results.

The theory is applied to radar observations of Venus made at wavelengths of 12.5 and 68 cm in an attempt to deduce the mean slope of Venus and the Venusian rotational rate. It will be shown that Venus appears very smooth at radar wavelengths; i.e., the mean slope parameters are small relative to those for the moon.

Values of the intrinsic angular velocity are computed from the 12.5-cm radar spectral observations of Venus and are found to be between the limits of 4.5×10^{-7} and 2.0×10^{-7} rad/sec. The spread in this result arises from the difficulties in determining the wavelength dependence for the slope parameters determined from the radar data.

I. INTRODUCTION

SIGNIFICANT radar observations of Venus have been accomplished by investigators at the Jet Propulsion Laboratory and the Lincoln Laboratory in particular. Early interpretations suggested that the intrinsic rotation of Venus was very slow and that it was highly likely that Venus rotates synchronously with respect to its orbit (Muhleman 1961; Victor and Stevens 1961). Repeated observations of Venus in 1962 lead Carpenter in particular to suggest that the rotation was actually retrograde (Goldstein and Carpenter 1963).

This paper presents a detailed analysis of the observations in an attempt to determine the Venusian radar-backscatter function which is consequently used to infer the planetary rotational rate. The development of the theory is heavily based on the considerable volume of lunar radar observations catalogued by many investigators. The analysis leads to a number of new results for the moon as well as for Venus.

II. DEVELOPMENT OF THE THEORY

Many investigators have made quantitative radar studies of the moon with sufficient precision to deduce certain detailed characteristics of the scattering behavior of the lunar surface for a range of wavelengths (see Evans and Pettengill 1963, for a rather complete list of references). Similar information concerning Venus and Mercury is available from the experiments of the Jet Propulsion Laboratory conducted at a wavelength of 12.5 cm. A statistical backscattering law that represents the measured characteristics to the accuracy of the measurements will be derived in this paper. The law contains one statistical parameter, H/L, which is a ratio of a surface-height statistic to a surface-scattering-length statistic and apparently varies with wavelength.

The computations are accomplished using ray optics only. Thus, the fundamental physical principles are the laws of geometrical reflection; that is, the angle of reflection from an individual (plane) scattering element is equal to the angle of incidence and the incident and reflected rays are coplanar with the normal vector to the scattering element. We assume that the planetary surface is covered with plane-scattering elements of unspecified size and that the statistics of the surface are described by the probability distribution of the element-normal vectors relative to the normal of the mean spherical surface. The geometry is illustrated in Fig. 1. The probability density function is assumed to be of the form (in spherical coordinates)

$$p(\theta,\phi)\sin\theta d\theta d\phi = p(\theta)\sin\theta d\theta(d\phi/2\pi), \qquad (1)$$

where θ is the polar angle measured from the normal to the mean surface to the normal of the local scattering

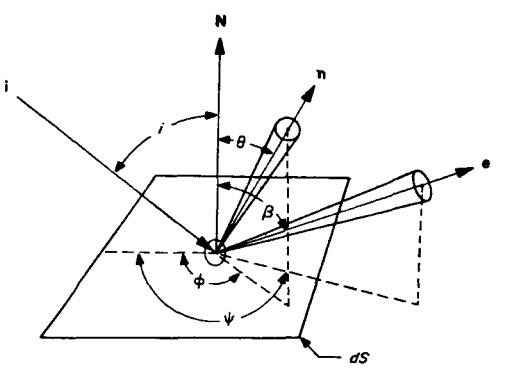

FIG. 1. Geometry defining the incident ray **i**; the reflected rays **e**; the normal to the scattering element **n**; and the normal to the mean surface **N**.

* This paper presents the results of one phase of research carried out at the Jet Propulsion Laboratory, California Institute of Technology, under Contract No. NAS 7-100, sponsored by the National Aeronautics and Space Administration.

element and ϕ is the azimuth angle of the element normal, which is assumed to be distributed uniformly. The normalization condition is

$$\int_0^{2\pi}\int_0^{\frac{1}{2}\pi} p(\theta)\sin\theta d\theta(d\phi/2\pi)=1. \tag{2}$$

Equation (1) gives the probability that the normal-to-the-surface element lies within a solid angle of $\sin\theta\ d\theta\ d\phi$ at an angle θ. If we now assume that unit flux is incident on an area dS of the mean surface at an angle of incidence from the mean normal of i (see Fig. 1), then the intensity δI scattered into a solid angle $d\Omega$ in the direction (β,ψ) is given by the number of individual scattering elements in dS that are so oriented that the laws of reflection are satisfied. Thus

$$\delta I d\Omega=\text{Prob}[\mathbf{n}\text{ in }\sin\theta d\theta d\phi](\mathbf{n}\cdot\mathbf{i})dS, \tag{3}$$

where (θ,ϕ) are related to (β,ψ) by the laws of reflection. Clearly, from Fig. 1, a scattering element will contribute if its normal, $\mathbf{n}$, is in the plane formed by $\mathbf{i}$ and $\mathbf{e}$ and midway between $\mathbf{i}$ and $\mathbf{e}$. Equation (3) written out in full is

$$\delta I\ \sin\beta d\beta d\psi=[p(\theta)/2\pi]\sin\theta d\theta d\phi(\mathbf{n}\cdot\mathbf{i})dS. \tag{4}$$

The relationship between $\sin\beta\ d\beta d\psi$ and $\sin\theta\ d\theta d\phi$ will now be derived. It can be seen from Fig. 2 that as the direction of observation $\mathbf{e}$ is moved, $\mathbf{n}$ (normal to the scattering element) must move so as to remain in the plane of $\mathbf{i}$ and $\mathbf{e}$ and bisect the angle γ between $\mathbf{i}$ and $\mathbf{e}$ if a reflection is to be detected. Thus there is a one-to-one mapping of the points contained in the element of solid angle $\sin\beta\ d\beta d\psi$ to the points in the solid angle $\sin\theta\ d\theta d\psi$. Consequently,

$$\sin\theta d\theta d\phi=|J(\theta,\phi)/(\beta,\psi)|\sin\beta d\beta d\psi, \tag{5}$$

where J is the Jacobian of the transformation which may be found from the relationships among the spherical triangles of Fig. 2. After an extensive reduction it can be shown that

$$J\frac{(\theta,\phi)}{(\beta,\psi)}=\frac{1}{4\cos(\frac{1}{2}\gamma)}\frac{\sin\theta}{\sin\beta}, \tag{6}$$

and Eq. (4) becomes

$$\delta I=[p(\theta)/8\pi]dS, \tag{7}$$

where

$$\cos\theta=\frac{\cos\beta+\cos i}{2\cos(\frac{1}{2}\gamma)}. \tag{8}$$

For the backscatter case $\gamma=0$ and $\beta=i$. Then

$$\delta I=(1/8\pi)p(i)dS. \tag{9}$$

Thus the probability frequency function of the tilt angles of the scattering elements (slope) is the same as the scattering law.

Application to a Spherical Surface

The element of spherical surface area in spherical coordinates with polar angle i and azimuth angle ν is

$$dS=R^2\sin i di d\nu. \tag{10}$$

As an example we will consider a perfectly smooth sphere. The probability density of the normal vectors for a smooth sphere can be represented by the Dirac delta function

$$p(i)=\delta(i)/\sin i \tag{11}$$

such that the integral over all angles is unity:

$$\int_0^{2\pi}\int_0^{\frac{1}{2}\pi}\frac{\delta(i)}{\sin i}\sin i di d\nu=1. \tag{12}$$

When Eq. (10) and (11) are used in Eq. (9), the intensity per unit solid angle scattered back is

$$I=\frac{R^2}{8\pi}\int_0^{2\pi}\int_0^{\frac{1}{2}\pi}\delta(i)didv=\tfrac{1}{4}R^2, \tag{13}$$

which is the correct result for a smooth sphere since the power intercepted by the sphere is πR^2 (for unit incident flux) which is isotropically scattered into 4π rad.

If $p(i)\propto\cos^2 i$ we get for the increment in intensity

$$\delta I\propto\cos^2 i\ \sin i di d\nu,$$

which is the correct result for a Lambert scatterer.

Surface Statistics

The idealized scattering elements considered in the preceding discussion can be characterized by two

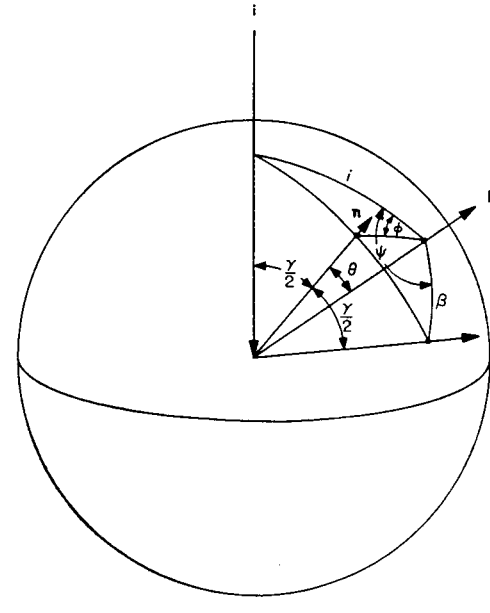

FIG. 2. Geometry showing the geometrical optics relationships among **i**, **e**, and **n**.

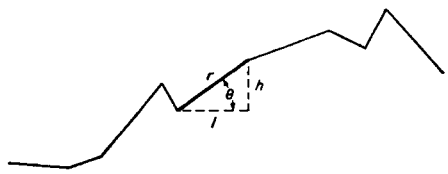

FIG. 3. One-dimensional surface contour.

factors: a tilt of the element normal from the mean surface and a characteristic length (or area) assumed to be on the order of several wavelengths. Equivalently, these factors can be thought of as scattering lengths along the surface and height increments perpendicular to the surface. Based on intuitive ideas of the earth's surface, two types of probability distribution functions will be analyzed: those related to the normal distribution and those related to the exponential distribution. The relative merits of the two will be evaluated from the radar observations.

Calling the length and height variables l and h, respectively, a (one-dimensional) scattering element can be represented in polar coordinates r and θ with the transformation (see Fig. 3):

$$h=r\sin\theta, \quad l=r\cos\theta. \tag{15}$$

The joint probability densities in the two coordinate systems are related by the equation

$$g(r,\theta)rdrd\theta=f(l,h)dldh. \tag{16}$$

If we assume that h and l are independent random variables, then

$$f(l,h)=f_1(h)f_2(l). \tag{17}$$

Given $f_1(h)$ and $f_2(l)$ and Eq. (15) we can compute the probability density of θ, the tilt angle, by integrating over all r, i.e.,

$$p(\theta)d\theta=d\theta\int_0^\infty g(r,\theta)rdr, \tag{18}$$

which, when generalized to two dimensions, is the desired function for the scattering law. In particular for the distribution functions:

(Gaussian)

$$f_1(h)dh=\frac{1}{(2\pi)^{\frac{1}{2}}\sigma_h}\exp(-h^2/2\sigma_h^2)dh, \quad -\infty\leq h\leq\infty, \tag{19}$$

and

(Rayleigh)

$$f_2(l)dl=\frac{l}{\sigma_l^2}\exp(-l^2/2\sigma_l^2)dl, \quad 0\leq l\leq\infty. \tag{20}$$

Equation (18) yields [after use of Eq. (15)]

$$p'(\theta)d\theta=\frac{1}{2}\left(\frac{\sigma_h}{\sigma_l}\right)^2\frac{\cos\theta d\theta}{[\sin^2\theta+(\sigma_h/\sigma_l)^2\cos^2\theta]^{\frac{3}{2}}}, \quad \tfrac{1}{2}\pi\leq\theta\leq\tfrac{1}{2}\pi. \tag{21}$$

Thus, the probability distribution of the tilt angles and, from Eq. (9), the backscatter law depends only on a single parameter $\alpha'=\sigma_h/\sigma_l$. If $\sigma_h=\sigma_l$ Eq. (21) reduces to

$$p'(\theta)d\theta=\tfrac{1}{2}\cos\theta d\theta, \quad \tfrac{1}{2}\pi\leq\theta\leq\tfrac{1}{2}\pi. \tag{22}$$

In terms of scattering this represents the Lommel–Seeliger scattering law. Thus $\alpha'=1$ yields a distribution which apparently represents a uniformly rough surface in a quantitative sense. The distribution function, Eq. (21), in terms of slopes $s=\tan\theta$ becomes

$$q'(s)ds=\tfrac{1}{2}(\alpha')^2\frac{ds}{[s^2+(\alpha')^2]^{\frac{3}{2}}}, \tag{23}$$

where the mean value of s is

$$E\{s\}=E\{\tan\theta\}=\alpha' \tag{24}$$

and the variance is

$$E\{s^2\}=\infty.$$

Thus, α' is the mean surface slope. Hence, the determination of a scattering law in the form of Eq. (21) is equivalent to measuring the mean surface slope α' and one should expect the measurement of α' to be wavelength-dependent.

Next, we will develop relationships analogous to Eqs. (21), (23), and (24) for probability densities related to the exponential distribution. Specifically, the functions

(Exponential) $f_1(h)dh=(1/H)e^{-|h|/H}dh, \quad 0\leq|h|\leq\infty,$ (25)

(Poisson) $f_2(l)dl=(l/L^2)e^{-l/L}dl, \quad 0\leq l\leq\infty,$ (26)

after the change of coordinates from Eq. (15) and integration in Eq. (18), yield

$$p(\theta)d\theta=2\left(\frac{H}{L}\right)^2\frac{\cos\theta d\theta}{[\sin\theta+(H/L)\cos\theta]^3}, \quad 0\leq\theta\leq\tfrac{1}{2}\pi, \tag{27}$$

which is again a function of one parameter $\alpha=H/L$. If the distribution is written as a function of slopes, $s=\tan\theta$, we get

$$q(s)ds=2\alpha^2\frac{ds}{[s+\alpha]^3}, \quad 0\leq s\leq\infty, \tag{28}$$

with the mean of s given by

$$E\{s\}=E\{\tan\theta\}=\alpha$$

and

$$E\{s^2\}=\infty.$$

Thus the parameter α is again the mean surface slope.

The nonexistence of the variances for the distribution Eqs. (25) and (28) is apparently due to allowing the height variations to be defined to infinity. Noninfinite variances would be obtained if the height-distribution functions were truncated at some finite value, say the height of the largest mountain on the planet. The distribution represented by Eq. (28) is the well-known F distribution with $m=2$ and $n=4$ degrees of freedom, which arises in probability theory in taking the ratio of two chi-square-distributed random variables with m and n degrees of freedom, respectively.

The distributions given by Eqs. (21) and (28) are very similar. Equation (28) can be written

$$p(\theta)d\theta=2\alpha^2\frac{\cos\theta d\theta}{[\sin^2\theta+\alpha^2\cos^2\theta+2\alpha\cos\theta\sin\theta]^{\frac{3}{2}}}, \quad (29)$$

which is essentially the same as Eq. (21) except for the cross term in the denominator of Eq. (29) and the difference in the measuring of α and α'. Thus in a practical application of these distributions we should expect difficulty in determining whether the statistics are fundamentally Gaussian or exponential.

Applications to Radar Measurements

The distribution functions are transformed to a two-dimensional surface distribution by assuming that the azimuth angles of the normal vectors to the scattering elements are uniformly distributed, as shown in Eq. (1). The distributions must be renormalized in accordance with Eq. (2), where θ is now defined in the interval of $(0,\frac{1}{2}\pi)$.

It is well known (Pettengill 1961) that the response of the sphere to an infinitely sharp radar pulse is the backscatter function of the surface, which from Eq. (9) becomes

$$F(i)\sin i di=kp(i)\sin i di, \quad (30)$$

where i is the great circle angle from the subradar point to the scattering element. The angle variable i in Eq. (30) is related to the time τ after the leading edge of the returned pulse by the relationship

$$\tau=(2R/c)(1-\cos i). \quad (31)$$

Equation (30) may then be expressed in terms of τ:

$$F(\tau)d\tau=k'p[i(\tau)]d\tau, \quad (32)$$

where $p[i(\tau)]$ is given by either Eq. (21) or (28) with the use of Eq. (31), with $i=\theta$. Thus

$$F(\tau)=(\alpha')^3\frac{\cos\theta}{[\sin^2\theta+(\alpha')^2\cos^2\theta]^{\frac{3}{2}}}, \quad (21')$$

or

$$F(\tau)=\alpha^3\frac{\cos\theta}{(\sin\theta+\alpha\cos\theta)^3}, \quad (28')$$

where

$$\tau=(2R/c)(1-\cos\theta).$$

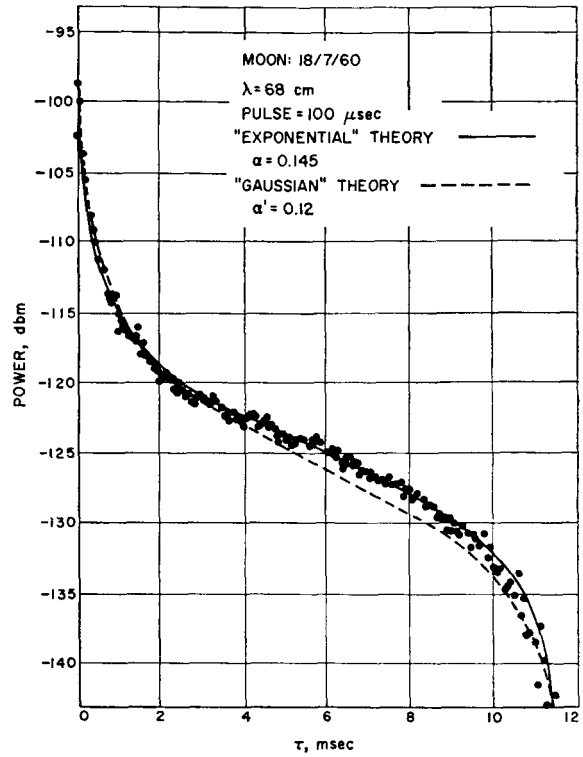

FIG. 4. Returned lunar pulses at 68 cm using a pulse width of 100 μsec.

The two expressions have been normalized so that $F(\tau)=1$ when $\theta=\tau=0$ (i.e., the pulse peak is 1).

Application to the Moon

Figure 4 shows the radar response of the moon as measured by Pettengill (1961) using 100-μsec pulses at a wavelength of 68 cm. The solid line in Fig. 4 represents the "exponential" model from Eq. (28′) and the broken line represents the "Gaussian" model from Eq. (21′) (after convolving the models with the pulse shape). It is easily seen that while both are excellent fits to the observations the exponential model is the superior fit over the entire lunar disk. Actually, the Gaussian model allows the best fit for the first 50 μsec of the data, but the parameter α' resulting from such a fit poorly represents the observations over the major part of the lunar disk. The value of $\alpha=0.145$ was found from the observations of Fig. 4.

The exponential character of the lunar radar response was first noted by Pettengill (1961). Equation (28′) yields for small θ

$$F(\tau)\simeq\exp[-(3/\alpha)\tan\theta], \quad (33)$$

in good agreement with Pettengill's result, and for large θ

$$F(\tau)\simeq\alpha^3\cos\theta(1-3\alpha\cos\theta), \quad (34)$$

which is essentially a $\cos\theta$ curve. Equation (34) offers

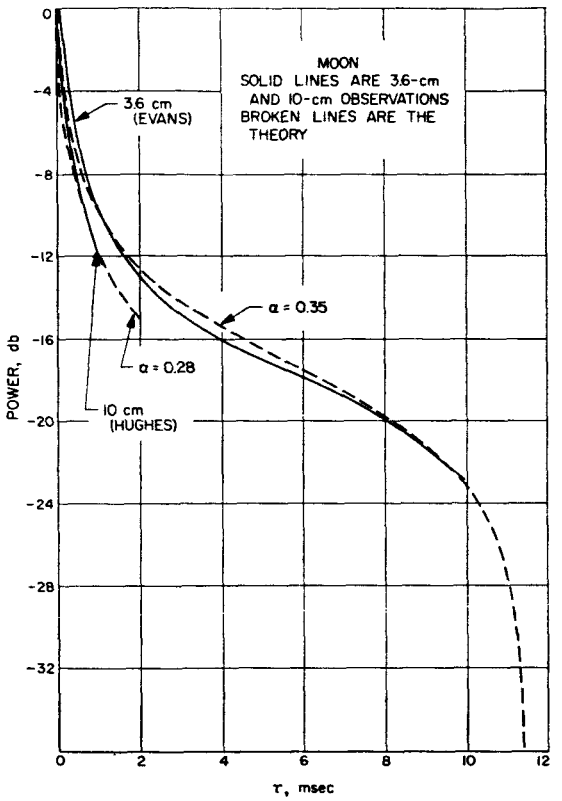

FIG. 5. Returned lunar pulses at 3.6 cm, pulse width of 30 μsec, and 10 cm pulses, pulse width 5 μsec.

another interpretation of the mean slope parameter α; i.e., α^3 gives the fraction of the returned power in the so-called "diffuse" component. However, this theory makes no use of the concept of a specular and diffuse component employed by many previous investigators.

Figure 5 shows the lunar radar response measurements at 10 cm and 3.6 cm along with the best fit of the exponential model (suitably corrected for pulse width). The values of the mean slopes from these observations are

$$\alpha_{10}=0.28, \quad \alpha_{3.6}=0.35.$$

For completeness, the lunar infrared observations at full moon of Pettit and Nicholson (1931) are shown in Fig. 6 along with the model for $\alpha=1.0$ (uniform roughness). It can be seen that the model adequately represents the observations except that a slight specular behavior is predicted. It is doubtful that Pettit and Nicholson's techniques could have detected such an effect. Clearly, the infrared radiation is not reflected radiation, but one would expect that any directional properties of the infrared emission would depend on the statistics of the slopes in a manner similar to the radar case.

The values of α are plotted against log-wavelength in Fig. 7 and apparently fall on a straight line. A poorly determined value for a wavelength of 12.5 cm computed from the author's CW lunar radar observations is included in the plot. This value was inferred from the spectra of radar signals in a manner described below, but the results are seriously in doubt because of uncertainties in the antenna pattern effects. The equation of the line in Fig. 7 is

$$\alpha(\lambda)=0.44-0.16\log\lambda. \tag{35}$$

Equation (35) yields $\alpha=1.0$ for $\lambda=2.2\,\mu$. However suggestive this result may be with respect to the infrared observations it may very well be fortuitous. Clearly, the equation must break down for $\lambda>5$ *m* since α must be greater than zero.

III. APPLICATIONS TO VENUS

Several significant questions concerning Venus can be studied with an application of the above theory to the radar observations of Venus. A direct consequence of such studies, assuming the availability of ideal observations, is a determination of the average mean slope of the Venusian surface or values of the mean slopes as a function of the orientation of the surface as it rotates beneath the subradar point. Since the measured value of α will probably be wavelength-dependent, data are required over a range of wavelengths in order to determine the properties of the true geometrical surface. However, the power returned near the limbs of the planet will be affected by the absorption of the planetary atmosphere (limb-darkening) which will also be wavelength-dependent. Muhleman (1963) has shown that the absorption in the Venusian atmosphere and ionosphere for 12.5-cm radar waves is probably negligible, but effects would become much more significant at longer wavelengths.

Finally, if the scattering law with the correct mean-slope parameter can be established, an estimate of the Venusian rotation rate can be made by fitting the model to observed radar spectra in the manner described below.

The radar observations of Venus are limited to two wavelengths: 12.5 cm from the Jet Propulsion Labora-

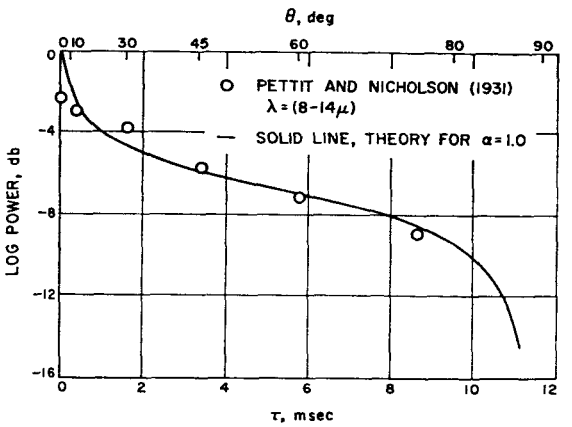

FIG. 6. Lunar infrared observations of Pettit and Nicholson (1931) plotted in the manner of radar pulses.

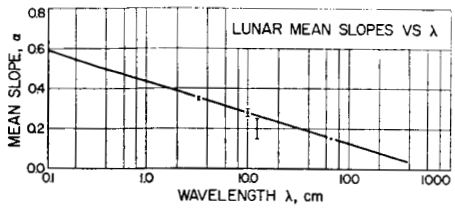

FIG. 7. Computed effective-mean slopes against the logλ.

tory work and 68 cm from the Lincoln Laboratory. The 68-cm observations were made in 1961 and are essentially limited to one rather low-quality, pulse-decay measurement made on 17 April 1961. This represents the only data from which the scattering law can be directly determined. The 12.5-cm observations taken at inferior conjunctions of Venus in 1961 and 1962 are all in the form of spectra, because the experiments were done in a CW mode. The scattering law can be uniquely determined from these spectra if the rotation rate of Venus is known. The approach that will be adopted here is as follows:

(1) Tentatively assume that the backscatter law for Venus has the same mathematical form as that for the moon.

(2) Determine the Venusian mean slope α (independent of the rotation rate) from the 68-cm observations of 1961.

(3) Apply the scattering law to the observed 12.5-cm spectra to establish that the mathematical law does fit the observations and to obtain an estimate of the Venusian rotation rate.

The pulse-response data for Venus (Smith 1963) at 68 cm are shown in Fig. 8. The heavy solid curve in Fig. 8 is the response of a perfectly smooth sphere to the 68-cm pulse employed by the investigators (500-msec pulses). The lunar scattering law from Eq. (28′) must be convolved with this function for comparison with the observations. The scattering laws with $\alpha=0.04$, 0.05, and 0.12 are also shown in Fig. 8. These curves suggest that the correct choice may be as small as 0.04 (2.3 deg), but all of the observations are within 1σ of the $\alpha=0.05$ curve except one. The $\alpha=0.12$ curve represents a surface that is nearly as rough as the moon (at 68 cm) and its significance will be explained in the following. Thus, we will tentatively adopt the lunar scattering law with $\alpha_{68}=0.04$ as a minimum value.

Derivation of Theoretical Spectra from the Scattering Law

The spectrum of the echoed-CW signal is a measurement of the power returned per cps as a function of the frequency measured plus-and-minus from the center of the spectrum. The power in a 1-cps frequency interval at frequency f is the integral of the echo intensity over a strip on the surface of the planet parallel to the axis of the apparent planetary rotation. It can easily be shown that the frequency f corresponds to an angle θ measured on a great circle about the rotational axis where

$$f=f_m \sin\theta, \tag{36}$$

and f_m is the maximum frequency from the center of the spectrum corresponding to the power returned from the limb on the equator. The frequency f_m is an exact measurement of the apparent rotation rate since

$$f_m=(2R/\lambda)\omega_a,$$

where R is the planetary radius, λ the wavelength of the CW transmission, and ω_a the apparent rotation rate. The intensity scattered by a surface element is given by Eq. (9) and for a spherical surface

$$\delta I=(R^2/8\pi)p(i)\sin i di dv. \tag{9′}$$

Recall that i is the angle from the subradar point to the scattering element and is equal to θ only when the

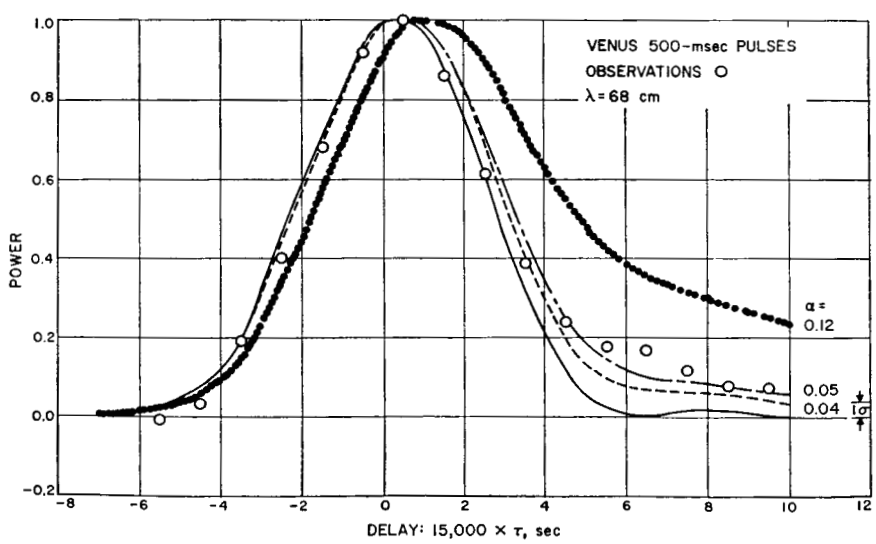

FIG. 8. Venus 68-cm pulse observations of Pettengill with the theoretical models for $\alpha=0.04$, 0.05, and 0.12.

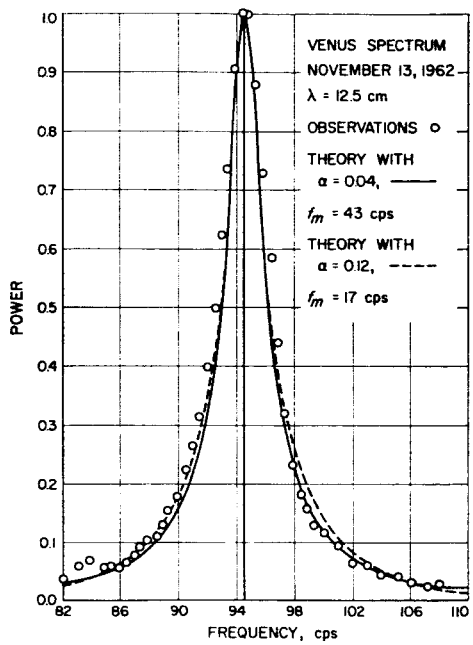

FIG. 9. Observed Venus-echo spectrum for 13 November 1962 and theoretical spectra for $\alpha=0.04$, $f_m=43$ cps, and $\alpha=0.12$, $f_m=17$ cps.

scattering element is on the rotational equator. It can then be shown from the geometry of the sphere that the integral for a constant $f=f_m \sin\theta$ is given by

$$P(\theta)d\theta = K\cos\theta\int_{i=\theta}^{\frac{1}{2}\pi}\frac{p(i)\sin i di}{(\cos^2\theta-\cos^2 i)^{\frac{1}{2}}}, \qquad (37)$$

where K will be chosen such that the peak power in the spectrum is unity, i.e., $P(0)=1$. The power-spectral density $P(\theta)$ can then be mapped onto the frequency scale with Eq. (36) for any given value of f_m. Inserting Eq. (28′) in Eq. (37) we get

$$P(\theta)d\theta = 2\alpha^3\cos\theta d\theta \times\int_{\theta}^{\frac{1}{2}\pi}\frac{\cos i\sin i di}{(\cos^2\theta-\cos^2 i)^{\frac{1}{2}}[\sin i+\alpha\cos i]^3}. \qquad (38)$$

This integral was evaluated numerically for several values of α.

Application to Venus Spectra

Figure 9 shows the observed Venus spectrum for 13 November 1962. This spectrum was chosen for discussion since it was taken at inferior conjunction when the signal-to-noise ratio was a maximum, and it is representative of all the spectra taken within a week of conjunction. The following discussion will be based on this particular spectrum, but the same conclusions are arrived at using any of the strong-signal spectra; indeed, even the strong spectra from the 1961 observations of Venus. The spectrum of Fig. 9 exhibits a significant "bump" on the low-frequency side (at about −9 cps), which consistently appeared in the observations for several weeks prior to conjunction, as pointed out by Goldstein and Carpenter (1963). These authors found that this anomaly moved to the left in the spectra as a function of date and have utilized this fact to estimate a rotation rate. Because of this anomaly, the high-frequency side of the spectra was used for this analysis, although each spectrum can be rendered symmetrical by simply "subtracting" the anomaly from the observed spectra. The dots in Fig. 9 are the observations, the solid line the best fit for $\alpha=0.04$ to the high-frequency side of the spectrum, and the dashed line the fit for $\alpha=0.12$. The curves were fitted slightly inside the observations to make a qualitative allowance for the ±0.5-cps jitter in the receiver. (The details of the spectral computations can be found in Muhleman 1963.) The $\alpha=0.04$ curve yields an $f_m=43$ cps, whereas that for $\alpha=0.12$ requires $f_m=17$ cps.

It can be seen from Fig. 9 that the $\alpha=0.04$ gives a superior fit to the data, but the difference may not be truly significant. However, the case $\alpha=0.12$ appears (at first) to be completely ruled out by the results from Fig. 8.

It is, of course, dangerous to use the α parameter determined from 68-cm observations in the calculations for the 12.5-cm spectra, since a definite wavelength-dependence of α has been established for the moon. If we assume the wavelength-dependence of Eq. (35) holds for Venus, the α value for 12.5 cm corresponding to $\alpha_{68}=0.04$ turns out to be $\alpha_{12.5}=0.13$. Consequently, we can only establish fairly large bounds on the total spectral width and, correspondingly, on the apparent Venusian rotation rate.

If we assume that the rotational axis of Venus is perpendicular to the Venusian orbit, the (slightly preferred) result for $\alpha=0.04$ and $f_m=43$ cps corresponds to a planetary rotational period of

225 days direct

or

180 days retrograde.

For $\alpha=0.12$ and $f_m=17$ cps, we get

570 days direct

or

250 days retrograde.

These results suggest three fairly distinct possibilities for the rotation of Venus: (1) the rotation is in synchronism with the Venusian orbital motion; (2) the intrinsic rotation is essentially zero with respect to inertial space; or (3) the rotation is retrograde and very slow.

Unfortunately, this method of analysis is unable to resolve the rotation problem any further and, more importantly for this paper, the 12.5-cm slope parameter remains relatively uncertain between the limits of 0.04 and 0.13 or 2.3 and 7.4 deg, respectively, although the

fit to the data is superior for the smaller value. However, the mathematical form of the scattering law appears to be well supported and the statistical parameter can be established when better pulse observations at a wavelength near 12.5 cm become available.

The rotational results obtained from the model using $\alpha = 0.13$ are in agreement with the conclusions reached by Goldstein and Carpenter (1963) based on several different approaches to the observations.

IV. CONCLUSIONS

The radar backscatter function has been shown to be equivalent to the probability distribution of the surface slopes. A particular backscatter function was derived from reasonable assumptions concerning the statistical properties of surface-height variations and horizontal scattering lengths. This function, which contains one parameter—the mean slope, was shown to fit all of the lunar radar observations available to the author within the accuracy of the measurements, by varying the single parameter. The effective mean slope was found to vary as the logarithm of the wavelength from 0.35 (20.1 deg) at 3.6 cm to 0.145 (8.3 deg) at 68 cm.

A backscatter function of the same form was found to fit the Venus radar spectral observations. When this function was applied to the 68-cm Venus pulse data, a mean slope of 0.04 to 0.05 (2.3 to 2.9 deg) was obtained. However, because pulse observations from Venus are available only at 68 cm, it is not possible to determine the wavelength-dependence of the measured mean slope and, consequently, α remains ambiguously connected with the Venusian rotation rate in the 12.5-cm spectra.

Application of this scattering theory to the 12.5-cm radar spectra has yielded a range of values for the effective mean slope (at 12.5 cm) from $\alpha = 0.04$ (2.3 deg) to $\alpha = 0.13$ (7.4 deg). A superior fit was obtained with the smaller values. In any case, the analysis shows that the Venus response to decimeter radar waves corresponds to a surface considerably more smooth than that of the moon. The establishment of the scattering law with correct parameters over a range of wavelengths will offer an important tool for the study of atmospheric and ionospheric limb darkening, surface-roughness anomalies, and the interpretation of the planetary surface emission in the radio domain.

The radar observations of Venus offer a unique opportunity to determine the rotation rate of the planet because the Venusian atmosphere is apparently transparent to high radar frequencies. The rotation rate may be easily determined once the total spectral width of a rotationally broadened radar echo can be accurately and unambiguously measured. However, the observations currently available are not of sufficient quality to reliably find the terminal points of the spectral wings in the background noise.

The method developed in this paper, utilizing the 68-cm Venus pulse data, has yielded a rotation rate of 4.4×10^{-7} rad/sec if the effective mean slope at 12.5 cm is taken equal to that from the 68-cm data. This value corresponds to a direct rotation of a 225-day period or a retrograde rotation with a 180-day period. When the effective mean-slope variation with wavelength given by lunar observations is used, a rotation rate of 2.0×10^{-7} rad/sec is computed, corresponding to the rotation periods of 570 days direct or 250 days retrograde.

Possibly the current deficiencies of the Venusian radar observations will be removed for the 1964 campaign on Venus, since the Jet Propulsion Laboratory's 12.5-cm radar has been improved by more than a factor of 10, and several other equally sensitive radars will be operated at several different wavelengths. When the new information becomes available, considerable progress will be made toward determining the quantitative characteristics of the Venusian surface and, perhaps, even the atmosphere.

ACKNOWLEDGMENTS

I am indebted to several colleagues for numerous discussions concerning the work presented here. In particular I wish to acknowledge the mathematical assistance on several points by Dr. J. Franklin of the California Institute of Technology and Dr. E. Posner of the Jet Propulsion Laboratory, as well as my colleagues through all of our radar astronomy efforts: Dr. R. Goldstein and R. L. Carpenter of the Jet Propulsion Laboratory.

REFERENCES

Evans, J. V., and Pettengill, G. H. 1963, *J. Geophys. Res.* **68**, 2, 423.
Goldstein, R. M., and Carpenter, R. L. 1963, *Science* **139**, 910.
Muhleman, D. O. 1961, *Astron. J.* **66**, 292.
Muhleman, D. O. 1963, "Radar Investigations of Venus," Ph.D. thesis, Harvard University, Cambridge, Massachusetts.
Pettengill, G. H. 1961, MIT course notes.
Pettit, E., and Nicholson, S. B. 1931, *Astrophys. J.* **71**, 102.
Smith, W. B. 1963, *Astron. J.* **68**, 15.
Victor, W. K., and Stevens, R. 1961, *Science* **134**, 46.

From the ASTRONOMICAL JOURNAL
69, No. 1, 1964, February—No. 1316
Printed in U. S. A.

Radar Observations of Venus at 38 Mc/sec

J. C. JAMES AND R. P. INGALLS
Lincoln Laboratory, Massachusetts Institute of Technology, Lexington, Massachusetts*

A series of radar measurements was made of the planet Venus at 38 Mc/sec during November and December 1962. The cross section most often measured when account was taken of Faraday rotation effects was the same as that measured at much higher frequencies; however, on some days the measured cross section was larger than usual. It is suggested that these increases in cross section were due to the appearance of solar plasma in interplanetary space or perhaps to changes on Venus which were not observed at higher frequencies.

I. EXPERIMENTAL PROCEDURE

IN November and December of 1962, radar observations of the planet Venus were made by the Lincoln Laboratory of the Massachusetts Institute of Technology. The radar system is located near El Campo, Texas, and is regularly used for solar radar studies. The transmitter produced a continuous power output of 490 kW at a frequency of 38.26 Mc/sec. The main antenna consisted of a horizontal array of half-wave dipoles linearly polarized in an east–west direction above a ground screen. For the Venus experiment, the antenna produced a fan-shaped beam having east–west dimensions of about 13 deg and north–south dimensions of about 2 deg. This antenna was used for both transmission and reception and a second array polarized in the north–south direction was used for reception only. Both antennas were transit instruments, but could be phased in declination. The gains above isotropic were about 30 dB for the main antenna and about 24 dB for the cross-polarized antenna. Because of the lower gain of the cross-polarized antenna, signals received on it were so buried in noise that the results were of little value other than showing that when the results of all the individual Venus experiments were combined, one-half the average echo energy was returned aligned with each of the two polarizations.

A series of five radar experiments was scheduled each day at a time when Venus was near the local meridian. For each experiment a transmitting period equal to the round-trip travel time of the signal to Venus was used. The transmitting period then was followed immediately by a receiving period of equal length. The round-trip time varied from 267 sec at the time of inferior conjunction on 13 November to 343 sec on 7 December when the experiments were terminated.

During the transmitting period, a pseudo-random binary code was used to switch the transmitted signal alternately between two frequencies separated by 16.7 kc/sec. This code was used to eliminate the range ambiguity which would result from a simple square-wave frequency-shift modulation. Basic coding periods of 1 and 2 sec were used. During reception, separate receiving channels were used for each of the two transmitted frequencies. Although the bandwidth of the signal reflected from Venus might be predicted to be of the order of 0.1 cps as a result of extrapolation of radar results at uhf (Pettengill 1962), a receiver bandwidth of 2 cps was chosen as it was known that spectral broadening due to scintillations in the ionosphere was of this order.

In order to keep the echo signal within ± 0.25 cps of the center of the 2-cps receiver bandwidth, it was necessary to continually tune the receivers according to a precomputed schedule of Doppler shifts. This schedule was determined from Doppler computations involving the rotation of the earth on its axis, the rotation of the earth about the earth–moon barycenter, and the relative motions of Venus and the earth–moon barycenter. The latter motions were based on Duncombes' corrected values which were made available on punched cards by the U. S. Naval Observatory in September 1962.

The tuning of the receivers to account for the changing Doppler shift was performed manually, but very carefully with a calibrated, frequency-stable circuit and a frequency monitor. The probability of an operator error was very small; however, such errors if incurred would have produced a smaller apparent cross section and a larger apparent Doppler spread.

The outputs of the two receiving channels were combined and processed in real time by analogue integration equipment. A delayed replica of the transmitted code was cross-correlated with the received signal in a manner similar to that used in the solar radar studies (Abel 1961). Analogue magnetic-tape recordings of the received signals were made during each experiment and were analyzed later to confirm that the width of the Doppler spectrum of the Venus echo was less than 2 cps.

The measured value of the received energy during each experiment was used to compute the apparent radar cross section of Venus. These cross-section computations involved the transmitted power, antenna gains, transmission-line losses, and target range. The most inaccurate of these parameters is antenna gain, which was determined by studies of radio stars and measurements made using a high-flying aircraft to be accurate within ± 0.5 dB at least along the antenna axis (Devane and Dion 1962). During each receiving period, analogue integrator circuits in the receiver obtained a measure of the ratio of echo-signal energy and the total measured

* Operated with support from the U. S. Army, Navy, and Air Force.

23

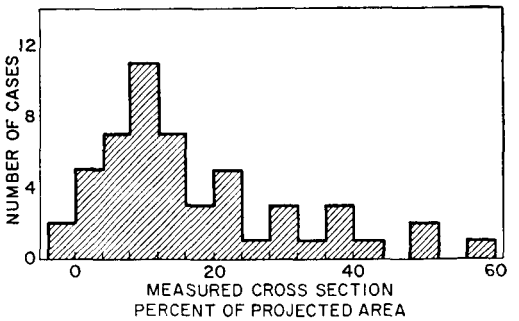

FIG. 1. Distribution of measured cross sections of Venus. Number of cases measured as a function of the cross section expressed as a percentage of the projected area of Venus.

energy. The predetection signal-to-noise ratio was less than unity and consequently postdetection integration was used to obtain a usable measurement. Most of the total energy was due to the background cosmic noise rather than system noise or received-signal energy and consequently an accurate measurement of cosmic noise power during the experimental period was required to make a signal-level calculation. The received cosmic-noise levels were determined by comparison with a calibrated-diode noise source and are believed to be accurate to within ± 0.5 dB. The antenna performance was monitored by a continual 24-h per day recording of cosmic noise.

II. OBSERVATIONS

The apparent cross section in square meters for each and every valid experiment is listed in Table I. The valid experiments are considered to be those for which the average product of transmitter and receiver gains was greater than one-fifth of the maximum gain product obtained at the zenith angles used during the experiment, and for which there were no obvious experimental difficulties. The apparent cross section was computed assuming that for a given experiment, one-half the echo energy was received by the main antenna and one-half by the cross-polarized array. This assumption is known to be true for the average of all the experiments, but is not necessarily true for any one given experiment. Standard deviations, expressed in the same units as the cross sections, are also listed in Table I. They represent the uncertainties in each cross section due to noise level during the signal-integration process.

The average value of the cross sections listed in Table I is 1.9×10^{13} m^2 when all the values are weighed according to the weighting factor shown in column four of Table I. This weighting factor is proportional to the expected (not actual) signal-to-noise ratio at the receiver input. The scatter of cross-section values about the mean is due in part to the assumption that one-half the echo energy was always received in a given polarization.

The projected area of Venus is 12.1×10^{13} m^2, which means that at 38 Mc/sec, the average observed cross section of Venus is about 15% of the projected area. At 440 and 2388 Mc/sec the radar cross section of Venus was measured to be about 1.3×10^{13} m^2, which is 11% of the projected area (Pettengill 1962; Victor and Stevens 1961).

The data of Table I are plotted in Fig. 1 as the number of cases of a given cross section vs that value of cross section. Each case corresponds to one experiment, which

TABLE I

Date 1962	Cross section 10^{12} m^2	One standard deviation 10^{12} m^2	Weighting factor
6 Nov	11.1	5.3	2.81
	−5.6	5.6	2.48
10 Nov	5.6	7.1	2.03
	11.6	4.9	3.03
11 Nov	14.7	6.1	2.46
	17.4	4.1	3.79
	9.5	4.8	3.05
12 Nov	45.3	9.8	1.61
	42.8	6.3	2.63
15 Nov	43.3	11.6	1.33
16 Nov	9.7	5.5	2.66
	27.9	4.7	3.39
17 Nov	58.9	6.0	2.94
20 Nov	7.2	4.6	3.17
21 Nov	10.5	5.7	2.53
22 Nov	11.3	6.9	2.09
23 Nov	14.5	5.1	2.89
24 Nov	25.6	5.4	2.85
	1.9	3.1	4.55
	18.1	4.2	3.63
26 Nov	36.5	6.0	2.70
	28.6	4.2	3.87
	37.0	4.7	3.54
	13.5	10.0	1.45
27 Nov	24.2	5.9	2.60
	16.8	4.3	3.53
	60.3	16.2	0.95
28 Nov	71.0	9.9	1.67
	46.9	5.7	2.99
29 Nov	7.9	10.5	1.37
	1.8	9.4	1.49
	27.0	17.1	0.85
30 Nov	9.6	7.1	2.02
	2.6	5.8	2.78
	8.6	5.3	2.72
	20.7	12.4	1.17
1 Dec	19.6	6.3	2.36
	−3.2	4.9	3.69
	51.2	5.3	3.27
	9.7	13.5	1.06
2 Dec	36.5	7.6	2.04
	10.4	4.2	3.51
	15.9	5.2	2.85
3 Dec	24.5	10.0	1.56
4 Dec	8.9	6.6	2.16
	8.2	4.5	3.17
	1.0	4.9	2.82
	13.9	15.6	0.91
6 Dec	15.6	8.3	1.76
	10.0	2.8	2.72
7 Dec	12.7	6.5	2.24
	1.2	8.3	1.67

consisted of one transmitting and one receiving period. Each value of cross section is the average value observed during that experiment and is plotted in Fig. 1 as percent of the projected area of Venus. The histogram of Fig. 1 shows that the cross section most often measured is about 10% of the projected area, which is very near the value measured at higher frequencies. The lack of gain in the orthogonal antenna prevented the accurate measurement of the distribution of energy between the two linear receiving polarizations. It was thus impossible to determine the cross section definitely for a given experiment although any single cross section in Fig. 1 may be at most twice as large as the true cross section because of the polarization uncertainty.

III. DISCUSSION

The data of Fig. 1 can be divided into two groups: (1) those cross sections that are less than 20% and which as a group imply an average Venus cross section of 10%, and (2) those anomalous cases which are significantly greater than 20%. If the echo signal were linearly polarized and the polarization angle changed 180 deg or more during a single experiment, then the shape of this first group would be very peaked at 10%. If the polarization-angle change were always much less than 90 deg, the shape would be more uniform, but peaked somewhat near zero and 20%. The observed distribution of cross sections for the first group indicates that the plane of polarization of the echo signal often does change somewhat during a single experiment, but the magnitude of the change is typically less than 90 deg.

The anomalous high cross sections of the second group could be due to one or more causes. One possibility is that Venus has an ionosphere that is becoming critically dense at 38 Mc/sec. The required ionization density is about 2×10^7 electrons/cm^3, which is about two orders of magnitude greater than the density of the earth's ionosphere. Danilov (1962) has computed that the ionization density on the sunlit side of Venus should be about 10^6 electrons/cm^3 if carbon dioxide were the only constituent and solar ultraviolet were the only ionizing radiation. Another possible explanation for the larger cross sections is some particular type of surface material or surface feature such as a layer of dielectric material covering a subsurface material having a larger dielectric constant. The top layer would have a depth which is large compared with the 440 Mc/sec wavelength and small compared with the 38 Mc/sec wavelength. If this depth varied over the surface of the planet, a change in cross section at 38 Mc/sec might be expected from day to day as the planet rotated. This effect may be the cause of the large range of cross-section values listed in Table I. It is also conceivable that streams of solar plasma could focus radio energy onto Venus. Such focusing action, if present, would be much stronger at lower frequencies. If these streams were generally aligned in the direction of earth and Venus, their tendency would be to increase the amount of signal energy striking Venus more often than to decrease this energy. This effect, if real, should also be more pronounced at some times than at others, depending on solar activity. A stream of plasma lying parallel and adjacent to a line from earth to Venus and having an electron density of the order of 10^3 to 10^4/cm^3 would be sufficient to produce a pronounced focusing effect.

The amount of Faraday rotation of the radar signal in the ionosphere of Venus is inversely proportional to the square of the frequency. For this reason 38 Mc/sec is more sensitive than higher frequencies to the presence of a magneto-ionic medium. There were no Faraday effects observed in the present experiment, however, that could not be attributed to the earth's ionosphere. Radar experiments on the moon performed with the El Campo radar system at 38 Mc/sec have yielded Faraday effects equivalent to those of the Venus echo. The rate of rotation of the polarization of the lunar echo is attributed to the earth's ionosphere and varied between 90 deg per 5 min or less at sundown to 90 deg per hour at midnight. It should be noted that a rough target beneath a magnetoionic medium should not return a composite echo which was linearly polarized because the echo would consist of signal components that were not in phase and that had undergone various degrees of Faraday rotation. If Venus were a rough target so that energy components were returned from various portions of the disk and there were no Faraday rotation, the composite echo would still likely be linearly polarized; however, if the radar energy to and from these various reflecting centers underwent different amounts of Faraday rotation, the composite echo would be elliptically polarized. It is possible that the distribution of cross sections between 0 and 20% in Fig. 1 is due to Faraday effects on Venus, but it seems more reasonable to attribute this small effect to the earth's ionosphere.

The significant results of this experiment are that the average Venus cross section was greater than that measured at higher frequencies and that the observed cross section changed from day to day by an amount greater than was expected on the basis of Faraday rotation alone. The results suggest that the most probable value of cross section is the same as the cross sections measured at 440 and 2388 Mc/sec, but that spurious effects at times cause the apparent cross section to be several times larger. The observed spurious effects are not explained, but three possible causes are suggested. These suggestions are (1) that Venus may have an ionosphere which in spots is critically dense at 38 Mc/sec, (2) that the surface of Venus may be stratified with an underlying layer having a larger dielectric constant, and (3) that at times in the earth–Venus interspace there may be solar plasma of sufficient density and orientation to cause a focusing of radio energy onto Venus.

ACKNOWLEDGMENTS

The authors would like to acknowledge the assistance of other members of the Lincoln Laboratory in helping construct equipment and plan and conduct the experiment. In particular should be mentioned J. H. Chisholm, L. P. Rainville, A. W. Bishop, W. Rutkowski, and J. B. Steele.

REFERENCES

Abel W. G., *et al.* 1961, *J. Geophys. Res.* **66**, 4303.
Danilov, A. D. 1962, "Model of Venus and Mars Ionospheres," Paper presented to Cospar Conference, Washington, D. C., May, 1962.
Devane, M. E., and Dion, A. R. 1962, "The El Campo Solar Radar Antenna," Tech. Rept. No. 276, Lincoln Laboratory, Massachusetts Institute of Technology, Cambridge, 17 August 1962.
Pettengill, G. H., *et al.* 1962, *Astron. J.* **67**, 181.
Victor, W. K., and Stevens, R. 1961, *Science* **134**, 46.

26

TABLE I. Jicamarca radar parameters.

Transmitter	
Peak power	4×10^6 W
Frequency	49.92 Mc/sec
Pulse-repetition frequency	20 cps
Pulse length (as used for Venus experiment)	3 msec and 500 μsec interlaced with gap at 1-sec intervals
Antenna	
Area	84 000 m²
Gain over isotropic radiator appropriate to this experiment (see text)	40 dB
Receiver	
Frequency	49.92 Mc/sec minus predicted Doppler
Noise figure	1.5
Sky-brightness temperature at time of experiment	~6000°K
Predetection bandwidths	300 cps 3 kc/sec
Frequency stability	2 parts in 10^9
Timing accuracy (range gates and tape recorder)	parts in 10^6

each day to the declination of Venus. A slight additional north–south adjustment was made by phase adjustment of the quarters. To compensate for earth's rotation during the round-trip time of the radar pulse, phasing by quarters was also programmed to affect a shift 1.3 deg west at the time of antenna-switchover from transmission to reception. A different phasing arrangement was used each day. The realized gain over the 10-day period varied from 39.4 to 40.6 dB as compared with a gain of 42.6 dB when the antenna is phased on axis (Bowles, Ochs, and Green 1962). Circular polarization was employed, thereby eliminating long-period fading from Faraday rotation.

The transmitted frequency was always 49.92 Mc/sec, stable to roughly 2 parts in 10^9. The receiver was tuned each day to a frequency below that of the transmitter by a precisely known amount and as near as possible to the predicted Doppler shift. All timing and gating pulses, as well as the transmitter-pulse repetition frequency and the Doppler offset frequency, were derived from a second highly stable crystal oscillator operating at 1 Mc/sec. The reference frequency for two orthogonal phase detectors used to preserve both the even and odd components of the complete received spectrum was derived from the same crystal oscillator feeding the transmitter by using a balanced modulator. Data were recorded in analogue form along with all timing and gating pulses on magnetic tape at 60 in./sec. Each day's run consisted of the entire transmitting period (4 min), the entire receiving period (4 min), plus several minutes of noise for comparison purposes. In principle, radar-echo delay time and Doppler information can be recovered from the tapes to an accuracy of a few parts in 10^7. We believe our present absolute echo delay

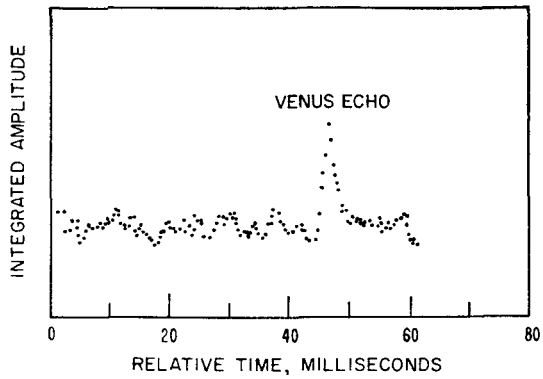

FIG. 1. Integrator readout, 3-msec echo. Integration time 12.5 sec, range boxes spaced 500 μsec apart.

time estimates are good to a few parts in 10^6 (±1 msec in 300 sec) using only the facilities available to us in Peru. For example, using the 3-msec pulse data at 15 h 12.5 m UT on 4 December, we observed an echo delay time of 326.704 ± 0.001 sec as compared to a round-trip time of 326.7036 sec derived from Duncombe's orbit of Venus. These are good enough to allow various echo characteristics such as fading and relative Doppler shift to be assessed, but not sufficiently accurate to study the effect of the interplanetary medium on propagation delay or absolute Doppler shift.

Radar-echo delay timing was facilitated in this experiment by the simple expedient of suppressing the transmission of every tenth 3-msec pulse. The returning pulse train then showed gaps at 1-sec intervals, very little integration being required to locate the gap within 0.1 sec with the favorable signal-to-noise ratio available. Since even a crude ephemeris can easily resolve the 1-sec echo delay time ambiguity, absolute range estimates could be made without the complexity of transmitting a pseudorandom code sequence. Furthermore, the Doppler measurements described in Sec. V could be easily carried out on the same data. With the echo delay time determined to within 0.1 sec for a particular section of data, integration was then

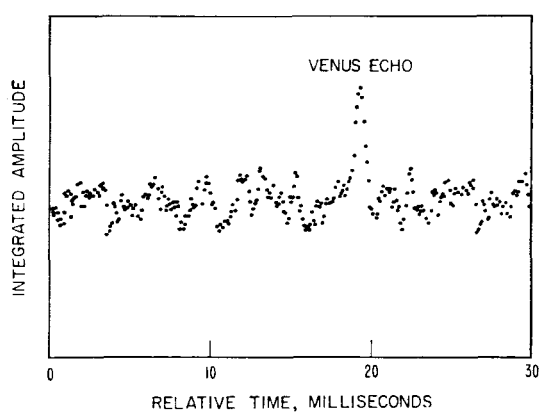

FIG. 2. Integrator readout, 0.5-msec echo. Integration time 1 min, range boxes spaced 100 μsec.

From the ASTRONOMICAL JOURNAL
69, No. 1, 1964, February—No. 1316
Printed in U. S. A.

Radar Echoes from Venus at 50 Mc/sec

W. K. KLEMPERER, G. R. OCHS, AND K. L. BOWLES
*Jicamarca Radar Observatory, Apartado 3747, Lima, Peru**

Radar echoes were obtained at 50 Mc/sec from Venus over a nine-day period late in 1962 using the 84 000-m² antenna array and 4-MW transmitter of the Jicamarca Radar Observatory in Peru. During local meridian transit of the planet on 2 December 1962 individual echoes were occasionally in excess of three times the received noise power. This favorably high signal-to-noise ratio permitted observation of the libration-fading and other short-term characteristics of Venus echoes. From comparison of the echo power, using long and short pulses, one finds that almost all the power received is returned from an area less than 1/40 of the visible disk of Venus. Accordingly, Venus is considerably smoother than the moon at radio wavelengths. The received-frequency power spectrum appears narrower than 0.03 cps for short periods, which should permit coherent integration to be carried out for 5 to 10 sec. A rotation period in the range 180 to 280 days would agree with the libration-fading observations.

I. INTRODUCTION

THE Jicamarca Radar Observatory, located near Lima, Peru, is one of the largest of several recent radar installations of extremely high sensitivity designed to acquire upper atmospheric electron-density profiles by the incoherent scatter technique. The experiment to be described in this paper was carried out from 28 November to 7 December, 1962, during which period the individual echoes from Venus of our 3-msec-transmitted pulses were often well above the received-noise level.

There are some rather severe limitations inherent in the use of a large, fixed antenna (such as the one at Jicamarca) for planetary radar astronomy. Only a limited range of declination can be accommodated before antenna efficiency drops off markedly. This meant that our radar studies of Venus in 1962 could not commence until almost one month after closest approach, and the experiment cannot be repeated until January 1966. Similar limitations in hour angle preclude the use of this antenna on targets distant by more than 10 light-minutes. Furthermore, only about 3 min of data could be obtained each day, as means for tracking the planet in hour angle were not available. Accordingly, the total amount of data obtained comprises only some 30 min, a rather short sample compared to the almost 12 h runs possible for months at a time with fully steerable paraboloids.

In spite of such limitations, the comfortably high signal-to-noise ratio obtained permitted observation of some interesting phenomena which may have escaped detection by radars of less sensitivity. In particular, Venus' libration fading can only be observed if the integration time required does not greatly exceed the typical fading period. We shall describe some of these short-term echo characteristics in the following sections.

II. DESCRIPTION OF THE EXPERIMENT

The parameters of the radar system used to obtain echoes from Venus are listed in Table I.

The antenna (Ochs 1963) is an array of 9216 crossed dipoles over a reflecting screen, 48 wavelengths on a side, and covers an area of some 22 acres. The array is composed of 64 identical modules whose relative phases can be changed by inserting cables of differing lengths at their point of connection to the branching feed system. In this manner the main lobe of the antenna may be deviated up to $3\frac{1}{2}$ deg from its main axis at declination -12.9 deg. A complete direction change by this means requires approximately 2 h. Since the inputs to each quarter of the antenna are available at the building, a more rapid but very limited adjustment may be made there. For the Venus observations, the phasing of the 64 modules was adjusted, with the fixed-length cables available, to point the antenna as nearly as possible

* A cooperative project of the Central Radio Propagation Laboratory, National Bureau of Standards, Boulder, Colorado, and the Instituto Geofisico del Perú, Lima, Perú.

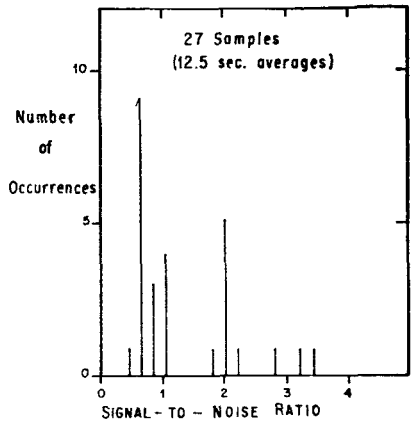

FIG. 3. Histogram of echo strength.

performed using a 100-msec time-base sampled every 500 μsec. An example of the integrator contents after 125 sweeps (12.5 sec) is shown in Fig. 1. Echoes of the 0.5-msec pulses (which are sent out 0.05 sec before the 3-msec pulses) are greatly attenuated in the 300-cps filter used and hence are not visible on the display. From data such as those shown in Fig. 1 the absolute echo delay time to Venus at a particular time can be determined within 1 msec.

Considerably higher accuracy is attainable in principle from the short-pulse data. Figure 2 shows the recovery from below-noise level of the echoes of our 500-μsec pulses. The same integrator was used for a longer period (1 min) with the range boxes spaced 100 μsec.

In practice, the longer integration time and the fivefold increase in the number of gating pulses required greatly complicate the problem. The gating pulses recorded along with the data each day are like a picket fence, motionless in Venus' frame of reference to the same degree of accuracy to which the Doppler shift has been set (as predicted by a good ephemeris). Absolute echo delay time determination consists of counting and keeping track of all the pickets in the fence; i.e., replacing those gating pulses missing due to tape dropouts during playback of the recorded data. This can be done, but is much more difficult to carry out than relative timing from an arbitrary point near Venus. None of the topics of the following sections require absolute range or Doppler information, but it is planned to attempt such determinations at a later date.

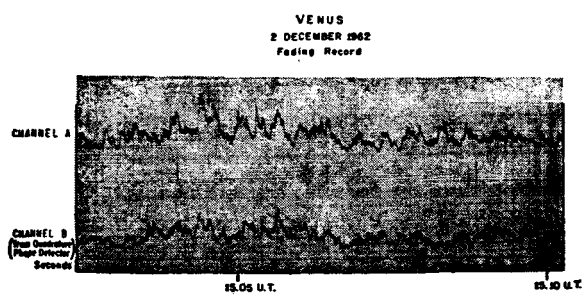

FIG. 4. Running average of echo strength (1-sec time constant) from each phase-detector.

III. FADING CHARACTERISTICS

Echo strength (or more precisely, the observed signal-to-noise ratio) was found to vary markedly for different 12.5-sec samples such as the one shown in Fig. 1. A histogram, Fig. 3, gives an indication of the spread of values found in 27 consecutive samples of the data of 2 December 1962. The temporal variation of echo strength is illustrated by the records of Fig. 4, which were obtained by squaring the outputs of the two phase-detector channels. The noise on the two channels is uncorrelated, while changes in signal level and strong peaks are fairly well correlated. The typical fading period is on the order of 5 to 10 sec. The fading is deep rather than shallow, as would be the case for a steady reflected signal.

The terrestrial ionosphere causes some intensity variations or scintillations of the received signal, but these are normally less than $\pm 20\%$ and fairly rapid at our latitude. The deep fading observed cannot be attributed to local ionospheric effects. We observe fading of lunar echoes, which is very similar in character but at a considerably faster rate (normally 0.5 to 1 cps). This is known as libration fading and the echo amplitudes are Rayleigh-distributed (Browne, Evans, Hargreaves, and Murray 1956). Evidently, the echo-strength variations we observe in Fig. 4 are also libration fading as caused by the relative motions of the earth and Venus.

To prove that this fading cannot be attributed to noise fluctuations alone, we examined the statistical distribution of power in ten equally spaced levels of (a) noise and (b) signal plus noise (echo) from the same tape. Normalized probability density distributions were constructed for each case. The theoretical distribution for the output of a square-law detector subjected to band-limited white noise is of the form

$$dP = \exp\{-Y\}dY,$$

where Y is the detected output power and P is the probability $0 \leq P \leq 1$ that Y exceeds Y_0. In Fig. 5 we show normalized data for cases (a) and (b), along with the theoretical curve. Plus and minus two standard deviations are indicated for each point. The data of Fig. 5(a) exhibit an excellent fit to the exponential law as would be expected of a pure-noise record. The data in Fig. 5(b), on the other hand, deviate from the theoretical curve by more than two standard deviations in nine out of ten power levels. Although this analysis strongly suggests the existence of a component or components other than noise alone, there are unfortunately insufficient data to identify the scattering law for Venus.

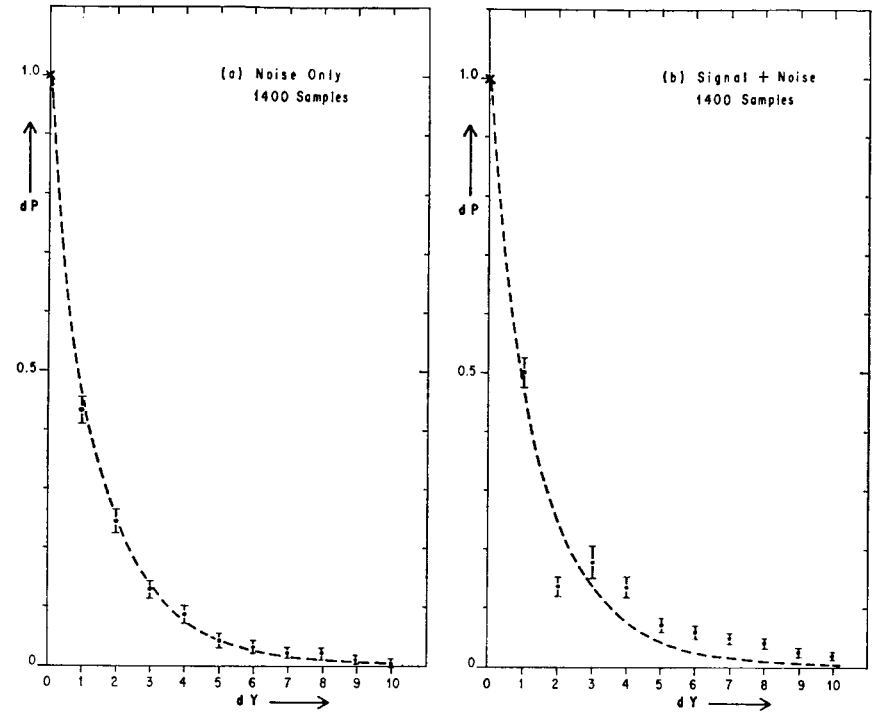

FIG. 5. Probability density distributions, 2½ December 1962 data.

Venus' libration fading complicates the problem of estimating the radar cross section σ. By definition

$$\sigma = g\rho\pi R^2,$$

where g is the directivity of the target and ρ is the mean surface reflectivity. Adopting the value $R = 6200$ km for Venus' radius, we find that the product $g\rho$ is somewhat less than 0.2, taking all the data into account. One may expect occasional values as great as 0.6 over a 12-sec period at our operating wavelength.

IV. ESTIMATES OF SURFACE ROUGHNESS

The 20-pulse/sec repetitive sequence transmitted, with 3-msec and 0.5-msec pulses interlaced, provided a convenient means for estimating Venus' surface roughness. Integration times were chosen sufficiently long to yield a reliable estimate of echo strength for the 0.5-msec pulses (usually 1 min). The signal-to-noise ratio obtained for the short-pulse echo was then compared with that for the long-pulse echo over the same interval and with due allowance for the different predetection bandwidth used. Comparisons made in this way have agreed to within ± 0.5 dB. Accordingly, almost all the power returned comes from a radar depth of 75 km (500 μsec) or less. Using a value for Venus' radius of $R = 5200$ km and the geometrical relationship

$$Z \cong (2Rx)^{\frac{1}{2}},$$

where $x = 75$ km, we obtain for Z, the radius of the zone from which most of the power is returned, a value of less than 1000 km. Therefore, the echoes come from an area less than approximately 1/40 of the visible disk of Venus.

At our operating wavelength, 6 m, most of the power in a long pulse reflected from the moon is returned from an area of not much less than 1/20 of the visible disk. Figure 6 shows on the same scale the average pulse shape returned by the moon and Venus for transmitted 500-μsec pulses and identical receiving equipment. This demonstrates that the surface of Venus is considerably smoother than that of the moon at meter wavelengths.

V. DOPPLER SHIFT MEASUREMENTS

The frequency of the 49.92-Mc/sec radar signal reflected from Venus was found to be Doppler-shifted by

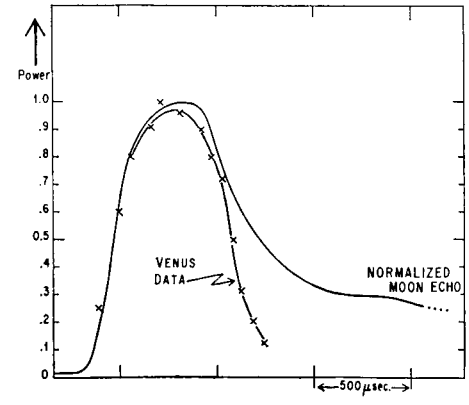

FIG. 6. Comparison of moon echo and Venus echo, 0.5-msec transmitter pulses, identical equipment.

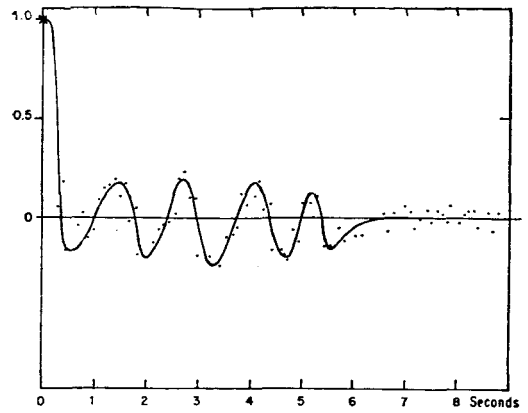

FIG. 7. Autocorrelation of data for Doppler shift and coherence time estimation. Lags spaced 0.1 sec apart.

-2.3 kc/sec to -3.3 kc/sec during the course of the experiment from 28 November to 7 December. The Doppler shift increased at an average rate of about 0.7 cps/min in agreement with the observed range rate and with ephemeris predictions. However, it was noted that at times of high signal level separated by as little as 10 sec, the Doppler frequency often changed by more than 0.1 cps in either direction.

A preliminary investigation of these short-term frequency variations was carried out late in 1962 using an analogue multiplier. The method employed was simply to record the beat-frequency between a stable oscillator and the filtered phase-detected output of the receiver. In this way the changes in frequency of the received signal could be observed. By utilizing reference frequencies recorded along with the data at the time of the experiment, the accuracy of translation of the Doppler-shifted 49.92-Mc/sec received signal could be checked. In this way, one could prove that the short-term frequency shifts were real and not introduced by the equipment. More accurate estimates of these frequency shifts have now been obtained by computing normalized autocorrelation functions, defined as

$$\rho(\tau)=\overline{f(t+\tau)}/\overline{f^2(t)},$$

where the phase-detector output $f(t)$ is delayed $0\leq\tau\leq 12.8$ sec. A typical example of $\rho(\tau)$ is given in Fig. 7. The oscillations shown were not significantly changed by varying the length of record analyzed, and noise from non-echo portions of the tape subjected to the same analysis showed no periodic oscillations whatever.

The coherence time (or phase stability) of the signal reflected from Venus may be estimated from Fig. 7 by noting the time required for the oscillations in $\rho(\tau)$ to die out. These are occasionally found to persist out to 10 sec, particularly at times when the signal is fading slowly. With phase stability over such a long period, coherent integration might be employed to great advantage for highly accurate ranging and Doppler measurements. The power spectrum $P(\omega)$ can be obtained from the autocorrelation function $\rho(\tau)$ by a Fourier transform (Wiener–Khintchine theorem). Without going to the trouble, one may estimate the main features of the frequency power spectrum for the example in Fig. 7 by inspection. Oscillations having a recurrence period of approximately 1.6 sec are seen to persist out to 6 sec. Using the relationship

$$\rho(\tau)=\int_{-\infty}^{\infty} P(\omega)\cos\omega\tau d\omega\cong A\cos(\omega_1\tau),$$

where $A\cong 0.2$ and is a constant depending on the signal-to-noise ratio, and $P(\omega)$ can be approximated by a narrow spike whose width can be estimated from the 6-sec coherence time. The half-width (3 dB) is less than the reciprocal of π times twice the coherence time or about 0.025 cps. The value for ω is approximately 4 rad/sec as obtained from the 1.6-sec recurrence period. This leads to the conclusion that the spectrum $P(\omega)$ is a narrow spike displaced from the reference frequency by 0.63 cps. The frequency resolution obtainable with this technique is, of course, far superior to that achieved earlier using the analogue multiplier. Other data analyzed show greater and smaller displacements in frequency, a typical frequency separation between consecutive samples being 0.06 cps, with occasional differences as great as 0.2 cps. We have estimated the possible influence of ionospheric scintillations in this regard and find that the "Doppler" broadening of the spectrum from this source at our station should be roughly 1/10 as great as actually observed. Similar effects are noted when lunar radar echoes are subjected to the same analysis. At our frequency, typical excursions about the mean lunar Doppler shift are ± 0.2 cps in a few seconds. This can be related to the moon's apparent libration and is caused by slow changes in the position and strength of each of the various scattering centers on the lunar surface. In contrast we believe that the slower changes observed in short-term Doppler spectra from Venus are evidence for the wandering of the principal reflection point over the surface of Venus.

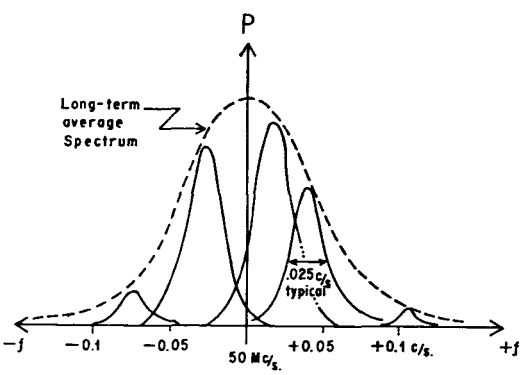

FIG. 8. Schematic representation of Venus power spectrum as a summation of short-term spectra.

It is interesting to compare our short-term data with the Doppler spectra obtained at higher frequencies with hour-long integration times (Malling and Golomb 1961; Goldstein and Carpenter 1963; Smith 1963). The half-width (3 dB) of the power spectrum has been estimated as 0.6 to 1 cps at 440 Mc/sec and about 9 cps at 2388 Mc/sec. This would scale down to an approximately 0.1-cps width at our frequency if the same scattering law were to apply, and would be somewhat less if Venus' surface looks smoother under longer wavelength illumination. Figure 8 shows schematically the expected long-term average spectrum at 50 Mc/sec (dotted) and the way it is built up from a summation of consecutive short-term spectra of the type we observe.

VI. DISCUSSION

Because of equipment limitations, neither accurate radar-echo delay timing (down to fractions of the 500-μsec pulse length) nor absolute Doppler measurements making use of coherent integration have as yet been carried out. There is, of course, considerable interest in making absolute measurements of high accuracy at as low a frequency as 50 Mc/sec, where propagation effects in the interplanetary medium become important. An excess delay of approximately 0.1 msec over that time required for a light pulse can be expected for a 50-Mc/sec radar pulse in traversing the ionosphere of the earth and Venus and the interplanetary medium. It is unlikely that the radar echoes obtained at 50 Mc/sec are reflections from Venus' ionosphere. The model proposed by Danilov (1962) predicts a maximum electron density of 10^6 electrons /cm^2 at about 100 km above the surface. An electron density more than thirty times as great would be required to achieve overdense reflections at 50 Mc/sec. The density gradient would have to be extremely steep to reflect the 500-μsec pulse with as little distortion as observed. This is highly unlikely for any reasonable model in diffusive equilibrium. The recent measurements of Venus' weak magnetic field (Smith, Davis, and Sonnett 1963) do not appear to predict any sizable magnetic control of the ionization. Furthermore, the echoes obtained near closest approach of the planet are all from Venus' dark side and it is difficult to conceive how a dense ionosphere could be maintained in the absence of sunlight.

The somewhat thorny problem of estimating surface roughness from radar data has been attacked by several competent theoreticians (Hargreaves 1959; Daniels 1961; Winter 1962) and has been reviewed recently (for the lunar case) by J. V. Evans (1962). Two important quantities for the statistical approach are (1) the operating wavelength, as no surface details smaller than roughly a wavelength are visible a short distance from the surface, and (2) the size of a Fresnel zone (which for a 50-Mc/sec radar and a plane target at the range of Venus is about 100 km^2). The roughness of Venus' surface is characterized by an angular power spectrum whose width is determined by both the surface gradient averaged over a few Fresnel zones, as well as by diffraction within these areas by smaller-scale irregularities down to about one wavelength in size.

In view of the narrow-band, almost "glint-like" character of the individual maxima of the Venus echoes, it is perhaps useful to speculate on the mechanism of their production. One would expect to receive individual maxima of radar echoes from a nearly spherical surface constructed of many large smooth surfaces, as from a many-faceted geodesic sphere. Each echo would arise when the corresponding individual plane surfaces were oriented essentially perpendicular to the path of propagation, thus satisfying the condition for specular reflection. Now the surface of Venus is certainly not like a geodesic sphere, yet it might be composed, on the average, of large, nearly flat valleys. Were this true, one might expect to find, at most times, only one large surface so oriented with respect to the earth as to produce a strong radar echo. The "valleys" not being perfectly flat, one might expect the echoes to arise, on the average, from a distributed area having some small fraction of the radius of the planet. This would account for the distribution of Doppler-shifted frequencies. The lack of interference, at most times, among several of these "glints" could account for the relatively long coherence times of the individual bursts of signal relative to the width of the distribution of frequencies observed during the complete observing period. Although the amplitude-distribution measurements do not prove that this conjecture is correct, the apparent departure of these results from the distribution expected of a collection of random scatterers may be consistent with the "glints" hypothesis.

The remarkably slow libration fading observed, no more than about 0.1 cps, indicates that the rotation of Venus with respect to the radar line of sight must have been very slow during the course of the experiment. Simple geometrical considerations show that the maximum fading frequency f_{max} can be related to Z, the radius of the reflecting zone, and L, the apparent rotation in radians per second, by the formula

$$f_{max} = 2ZL/\lambda,$$

where λ is the operating wavelength (6 m). The apparent rotation L is the projection onto a plane perpendicular to the line of sight of a number of components, not all of them important. These can be listed as follows:

(1) A diurnal component due to the earth's rotation. This is approximately 10^{-8} rad/sec and always positive at transit.

(2) A component (libration in longitude) due to Venus' passing the earth in space. This is greatest at closest approach, but becomes vanishingly small at

the two "stationary" points of Venus' orbit, one of which occurred 1 December 20 h UT and hence can be neglected for 2 December observations.

(3) A component due to the 3.4-deg tilt of Venus' orbit relative to the ecliptic. The magnitude of this component can be estimated from the daily change in Venus' apparent declination. It amounted to less than 10^{-11} rad/sec during the course of the experiment.

(4) A component due to an inclination of Venus' axis of rotation to the plane of its orbit (unknown).

(5) The component due to Venus' rotation. For synchronous rotation, a value of $+3.26\times10^{-7}$ rad/sec is appropriate if it is assumed that the inclination (4 above) is zero.

Adopting a value for L total of 3.3×10^{-7} (appropriate for synchronous rotation and zero inclination) and with $Z\cong10^{6}$ m as the radius of the zone from which most of the power is returned, the predicted maximum libration-fading rate is then slightly greater than 10^{-1} cps, which is in excellent agreement with the observed rate. The sense of rotation cannot be determined without observing at more points of the orbit.

VII. SUMMARY

An investigation of the characteristics of radar echoes from Venus at 50 Mc/sec has yielded the following information:

(1) Intensity variations in the reflected signals have been identified as libration fading. The fading is considerably slower than the usual libration fading observed for lunar echoes.

(2) A comparison of the power received using long and short pulses shows that almost all the power received is returned from an area less than 1/40 of the visible disk of Venus at 50 Mc/sec.

(3) Small changes in Doppler shift, which appear to be correlated with libration fading, show good phase stability for periods as long as 10 sec. The short-term power spectrum is considerably narrower than the average which would be obtained by integration for several hours. This should allow absolute Doppler and ranging experiments of high accuracy to be carried out, yielding information about the interplanetary medium and the ionosphere of Venus.

(4) The rotation period for Venus appears to be greater than 180 but less than 280 days as deduced from the observed fading rate.

ACKNOWLEDGMENTS

We wish to thank members of the Staff of the Jicamarca Radar Observatory and the Instituto Geofísico del Perú, especially A. A. Giesecke, Jr., for their contributions to the success of the Venus experiment. J. L. Green was largely responsible for the faultless performance of the transmitter. We wish to acknowledge the kind assistance of G. H. Pettengill (formerly of MIT Lincoln Laboratory) in providing us with a highly accurate ephemeris. We thank F. D. Drake of NRAO for first pointing out that Venus' declination near closest approach was suitable for the Jicamarca radar. We also wish to thank Robert Lawrence and others at the NBS Boulder Laboratories for their interest and advice.

REFERENCES

Bowles, K. L., Ochs, G. R., and Green, J. L. 1962, *J. Res. Natl. Bur. Stds.* **66D**, 395.

Browne, I. C., Evans, J. V., Hargreaves, J. K., and Murray, W. A. S. 1956, *Proc. Phys. Soc.* (*London*) **B69**, 901.

Daniels, F. B. 1961, *J. Geophys. Res.* **66**, 1781.

Danilov, A. D. 1962, *Model of Venus and Mars Ionosphere*, Paper No. 3.17 presented at 3rd International Space Science Symposium (COSPAR), Washington, D. C., May 1–9.

Evans, J. V. 1962, "Radio Echo Studies of the Moon," Chap. 12 of *Physics and Astronomy of the Moon*, edited by Z. Kopal (Academic Press Inc., New York).

Goldstein, R. M. and Carpenter, R. L. 1963, *Science* **139**, 910.

Gordon, W. E. 1958, *Proc. IRE* **36**, 1205.

Hargreaves, J. K. 1959, *Proc. Phys. Soc.* (*London*) **B73**, 536.

Malling, L. R., and Golomb, S. W. 1961, *British Inst. Radio Engrs.*, October, 297.

Ochs, G. R. 1963, "The Large 50 Mc/s Dipole Array at Jicamarca Radio Observatory," *1963 PTGAP International Symposium Digest*, pp. 237–241.

Smith, E. J., Davis, L., Jr., and Sonnett, C. P. 1963, *Science* **139**, 909.

Smith, W. B. 1963, *Astron. J.* **68**, 15.

Winter, D. F. 1962, *J. Res. Natl. Bur. Stds.* **64D**, 215.

From the ASTRONOMICAL JOURNAL
69, No. 1, 1964, February—No. 1316
Printed in U. S. A.

Mariner 2 Microwave Radiometer Experiment and Results

F. T. BARATH
Jet Propulsion Laboratory, California Institute of Technology, Pasadena, California

A. H. BARRETT
Research Laboratory of Electronics, Massachusetts Institute of Technology, Cambridge, Massachusetts

J. COPELAND
Ewen Knight Corporation, Natick, Massachusetts

D. E. JONES
Jet Propulsion Laboratory and Brigham Young University, Provo, Utah

AND

A. E. LILLEY
Harvard College Observatory, Cambridge, Massachusetts

On 14 December 1962 the Mariner 2 spacecraft passed within 34 350 km of the surface of Venus after a flight of 109.5 days from earth. During the passage, a microwave radiometer experiment abroad the spacecraft successfully measured emission from the planet at wavelengths of 13.5 and 19 mm on three scans of the planetary disk. The areal resolution was high, the half-power beamwidths of the antennas being approximately 1/6 of the angle subtended by the Venusian disk. The purpose of this paper is to: (1) Review the background and objectives of the experiment and the design constraints imposed by spacecraft technology. (2) Provide an engineering description of the experiment. (3) Describe the in-flight performance of the equipment and its effect on the planetary results. (4) Present the microwave data acquired. (5) Present an analysis and interpretation of the data and the conclusions drawn therefrom. The results provide quantitative data for microwave limb darkening of Venus and thus give strong support to that class of model atmospheres which have high temperatures originating at, or near, the surface of the planet.

I. INTRODUCTION

MANY ground-based observations of radio emission from the planet Venus made since 1956 have shown that the brightness temperature of the planet is approximately 600°K for wavelengths of 3 cm and longer. On the other hand, for wavelengths of 8 and 4 mm, a brightness temperature of 350° to 400°K is appropriate. These discoveries have stimulated many observational and theoretical investigations related to Venus, directed principally toward defining the origin of the high-temperature emission. Most of the theoretical discussions have either assumed or tried to justify a high-temperature surface as the origin of the radio emission (Barrett 1961; Öpik 1961; Sagan 1962), but alternative explanations have suggested that the origin is thermal emission from the ionosphere (Jones 1961), electrical discharges in the atmosphere (Tolbert and Straiton 1962), or plasma instabilities in the ionosphere (Scharf 1963). A recent review of these topics has been published by Roberts (1963). The use of satellite and spacecraft radio telescopes in planetary radio astronomy problems with emphasis on Venus has been presented by Lilley (1962).

In 1960, when the Mariner spacecraft design and experiment selection was begun, a microwave radiometric experiment was proposed to provide definitive answers to some of the puzzling problems raised by the radio observations of Venus. The spacecraft was designated Mariner A and was to be launched by the Atlas-Centaur combination of launch vehicles. The major objectives of the Mariner A microwave experiment were:

(1) To establish the place of origin and the radiation mechanism responsible for the centimeter and millimeter wave emission spectrum.

(2) To investigate the variations in intensity and spectrum from different positions of the planetary disk, including the daylight and dark hemispheres, and in the region of the terminator.

(3) To place upper limits on the effect of water vapor on the microwave spectrum.

To satisfy these objectives, a radiometer experiment was designed which was to measure planetary radiation at wavelengths of 19.0, 13.5, 8.0, and 4.0 mm, and the design and construction of flight units was begun. Further details of the experiment, its objectives, and its ability to distinguish various mechanisms of planetary radiation have been documented elsewhere (Barrett, Copeland, Jones, and Lilley 1961).

By mid-1961, it became apparent that the Atlas-Centaur rocket combination would not be sufficiently developed to meet a launch date of July 1962. A review of the program showed that it would be feasible to launch a smaller spacecraft using the Atlas–Agena combination of vehicles. Accordingly, a spacecraft of 447-lb total weight was designed for the Venus mission, as compared with the approximately 1100 lb of the Mariner A spacecraft. Two models of the modified spacecraft, designated as Mariner R-1 and R-2, were

launched in the fall of 1962. Of the two, only Mariner R-2, more often referred to as Mariner 2, performed a successful mission.

The reduced capabilities of the Mariner R spacecraft forced a cutback in the scientific payload which could be accommodated. The microwave radiometer experiment was reduced to two channels, the 19.0- and the 13.5-mm channels, a choice largely dictated by engineering considerations and the rigid time table imposed on the spacecraft designers. This change alone made it impossible to meet objective (3) listed above, as at least three frequencies would be required to define the water vapor resonant line. Severe limitations were also imposed on the planetary scan system. The elimination of an optical planetary seeker led to a scan program actuated by the outputs of the microwave radiometer. A stepping scan, or start–stop scan, had been planned for Mariner A to avoid complications caused by time-constant effects in the data. A continuous scan, because of its simplicity, was adopted for Mariner R. This imposed engineering change, coupled with the increase of the time constant during flight, had a serious effect on the microwave data, as is shown later.

II. MICROWAVE RADIOMETER—INSTRUMENTATION AND CALIBRATION

Two basic factors governed the design of the radiometer: the scientific goals proposed for the experiment, and the spacecraft environment to which the instrument was to be subjected. Of these, the second factor was by far the more predominant and most of the design parameters were arrived at for engineering reasons, provided the scientific goals were not seriously compromised. The following are some the the major constraints imposed on the radiometer by the spacecraft:

(1) Weight: 21 lb maximum allowable for the whole instrument. The total scientific payload of the Mariner R spacecraft was approximately 41 lb.

(2) Power consumption: 5 W maximum average, 10 W peak.

(3) Operating temperature range: $-10°$ to $+65°$C.

(4) Vibration survival: 12 g rms, noise-type.

(5) Mechanical interface with spacecraft: two-point mounting, one a bearing, the second an actuator permitting a 120-deg scan of the antenna beams.

(6) Electrical interface with spacecraft: prime power input from the central power-switching unit; data output in analogue form to the Data Conditioning System (DCS).

Added to these and other constraints governing the materials and processes used in the construction of the radiometer was the reliability requirement of a minimum unattended operational life of 3000 h under space conditions and a schedule calling for the delivery of three flight units five, six and seven months, respectively, after the start of the project.

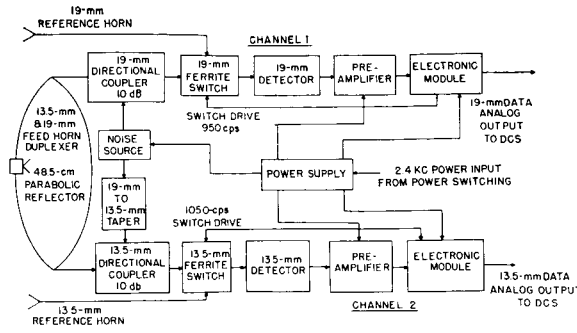

FIG. 1. Mariner 2 microwave radiometer block diagram.

The Radioscience Group of the Division of Space Sciences at the California Institute of Technology's Jet Propulsion Laboratory designed and built the instrument and associated equipments, the designs being largely based upon components developed for the Mariner A microwave radiometer. Three units were built, referred to as Serial 1, 2, and 3.

The radio telescope operated simultaneously at wavelengths centered at 19 mm (15.8 Gc/sec) and 13.5 mm (22.2 Gc/sec). In this discussion, the 19-mm wavelength will be referred to as Channel 1 and the 13.5-mm as Channel 2. Both radiometers were of the crystal video type so that the weight and power consumption would satisfy restrictions imposed by spacecraft engineering capabilities. Superheterodyne systems of various types were evaluated in order to achieve greater sensitivity, but had to be discarded because of excessive weight and power requirements. Both channels used a Dicke switching system for gain stability and were essentially identical electronically.

Figure 1 is a block diagram of the instrument. The effective diameter of the parabolic reflector used was 48.5 cm with a focal length of 19.3 cm. These values resulted in theoretical half-power beamwidths of 2.7 deg for Channel 1 and 2 deg for Channel 2, and gains of 35 and 38 dB, respectively.

The energy concentrated by the antenna entered a feed-diplexer unit at the focus where the two waveguide bands were separated by filters. The two channels of the radiometer were thereafter completely isolated. Both reference horns had 12-deg beamwidths in each plane, a gain of approximately 22 dB above an isotropic radiator, and were oriented to avoid pointing at either Venus or the sun.

In each channel, a 4-port ferrite device switched at approximately 1000 cps between the feed and the reference horn pointing at space. The output of the switch was fed to a high-sensitivity crystal video detector, and subsequently to a preamplifier–amplifier chain.

The amplified signal, with an amplitude proportional to the difference in temperature seen at the switch inputs, was rectified by a phase-sensitive detector and integrated. Since the reference horn viewed a source of temperature $\sim 0°$K, the output amplitude of the inte-

grator was proportional to the source temperature of the main antenna feed.

A reference oscillator provided signals for the ferrite switch drive amplifier and the phase detector. This oscillator was a miniature tuning fork chosen for its stability with temperature and voltage variations. To avoid crosstalk, reference frequencies of 950 and 1050 cps were used for Channel 1 and Channel 2, respectively.

The circuitry was solid state, and silicon semiconductors were used exclusively to permit high-temperature operation. The preamplifier was of conventional LC-tuned circuit design, with a low-noise input transistor; the amplifier which followed the preamplifier was also of conventional design, but with a twin-tee feedback network. The bandwidth of both the amplifier and the preamplifier was approximately 20 cps. Demodulation was accomplished by a transistor driven by the reference oscillator; the integrator was a dc amplifier in a Miller configuration. The time constant of the integrators (0 to 63% points) was set at values of about 20 sec. The over-all ac amplification had a voltage gain of approximately 120 dB, and the dc gain was 30 dB.

An important feature of the system was a builtin calibration unit. It consisted of a 5000°K gas-discharge tube made specially rugged coupled to both channels through 10-dB directional couplers. The outputs of the tube were in the 19-mm waveguide band, and a taper was used in front of the coupler to transduce into the 13.5-mm waveguide band. When the gas tube was fired upon external command, a known signal of approximately 350°K was injected into the main signal path to provide system calibration.

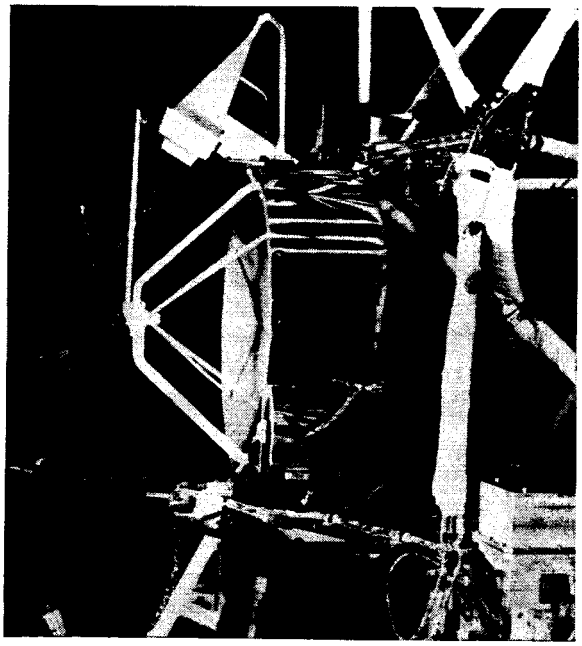

FIG. 2. Over-all view of the radiometer, with the reference horns, the feed assembly, and the thermal shield installed. The instrument is shown mounted on the spacecraft, with the scan-actuation mechanism.

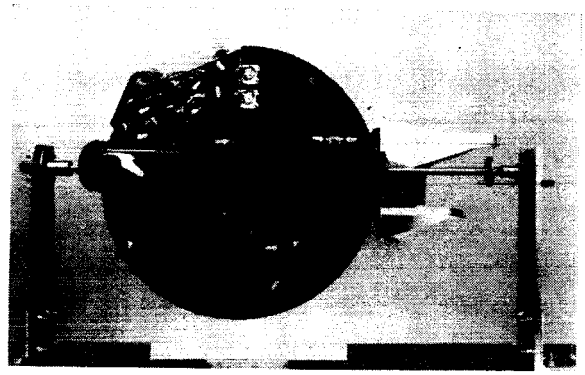

FIG. 3. Rear view of the radiometer in test stand, with heat shield removed. Note on lower left the infrared instrument mounting flanges.

The output voltages varied from 1 V dc for 0°K input temperature to 6 V dc for an antenna temperature increment of approximately 800°K. The response of the system was linear with antenna temperature for any combination of antenna temperature, reference temperature, and phasing, as well as shifts with temperature of the operating point of the circuits. Nonlinearities of output vs input were detectable only after the output voltage level exceeded ±9 V. Each channel output was fed to the DCS, where it was sampled every 20.16 sec for transmission through the spacecraft telemetry.

Of prime importance in the mechanical design were extreme ruggedness to withstand the spacecraft launch environment, high accuracy of the parabolic reflector for maximum efficiency, and lightest possible construction to stay within the weight allowance of the instrument.

To meet these requirements, a one-piece frame was designed, integrating the parabolic reflector unit, the instrument mounting flanges, and all waveguide and electronics mounting supports on the convex surface. Flanges were also provided near the side to allow installation of an infrared instrument on the frame. The frame was machined out of a solid aluminum billet and successfully met all the rigidity, accuracy, and weight specifications. All the microwave components, with the exception of the feed and reference horns, and all the electronic modules located in individual chassis were mounted on the back supports of the antenna unit. The back of the frame was then covered with a lightweight aluminum thermal shield. Figure 2 shows the front of the instrument with a portion of the polished thermal shield; Fig. 3 is a view of the uncovered back of the radiometer giving an idea of the construction and compactness of the system.

To maintain the temperature of the instrument within the specified limits, all outside surfaces were polished to reflect as much of the solar heat as possible. All internal surfaces were painted black to distribute and dissipate the heat generated by the electronics and the absorbed solar heat. The radiometer was completely exposed to

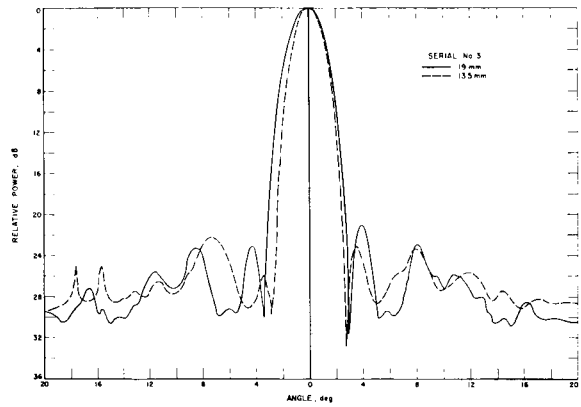

FIG. 4. E-plane antenna patterns.

sunlight during the flight to Venus and the change in solar constant from earth to Venus was sufficient to raise the temperature by about 60°C during the flight.

It can be noticed in Fig. 2 that the front surface of the paraboloid is of a stepped construction. The steps act as plane reflectors for infrared energy and thus avoid concentration of excessively high heat at the feed, should the instrument point at the sun during spacecraft maneuvers. The steps are small enough not to affect the microwave frequencies of interest, as proved by measurements of the antenna patterns.

Because of the constraints of power, weight, and time, it was necessary to utilize the outputs of the radiometer to provide actuating signals to the scan-control logic circuitry. The signals were all obtained from the drift-scan voltage levels as the antenna beams traversed the planet.

The complete instrument package was designed to execute a 1-deg/sec search-mode scan with an angular amplitude of ± 60 deg upon initiation of the spacecraft "encounter mode." The plane of the scan was perpendicular to the earth–spacecraft–sun plane. The 1-deg/sec rate was determined by the time constant and sensitivity of the instrument, the expected size and brightness temperature of the planetary disk, and the total time available for the gathering of planetary data (length of time that the scan plane intersects some portion of the planet). The scan angle coverage of 120 deg was necessary because of the anticipated uncertainty of the location of planetary disk as seen from the spacecraft. In addition, the experiment required that "cold sky" data on either side of a scan be obtained.

If the output of either radiometer channel exceeded 1.5 V (i.e., went 0.5 V above the 1.0-V baseline), a data-acquisition mode was initiated. In this mode, the scan rate was reduced from 1 deg to 0.1 deg/sec, and the reversal logic activated. In order for the reversing signal to be "armed," it was necessary for one of the radiometer outputs to exceed 2.25 V (or 1.25 V above the baseline). After the 2.25-V level had been exceeded, six consecutive combined readings from both channels below 1.5 V would cause scan reversal and return toward the planet. The delay produced by this action allowed the main beams to go far enough beyond the limit of the planet to obtain cold sky references from either side of the planet. The length of time spent off the planet was a compromise between time-on vs time-off the planet and the establishment of a satisfactory cold sky reference.

If while scanning both radiometer outputs were to fall below 1.5 V for 160 sec or longer for any reason, the fast scan mode would be initiated and the internal calibration noise tube activated for 120 sec. During this calibration period, the scan logic would prevent the system from going automatically into slow scan. This reinitiation of the search mode was to ensure that as little data time as possible be lost if a large burst of noise accidentally triggered slow scan prior to actual acquisition of the planet. Without this feature, the system would go into slow scan and stay there after a single random data point exceeding 1.5 V, a likely possibility on a spacecraft. It will be shown later that it was the fast-scan search mode logic which permitted, because of unexpected circumstances, the third scan across the sunlit portion of the planet.

The scan actuator consisted of a small, pressurized unit bolted to the spacecraft frame with a flanged shaft connecting it to the upper part of the radiometer. Two geared-down 12 000-rpm synchronous motors drove the shaft through a differential coupling. The motors were geared differently by a factor of 10 and scan rates of 1 deg or 0.1 deg/sec were obtained by simply stopping and starting alternate motors. Reversal of the scan direction was accomplished by reversing the motors either by command from the DCS or by mechanical limit switches. A precision potentiometer on the output shaft permitted a knowledge of the scan position by reading out a dc voltage.

The E-plane antenna pattern of Serial 3, the instrument flown to Venus, is shown in Fig. 4. No H-plane patterns were made of Serial 3. However, the eccentricity of the pattern could not have departed significantly from those of Serial 1 and 2, and these were found to have an eccentricity less than 0.25.

The primary calibrations of the radiometer gas-discharge noise tube and antenna pattern were performed simultaneously by constructing an absorbing disk, or "artificial planet," to simulate a planet of large angular size compared to the antenna beamwidth. The disk was made of microwave-absorbing material and suspended 15 m vertically above the radiometer so that it subtended an angle of 13 deg as seen from the radiometer. The angular size was chosen to approximately coincide with the expected angular size of Venus during the planetary passage. The emissivity of the absorbing material was within 1% of unity so that the physical temperature of the material was equal to the brightness temperature. The antenna temperature $(T_A)_D$ as the radiometer antenna beams are scanned across the disk,

through its center, is given by

$$(T_A)_D=\frac{1}{4\pi}\int_{\Omega_D} T_{BD}G(\theta,\phi)d\Omega, \qquad (1)$$

where $G(\theta,\phi)$ is the antenna gain pattern for each channel, T_{BD} is the brightness temperature of the disk, and Ω_D is the solid angle subtended by the disk. If $(T_A)_C$ is the effective antenna temperature, referred to the antenna input terminals of the internal calibration noise tube, then a quantity of interest is the ratio $\beta_1=(T_A)_D/(T_A)_C$ given by

$$\beta_1=\frac{T_{BD}}{4\pi(T_A)_C}\int_{\Omega_D} G(\theta,\phi)d\Omega, \qquad (2)$$

where T_{BD} has been removed from the integral because it was constant over the disk. For the actual flight unit, $\beta_1=0.174\pm0.015$ for Channel 1 and $\beta_1=0.340\pm0.024$ for Channel 2.

Note that the above method of calibration does not relate the temperature of the calibration signal to a known change of antenna temperature at the antenna terminals, as is usual in radio astronomy. Instead, the calibration signal is related to the change in antenna temperature as the antenna beams scan a target of large angular extent and of known brightness temperature. In this manner, the calibration procedure not only provides a measure of the radiometer sensitivity, but includes effects of the sidelobes on the target. The method was chosen, of course, to most nearly represent the actual conditions to be expected at planetary passage. Note also that the system electronic transfer function does not appear in β_1 and that the reference temperature is unimportant as long as it is stable and the linear dynamic range of the system is not exceeded during the calibration.

The calibrations obtained above were corrected for changes in atmospheric radiation and ground radiation as the antennas scanned the disk. The tests were performed on Table Mountain, in the California desert, at an altitude of 2.5 km under conditions of very low relative humidity so that atmospheric radiation, mainly from water vapor, was small. Ground radiation could be included in the calibration procedure by making scans with and without the absorbing disk being in the beam. Effects of the ground radiation were also checked by making scans with a metal ground screen in the immediate neighborhood of the radiometers. All ground radiation effects were undetectable. During the disk calibration, the comparison horns were terminated with microwave-absorbing material to prevent variable ground radiation from entering the horns as the equipment was scanned across the disk.

On–off measurements of the sun were also taken at Table Mountain on 18 May 1962 to check on the over-all calibration procedure. The resultant brightness temperatures obtained are $10\,000\pm1000$°K for Channel 1 and 9450 ± 650°K for Channel 2. These may be compared with the value of 8870 ± 980°K at 11.8-mm wavelength (data presented in another paper in this issue, by Staelin *et al.*).

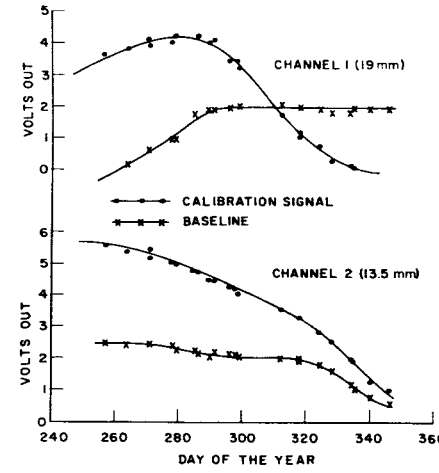

FIG. 5. Flight calibration history.

III. FLIGHT PERFORMANCE

In-flight calibration consisted of periodic firing of the noise tube. Every 189.12 h during cruise (pre-encounter) there were to be three successive noise-tube on–off calibrate sequences 15.76 h apart. A calibrate sequence consisted of the noise tube on for 185 sec and off for an equal time. During the planetary encounter mode the noise tube was to be fired for 120.96 sec every 32.256 min, provided the planet had not been acquired.

Throughout the 129-day mission, there were a total of 24 noise-tube calibrations. Of these, 22 occurred prior to planetary encounter and two after planetary passage. These calibrations gave a valuable history of the baseline and "calibrate-on" voltage levels. The noise-tube amplitudes as a function of time gave a history of the gain in both channels. As the probe approached Venus, the spacecraft temperatures increased beyond design limits. In view of the spacecraft temperature-control problems that developed, both channels showed pronounced gain changes, but the calibration history permits the data to be used with confidence. Plots of the baseline and calibrate-on voltage levels vs day after launch are seen in Fig. 5. The baseline of Channel 1 shifted down by approximately 2 V and the baseline of Channel 2 shifted up by 1.5 V during launch. The prelaunch values were 1.0 V. The only way shifts of this magnitude could be duplicated in the laboratory was by removing the screws securing the thermal shield to the rim of the radiometer and permanently distorting the shield. It is our opinion that the observed baseline shifts were due to launch vibrations which exceeded the Flight Approval Test levels and which

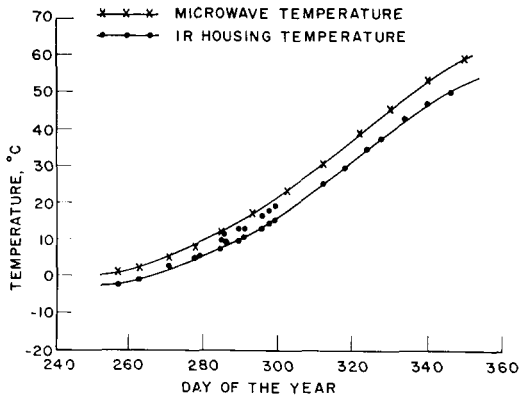

FIG. 6. Flight temperature history.

probably loosened the thermal shield from the screws securing its edge to the radiometer.

Gradual changes of the baseline and calibration amplitude (i.e., sensitivity) of Channel 1 during flight are attributable to the basic design of the audio amplifier chain. This chain consisted of two amplifiers in cascade, each with a narrow 20-cps bandwidth centered at the ferrite switch frequency. The phase-shift characteristics of these amplifiers were quite sensitive to passband and signal-frequency variations. The design was dependent on component stability in the reference oscillator, passband, and gain-determining elements. All components used were of high quality and no phase-passband shifts sufficient to cause substantial output variations were observed in the laboratory. Accordingly, we believe that one or possibly several components slowly degraded under the extended vacuum and heat conditions of the flight. Enough phase shift was observed in Channel 1 to cause actual phase reversal, resulting in a negative instead of positive output for a given input signal.

Channel 2 also experienced some phase shift, but its gradually decreasing sensitivity was basically due to a deteriorating video crystal as evidenced by a proportionally decreasing signal-to-noise ratio of the calibration signal. The sensitivity of Channel 2 at encounter was 13% of its value at launch.

Planned temperature control for the radiometers should have provided a temperature at encounter of 35 ± 10°C. The graph of Fig. 6 shows actual performance: 35°C was exceeded on day 317, and at encounter (day 348), the temperature was estimated to be 58°C. This came dangerously close to the maximum permissible operating temperature (65°C) of the video detector crystals. The microwave radiometer temperatures are based on the temperature values of the infrared instrument housing. No sensor was carried directly on the microwave instrument itself; the infrared-microwave radiometer temperature relation is based on ground calibrations.

Both channels exhibited changes of postdetection time constant during flight. The time constant determined from the calibration on day 348, the day of encounter, was determined to be 39 sec for Channel 1, as shown in Fig. 7, and 50 sec for Channel 2. These can be compared with the design and prelaunch value of 20 sec. The increase in time constant has forced the use of large correction factors on the raw data, as discussed in the following section. Tests performed on a radiometer identical with the flight unit have indicated that the time-constant change may be traced to a large bipolar, tantalum capacitor which exhibited excessive leakage varying with time and temperature.

After 8 October 1962, the analogue signals from other instruments on the spacecraft showed deviations from their normal values, and in some cases there seemed to be a marginal correlation of these changes with the output level of the microwave radiometer. However, a careful study of all the data from both channels of the radiometer taken prior to the planetary data has shown no detectable "crosstalk" effect on the microwave outputs caused by other instruments, or of the microwave radiometers on themselves.

Approximately $6\frac{1}{2}$ h prior to closest approach on 14 December 1962 the spacecraft responded to a radio command to begin the encounter mode of operation, transmitted from the JPL/NASA Deep Space Instrumentation Facility at Goldstone, California. In this mode, the telemetry of engineering information was terminated, the microwave and infrared instruments were energized, antenna scanning was started, and the telemetry was devoted entirely to the scientific experiments with a readout of each channel every 20.16 sec. Prior to the encounter mode, the radiometers had been energized, without antenna scanning, for only 4-min intervals during calibrations; consequently, the start of the encounter mode was the first chance to observe the long-term stability and over-all operation of the instrument. As expected, the baseline shift of Channel 1 caused the scan logic circuitry to immediately begin the planetary-scan rate of 0.1 deg/sec instead of the faster search scan of 1.0 deg/sec. A further result of the base-

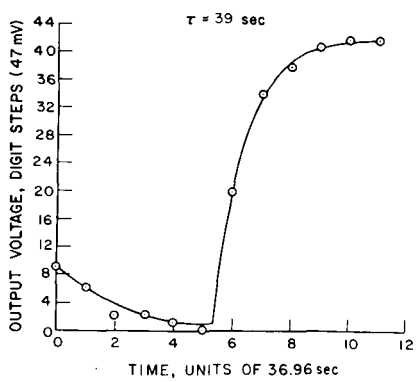

FIG. 7. Channel 1 calibration—day 348. The output voltage is quantized in the DCS into 47-mV steps for transmission through the spacecraft telemetry; the timing is determined by the DCS sampling rate of one sample per 36.96 sec during spacecraft "cruise mode."

39

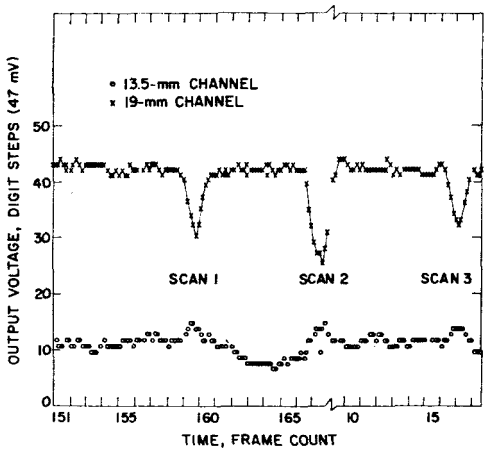

FIG. 8. Encounter data in unreduced form. The timing here is by DCS "frame count" in which each frame contains six spacecraft "encounter mode" sampling intervals of 20.16 sec each. The frame count was accidentally reset when fast scan occurred on Scan 2. Frame count 156 started at 18:53 GMT, 14 December 1962.

line shift was the failure to obtain radiometer noise-tube calibrations every 32.256 min before planet acquisition, as planned.

During the approximately 5½ h before planetary detection, the baseline level and stability were consistent with that determined from the in-flight calibrations. No baseline instabilities as a result of the scan motion of the radiometer were noticed. There was, however, a baseline shift in Channel 2 at one extremity of every scan. This shift, in the direction of "negative" temperature, as shown in Fig. 8, is attributed to the Channel 2 comparison horn "seeing" the solar panel at the extremity of the scan motion. This effect occurred during every scan for the entire operation of the encounter mode, was systematically repetitious, and can be averaged and removed from the remaining data.

Since the baseline level of Channel 1 exceeded 1.5 V but remained less than 2.25 V, the antenna scanned at the rate of 0.1 deg/sec without the scan-reversal mechanism being energized upon loss of planet signal. The possibility existed, however, that when the planet was acquired the fast-scan rate of 1.0 deg/sec would occur. This would occur because the Channel 1 signal had reversed in polarity so that a planetary signal would appear to the scan-logic circuitry as cold sky and energize the fast scan and subsequent noise-tube calibration, provided the signal exceeded 160 sec in duration.

The antenna was constrained to scan ±60 deg from the sun–probe–earth plane about an axis parallel to the sun–probe line. This constraint, combined with the motion of the spacecraft, resulted in the planetary scans being made prior to closest approach. First contact with Venus was made at 18:59 GMT when the spacecraft was 46 500 km from the center of the planet. The location of this and subsequent scans is shown in Fig. 9, and parameters pertinent to each scan are given in

TABLE I

Scan number	Location	Spacecraft distances from center of Venus[a]	Angular extent of scan
1	Dark hemisphere	46 800 km	10 deg
2	Terminator	44 350 km	15 deg
3	Sunlit hemisphere	42 500 km	10 deg

[a] At center of scan.

Table I. It can be seen from Fig. 9 that three scans across the planet were obtained and their juxtaposition on the planetary disk was ideal. In view of the difficulties with the baseline levels and their vital role in the scan logic, the positioning of the scans on the planet and the acquisition of the third scan were extremely fortuitous. Because of the large angular extent of the terminator scan and the phase reversal in Channel 1, the radiometer output dropped below 1.5 V for a time longer than 160 sec. This resulted in the antenna scan rate changing from 0.1 deg to 1.0 deg/sec just after the beam axis passed off the planet at the end of the second scan. Therefore, the antenna moved to its scan limit rapidly and returned to its slow scan rate as the radiometer output rose above 1.5 V again. Furthermore, during the fast scan, the noise tube did not fire. Had it fired, the antenna could not have returned to the slow scan rate before the beam axis crossed the planet. After changing back to 0.1 deg/sec, the antenna beam scanned across the sunlit hemisphere and successfully achieved the vital third scan. These circumstances are clarified in the scan angle vs time diagram shown in Fig. 9. Had the entire scan system functioned as designed, approximately 15 scans would have been obtained.

Approximately ½ h after closest approach, the spacecraft was commanded to return to the cruise mode of

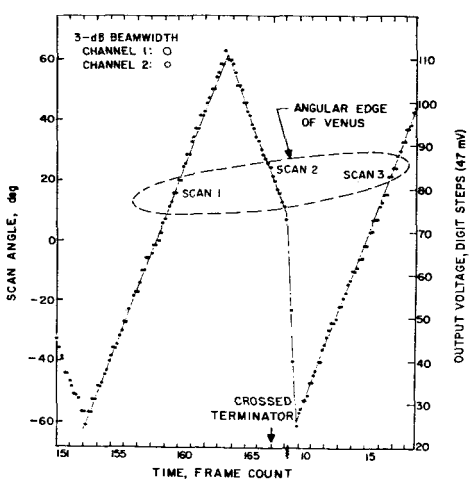

FIG. 9. Radiometer scan pattern during encounter. The sizes of the 3-dB antenna beamwidths are shown to scale in the upper left to give an idea of the resolution. Of course the intersection of the conical beam with the spherical planet will yield a circle of that size at only one point in each scan.

40

operation, during which the radiometers are off except for periodic calibrations, as in the pre-encounter flight. Upon receipt of this command, the antenna scan stopped and the noise tube fired, thereby calibrating the radiometers. This was a fortunate situation because a calibration was available after the radiometers had been in operation for approximately 7 h and within 1 h of the taking of planetary data. This calibration, shown in Fig. 7, was used for the reduction of the data. Subsequent calibrations which occurred until the spacecraft became silent on 3 January 1963 were of little value.

The basic data of the microwave radiometer experiment consisted of (1) the digital voltage outputs of both Channel 1 and Channel 2, and (2) the voltage output of the previously calibrated antenna-position potentiometer. The latter was used, for example, in constructing Fig. 9. The raw data from the radiometer outputs are shown, for the time of planetary encounter, in Fig. 8. To interpret the radiometer data, auxiliary data were required on the position of the spacecraft relative to the planet as a function of time. These data, supplied by the Jet Propulsion Laboratory, were accurate to approximately 0.1% and the errors introduced thereby into the experimental results are neglected.

IV. DATA REDUCTION AND RESULTS

The digital presentation of radiometer output across the planet in Fig. 8 is the "raw" data of the experiment from which the temperatures at selected positions on the planet may be determined. In the analysis that follows, the discussion is restricted to a determination of the brightness temperature of the planet at the central position, or midpoint of the three scans across the planet. The procedure followed in determining these temperatures is as follows:

(1) A determination of the base level of the radiometer output when the antenna beams were not directed at the planet was made.

(2) The time-constant "smearing" of the data was removed. The scans obtained after this process are referred to as the "restored scans."

(3) The ratio of the amplitude of the restored scans to the amplitude of the radiometer calibration signal was obtained. This will be designated β_2.

(4) A correction factor was computed from the previously measured antenna pattern and the geometry of the situation when the antenna beam was at the center of each scan.

(5) The brightness temperature was computed from Eq. (2) and items 3 and 4 above.

The base level of the radiometer outputs was determined from the telemetry data for the times when the antenna beams were off the planet. This consisted of determining the average output of the radiometers after removing any systematic effects. In the case of Channel 2, the effect of the solar panels in the comparison-horn antenna beam was removed.

The effect of the receiver time constant was removed by considering the transfer function of the integrating circuit. If the voltage output of the integrator as a function of time t is $V_o(t)$, then the input voltage $V_i(t)$ is given by

$$V_i(t)=V_o(t)+\tau[dV_o(t)/dt], \tag{3}$$

where τ is the time constant of the integrator. This procedure provides a measure of the output which would be observed with zero time constant. The application of Eq. (3) increases the uncertainty, or fluctuations, in the data. This equation also serves to bring out the serious degradation in the data that resulted from the increase in the time constant throughout the flight.

The amplitude of the input voltage $V_i(t)$ to the integrator is related to the brightness temperature of Venus by the equation

$$V_i(t)=\frac{k}{4\pi}\int_{\Omega_V(t)} T_{BV}G(\theta,\phi)d\Omega, \tag{4}$$

where the integral is evaluated over the planetary solid angle Ω_V (which is a function of time), and k is a constant which includes the response characteristics of the radiometer crystal detector, electronics, etc. Taking the ratio of this voltage to the calibration signal voltage removes the constant k and gives the parameter β_2, where

$$\beta_2(t)=\frac{1}{4\pi(T_A)_C}\int_{\Omega_V(t)} T_{BV}G(\theta,\phi)d\Omega. \tag{5}$$

By referring $V_i(t)$ to the calibration signal voltage, variations in the system electronic transfer function are effectively removed. Recall that a similar situation exists in the case of β_1.

The ratio β_2 is determined for the midpoint of each scan from the retored scans and the radiometer calibration which occurred as the spacecraft was commanded to the cruise mode following the planetary encounter.

The mean brightness temperature $\bar{T}_{BV}$ is obtained from Eqs. (2) and (5) by the equation

$$\bar{T}_{BV}=\bar{T}_{BD}\left(\frac{\beta_2}{\beta_1}\right)\frac{\int_{\Omega_D} G(\theta,\phi)d\Omega}{\int_{\Omega_D} G(\theta,\phi)d\Omega}. \tag{6}$$

The integrals in this equation must be evaluated numerically from the antenna-pattern measurements taken prior to launch. In the case of the integral over the planetary solid angle, the evaluation must be made only after the coordinates of the antenna beams on the planetary surface are known.

TABLE II

Channel	Scan	Integration time (sec)	Calibrator amplitude (V)	β_1	β_2	Calibration disk temperature	$\frac{\int_{\Omega_D} G(\theta,\phi)d\Omega}{\int_{\Omega_V} G(\theta,\phi)d\Omega}$	Peak amplitude digit step units	Peak amplitude (V)	$\bar{T}_p$
1	1	~40	2.2	0.174	0.291	287°K	0.998	13.6	0.640	480
(19 mm)	2				0.370		0.970	17.3	0.814	590
	3				0.246		1.135	11.5	0.541	460
2	1	~50	0.44	0.340	0.492	280°K	0.972	4.6	0.216	393
(13.5 mm)	2				0.513		0.944	4.8	0.226	400
	3				0.460		1.052	4.3	0.202	396

It is strongly emphasized that the entire analysis and the subsequent results assume that the calibration temperature $(T_A)_C$ remained constant throughout the entire flight and equal to the value it had during the prelaunch calibration on Table Mountain.

The factors entering into Eq. (6) and the results derived thereby for both channels are given in Table II. The values given there represent slight revisions of previously published values (Barath *et al.* 1963), due principally to the use of refined trajectory information.

Considerable importance is attached to the phenomenon of limb darkening or brightening as a means of defining the origin of the radiation from Venus. It is apparent from the values in Table II that the peak temperatures of the scans near the limbs of the planet are less than that of the central scan. This result could follow from two causes: (1) the planetary brightness temperature may indeed be less near the limbs than at the center, i.e., true limb darkening, or (2) the antenna beam filling may be sufficiently less near the limbs than at the center to account for the apparent limb darkening. In actuality, the second cause will indeed be operative and must be removed before any conclusions about a true limb darkening can be reached. The temperature reductions near the limb due solely to the antenna beam effects can be estimated by numerical integration using the actual antenna patterns measured prior to launch. The reduction factor for either Scan 1 or 3 is the ratio of the respective integral in the denominator of Eq. (6) to the corresponding integral for Scan 2, and represents the apparent limb darkening due to the antenna pattern that would be obtained by scanning an isothermal planet. The limb darkening due to the beam filling and the observed values are compared in Table III for the 19-mm wavelength data. It is immediately obvious that only a small fraction of the total observed limb darkening may be attributed to the effect of antenna beam filling and that true limb darkening has been observed. It should be emphasized that this result depends only upon voltage ratios and is not dependent upon the absolute calibration of the radiometers. Furthermore, if we deliberately lower the Scan 2 temperature and raise the other two scan temperatures by the maximum possible error in the digital telemetry data in an attempt to destroy the limb darkening, the limb darkening is still present. Therefore, we conclude that the results show unambiguously that limb darkening is present and that the origin of the microwave radiation from the planet is at or near the surface.

It will be noted from Table II that limb darkening is strongly evident only in the 19-mm data. This reflects the low signal-to-noise ratio which was experienced on the 13.5-mm channel, and further work is under way to determine the magnitude of limb darkening at this wavelength.

V. CONCLUSION

An estimate of the precision of the results is difficult because of the nature of the experiment, and particularly because of the limited amount of data. At the 19-mm wavelength, the estimated error is $\pm 5\%$, whereas the 13.5-mm results must be assigned an error of $\pm 25\%$ because of the poor quality of the data. The possibility exists that a large systematic effect could have occurred during the flight which would have been beyond our control and our ability to determine, but such an effect would not have altered, in all likelihood, the relative amplitudes of the individual scans. Therefore, the major conclusion of limb darkening and its importance to the origin of the radiation seems to be well established. Furthermore, the values of the planetary temperatures obtained at 19-mm wavelength are consistent with the current ideas of microwave radiation from Venus.

Further data analysis, directed toward analyzing the individual scans in detail, is in progress. This effort will be restricted almost entirely to the 19-mm data and will attempt to relate the observed temperatures to (1) the surface temperature distribution, (2) the absorption in the atmosphere, and (3) the emissivity of the surface.

TABLE III

Scan	Ratio of observed maximum voltage relative to Scan 2	Ratio of maximum voltage relative to Scan 2, beam-filling effect only
1	0.79	0.973
3	0.67	0.856

4/2

ACKNOWLEDGMENTS

The work of A. H. Barrett was supported in part by the U. S. Army Signal Corps, the Air Force Office of Scientific Research, and the Office of Naval Research, and in part by the National Aeronautics and Space Administration (Grant NsG-250-62). A. E. Lilley gratefully acknowledges the support of the Alfred P. Sloan Foundation and the Research Corporation for his research. J. Copeland acknowledges the support of the Army Missile Command during the early phases of this program. The work of F. T. Barath and D. E. Jones presents the results of one phase of research carried out at the Jet Propulsion Laboratory, California Institute of Technology, under Contract No. NAS 7-100, sponsored by the National Aeronautics and Space Administration.

The authors are also indebted to many associates for assistance in the design, construction, testing and calibration of the instrumentation, as well as in the reduction of the data. Special thanks are due E. J. Johnston of the Jet Propulsion Laboratory, who was largely responsible for the design of the radiometers.

REFERENCES

Barath, F. T., Barrett, A. H., Copeland, J., Jones, D. E., and Lilley, A. E. 1963, *Science* **139**, 908.
Barrett, A. H. 1961, *Astrophys. J.* **133**, 281.
Barrett, A. H., Copeland, J., Jones, D. E., and Lilley, A. E. 1961, "Objectives of the Mariner Venus Microwave Radiometer Experiment," Tech. Rept. No. 32-156, Jet Propulsion Laboratory, Pasadena, California.
Jones, D. E. 1961, *Planetary Space Sci.* **5**, 166.
Lilley, A. E. 1962, *Space Age Astronomy* (Academic Press Inc., New York), pp. 253–273.
Öpik, E. J. 1961, *J. Geophys. Res.* **66**, 2807.
Roberts, J. A. 1963, *Planetary Space Sci.* **11**, 221.
Sagan, C. 1962, *Icarus* **1**, 151.
Scharf, F. L. 1963, *J. Geophys. Res.* **68**, 141.
Tolbert, C. W., and Straiton, A. W. 1962, *ibid.* **67**, 1741.

43

From the ASTRONOMICAL JOURNAL
69, No. 1, 1964, February—No. 1316
Printed in U. S. A.

Microwave Observations of Venus, 1962–1963

F. D. DRAKE
Jet Propulsion Laboratory, California Institute of Technology, Pasadena, California

Venus was observed at 10.0-cm wavelength on 40 days during the period 15 September 1962 through 1 March 1963. The NRAO 85-ft telescope was used with the same radiometer, calibration procedure, and observing technique as in similar 1961 observations. The results give an intensity versus phase-angle relation which is identical, within the errors, with the result obtained in 1961. This indicates that either Venus has a small pole-to-equator temperature differential, or that its pole is very nearly perpendicular to the ecliptic. The data of 1961 and 1962 give a statistical probability of 0.991 that the minimum brightness temperature is observed after inferior conjunction, a situation to be expected with retrograde rotation.

Venus was observed at 21.4- and 40-cm wavelengths during the period 21 November through 4 December 1962 with the NRAO 300-ft radio telescope. Good measurements were possible at 21.4 cm, leading to a mean equivalent disk brightness temperature of 528±33 (m.e.)°K. The observations at 40 cm were appreciably harmed by sidelobe reception of solar emission, but lead to a preliminary value of the equivalent blackbody disk temperature of 400°K at that wavelength.

I. 10.0-CM OBSERVATIONS

THE author has previously reported observations of Venus made over a time interval including the inferior conjunction of 1961 (Drake 1962). These results will hereafter be referred to as the 1961 experiment. They indicated the existence of a small variation in the equivalent blackbody disk temperature T_{BB} of the planet with the phase angle, the angle between sun and earth as viewed from Venus. They also indicated that the minimum value of T_{BB} occurred after inferior conjunction, a situation consistent with retrograde rotation of the planet, barring the presence of a peculiar meteorology.

To verify these results, and to search for any long-term variations in the Venus emission, similar measurements were made on 40 days during the period 15 September 1962 through 1 March 1963 near the time of the 1962 inferior conjunction. The National Radio Astronomy Observatory 85-ft radio telescope with a traveling-wave-tube radiometer was used for both the 1962 and the 1961 observations. The 1962 observing procedure was the same as in the 1961 experiment, and consisted of observing a point 30′ from Venus for 30 sec, then Venus, then a point symmetrically opposite Venus for 30 sec, and so on until four observations of Venus, sandwiched between five observations of comparison positions, were obtained. The pairs of comparison positions used were either 30′ east and west, or north and south of the planet. After eight such sets of observations were made, a similar observation was made of an argon gas discharge tube. Once a day, three such sets of observations were made of the radio source 04N3A(3C123). All data were recorded digitally. The observations thus taken could be reduced to give the ratio of flux densities of Venus to 04N3A for the day's observations. Using a flux density for 04N3A of 23.7 flux units, as with the 1961 observations, and the standard radiation formulas, a value of T_{BB} for the day's observations could be readily obtained. Details of this procedure are given in the description of the 1961 experiment (Drake 1962).

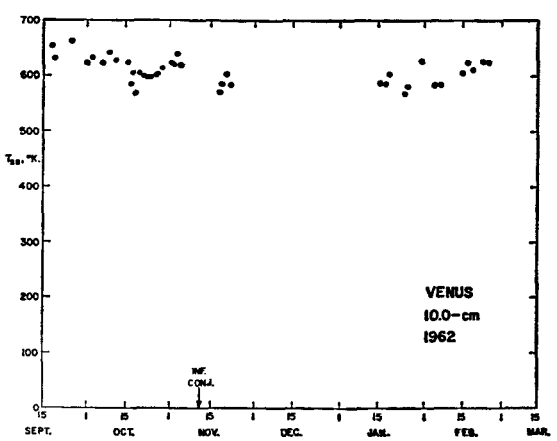

FIG. 1. Daily mean value of equivalent blackbody disk temperature observed at 10.0 cm, 1962–63.

The resultant daily mean values of T_{BB} are shown in Fig. 1. The gap in the data between 24 November and 15 January resulted from the telescope being assigned to other projects. The results show again the high values of T_{BB} of about 600°K, which occur at centimeter wavelengths, and the small variation in T_{BB} with time again appears.

The daily values of T_{BB} are plotted as a function of the phase angle i in Fig. 2. To these points has been fitted, by least-squares, the first two terms of a Fourier series in i, as was done with the 1961 data. The resultant best-fitting phase curve is indicated by a solid line in Fig. 2, and is expressed by

$$T_{BB\ 1962} = \underset{(6)}{622} + \underset{(12)}{43}\cos(i \pm \underset{(20)}{35})°\text{K}, \qquad (1)$$

where the plus sign is taken for values of i occurring after inferior conjunction, and the minus sign for values occurring before. The numbers in parentheses are the mean errors of the values immediately above them. Again, a statistically significant phase effect appears, and the minimum temperature occurs significantly after inferior conjunction. For comparison, the similar equa-

62
4/4

tion given by the 1961 data is

$$T_{BB\ 1961}=\underset{(9)}{622}+\underset{(15)}{39}\ \cos(i\pm\underset{(11)}{17})°\text{K}. \qquad (2)$$

This result is shown by a dotted line in Fig. 2. It is evident that the two results do not differ significantly, and that T_{BB} varied in 1962 in the same manner as in 1961 to a very high accuracy.

Since we observe Venus in different orientations in an inertial frame of reference from one conjunction to the next, we would expect systematic differences in the run of T_{BB} observed at different conjunctions if the pole of Venus was markedly tilted and there was an appreciable pole-to-equator temperature difference. The lack of such a systematic difference indicates either that the pole is nearly perpendicular to the ecliptic, or that there is a small pole-to-equator temperature difference at the planetary surface. It is also evident that the radio emission from Venus changes very little over periods of at least 18 months, a situation consistent with either the greenhouse or aeolosphere theories, but unlikely with an ionospheric theory.

Assuming that the run of T_{BB} was identical in 1961 and 1962, it is possible to combine the data from the two conjunctions to produce a more accurate mean phase curve for Venus. This is

$$T_{BB}=\underset{(6)}{622}+\underset{(12)}{41}\ \cos(i\pm\underset{(9)}{21})°\text{K}. \qquad (3)$$

Mayer, McCullough, and Sloanaker (1963) have made a similar analysis of their data and obtain for a wavelength of 3.15 cm

$$T_{BB}=\underset{(7)}{621}+\underset{(9)}{73}\ \cos(i\pm\underset{(33)}{11.7})°\text{K}.$$

Thus there is remarkably good agreement between the values of the constant term found at 10- and 3-cm wavelengths, indicative that the radiation is emitted from a solid surface whose emissivity does not vary at centimeter wavelengths.

However, there is a statistically significant difference in the amplitude of the variable term. This implies that Venus is not in synchronous rotation. The phase effect is a measure of the diurnal temperature variation in the radiating layers. Were the planet in synchronous rotation, any element of the surface would be subjected to virtually the same ambient temperature at all times, and the element of surface would acquire this temperature to great depths. We would thus observe this temperature at all wavelengths, despite the fact that radiation at different wavelengths emanates from different depths below the surface. The mean disk temperature at a given i, the net effect of many such elements, would then be independent of wavelength. The same phase effect would be observed on all frequencies. However, when a planet is not in synchronous rotation, a surface element is subjected to a diurnal temperature

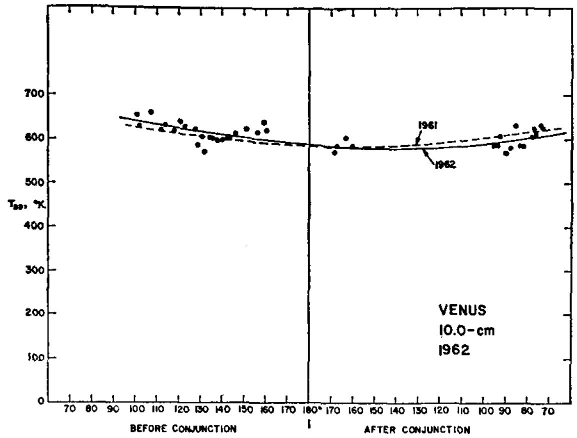

FIG. 2. Observed values of equivalent blackbody disk temperature vs phase angle i, 1962 inferior conjunction.

variation, causing a temperature wave to be transmitted below the surface. The amplitude of this wave decreases with depth, so that deeper layers have a smaller diurnal temperature variation. Since longer wavelengths emanate from deeper layers, we would observe a smaller phase effect at longer wavelength. This is the situation observed, arguing strongly for nonsynchronous rotation.

The mean error of the observed phase lags can be used to determine the probability that the minimum T_{BB} occurs after inferior conjunction. This probability is 0.96 for the 1962 data, and 0.94 for the 1961 data. The probability given by the combined data of 1961 and 1962 is 0.991. Thus it is extremely probable that the minimum T_{BB} occurs after inferior conjunction. This is consistent with retrograde rotation, if the planetary meteorology is similar to terrestrial meteorology, in which the maximum daily temperature usually occurs after noon, and the minimum temperature usually after midnight. Thus, unless a peculiar meteorology exists, retrograde rotation is indicated by the data, consistent with the radar results of Carpenter, presented in a companion paper in this issue.

II. 21.4- AND 40-CM OBSERVATIONS

During the period 21 November through 4 December 1962, Venus was observed at 21.4 and 40 cm with the NRAO 300-ft transit radio telescope. Conventional Dicke radiometers with superheterodyne receivers were used, except that a tunnel-diode amplifier with a noise temperature of about 300°K was used as a preamplifier with the 21.4-cm radiometer. Observations consisted of drift curves as the planet crossed the antenna beam. An argon noise tube calibration signal was measured immediately before and after each observation. The source flux density was computed by measuring the area under the response curve generated by the source transit, and comparing this integral with the integrals obtained in a similar manner for the radio sources 3C123, 3C348,

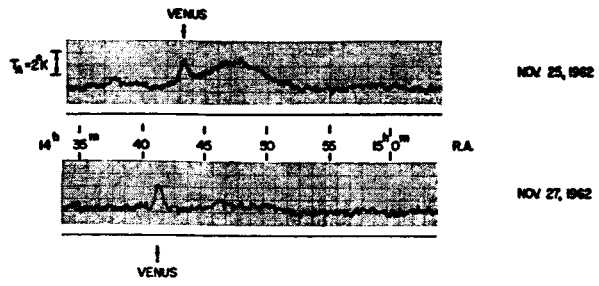

FIG. 3. 21.4-cm wavelength drift curves at the declination of Venus, NRAO 300-ft telescope, 5-sec time constant.

and 3C353. The flux densities assumed for these sources, in flux units, were at 21.4 cm: 3C123, 50.1, 3C348, 44.7, and 3C353, 56.2; at 40 cm they were 3C123, 78.0, 3C348, 89.0, and 3C353, 96.0. The gain of the 300-ft telescope varies by as much as 10% with changing declination; the gain versus declination function has been established by the observation of many sources. Corrections were made to the observed source intensities for this effect. Since the calibration sources were at declinations close to those at which Venus was observed, errors in the gain-declination relation will introduce negligible errors in the computed values of T_{BB}.

Figure 3 shows two of the 21.4-cm analogue tracings of Venus made with a 5-sec time constant. The response caused by the Venus radiation is readily visible. The tracings also contain large "zero drifts" or apparent "extended sources" centered near right ascension 14 h, 47 min. These are a result of sidelobe pickup of solar radiation. They produced considerable uncertainty in the records of 21 to 25 November at 21.4 cm and these records were discarded. Seven excellent records, with no significant solar effects, were obtained during the period 27 November through 4 December. The values of T_{BB} given by these records range between 447° and 580°K. The mean of all the values of T_{BB} from acceptable records is

$$T_{BB\ 21.4} = 528 \pm 33°\text{K (m.e.)}.$$

The mean phase angle for the observations used was $i = 142°$K, after inferior conjunction.

All of the 40-cm records were considerably confused by sidelobe pickup of solar radiation. The observed values of T_{BB} varied between 260° and 720°K during the period 29 November through 4 December when the solar interference was least. The mean value of T_{BB} from six observations of this latter period is $T_{BB} = 400 \pm 60$°K (m.e.). Because of the small number of observations, and the solar interference, the statistical error of 60°K given by the observations should be treated with suspicion, and may be an underestimate of the true error in the above value of T_{BB}.

Nevertheless, the results here indicate that the Venus spectrum approximates closely to a blackbody spectrum to wavelengths of 40 cm. Gibson and Corbett (1963) have measured $T_{BB} = 520 \pm 40$°K (p.e.) at 1.35-cm wavelength. This, with the above results, shows that the Venus microwave spectrum is a very close approximation to a blackbody spectrum over a wavelength interval of 30/1. As previously discussed in the 1961 paper, this is a strong argument for the idea that the emission originates at the planetary surface. Lastly, these results give no evidence for nonthermal radiation from radiation belts, such as are observed with Jupiter. This is to be expected, in view of the lack of magnetic field indicated by the Mariner 2 magnetometer observations.

REFERENCES

Drake, F. D. 1962, *Publ. Natl. Radio Astron. Obs.* 1, 165.
Gibson, J. E., and Corbett, H. H. 1963, Report 5937, Office of Naval Research, Naval Research Laboratory, Washington, D. C.
Mayer, C. H., McCullough, T. P., and Sloanaker, R. M. 1963, *Mem. Soc. Roy. Sci. Liege* 7, 357.

4/6

From the ASTRONOMICAL JOURNAL
69, No. 1, 1964, February—No. 1316
Printed in U. S. A.

Observations of Venus, the Region of Taurus A, and the Moon at 8.5-Millimeter Wavelength

V. L. LYNN, M. L. MEEKS, AND M. D. SOHIGIAN
Lincoln Laboratory, Massachusetts Institute of Technology, Lexington 73, Massachusetts*

A precisely calibrated 28-ft antenna, operating at a wavelength of 8.5 mm with a beamwidth of 4.3 min, has been utilized to observe emission from Venus near inferior conjunction, from the region of Taurus A, and from the moon. Simultaneous observations at 12 mm with the same antenna were also performed.

The mean brightness temperature of Venus, observed approximately one month after inferior conjunction, was found to be 380 (+72, −34)°K, in close agreement with previously reported results. Observations of Taurus A in the millimeter band have been previously reported only by Kuz'min and Salomonovich (1961) at 8 mm. They observed the presence of a second source to the east of Taurus A. Some evidence was found to support the existence of this second source, but the results are inconclusive. Taurus A was found to have a width of 2.4±0.5 min in right ascension. Based on a Guassian distribution of brightness and circular symmetry with this half-intensity width, the flux density is found to be $[260(+80, -55)]\times10^{-26}$ W m^{-2} cps^{-1}. The mean central brightness temperature of the moon was observed to be 254±20°K.

I. INTRODUCTION

DURING a period of nine days in December 1962 a series of joint radiometric observations was made by groups from Lincoln Laboratory and from the Research Laboratory of Electronics. These measurements were made simultaneously at wavelengths of 8.5 and 11.8 mm with the precision 28-ft paraboloid antenna at Lincoln Laboratory. The primary goal of the observations was the determination of the mean brightness temperature of Venus near the time of inferior conjunction. In addition, some other measurements were made, notably in the region of Taurus A.

This paper is concerned with the 8.5-mm measurements; the results at 1.18 cm are reported in a companion paper in this issue. A more detailed account of the equipment, measurements, and data reduction described herein can be found in a Lincoln Laboratory Report (Lynn, Meeks, and Sohigian 1963).

II. EQUIPMENT

The antenna consists of a 28-ft paraboloid with a modified form of Cassegrainian feed. A length of oversize circular waveguide operating in the TE_{11} mode extends along the axis from an equipment housing behind the vertex to a point several wavelengths from the secondary reflector, a 5-in.-diameter flat, circular plate. An antenna pattern range is an important, integral part of this system and is available for periodic monitoring of the radiation characteristics. With this range, the antenna has been measured extensively under varied conditions of wind and solar heating. The results of this evaluation, summarized in Table I, are given in detail elsewhere (Fitzgerald, Lynn, and Keeping 1963). The antenna is installed on an azimuth-elevation drive system and is directed either manually by means of boresighted optical telescopes at the controls or by reference to synchro readouts and precomputed azimuth-elevation positions.

* Operated with support from the U. S. Army, Navy, and Air Force.

A microwave, frequency-separating filter divided the signal between the two radiometers and was preceded by a weakly coupled, gas-discharge noise source providing a calibration signal common to both receivers. The 8.5-mm radiometer was a conventional Dicke system with a sensitivity, referred to the antenna focal point, of approximately 2°K per sec. The receiver characteristics are given in Table II.

Noise-balancing was accomplished at rf by adding noise to the antenna input with another gas-discharge source and utilizing a precisely calibrated variable-coupling system. Both the calibration source, used for comparison with Venus and Taurus signals, and the balance source, used in conjunction with the lunar signals, were calibrated by comparison with thermal loads.

TABLE I. Measured antenna parameters at 8.5 mm.

Gain above isotropic level	67.5±0.5 dB
Effective area	31.5±1.5 m^2
Half-power beamwidth	4.3±0.1 min
Aperture efficiency	55±5%
Feed-line loss	1.4±0.1 dB
Cross-polarized pattern below peak gain	>20 dB

III. PROCEDURES

Observation of Venus employed two basic modes of operation. In the first, the antenna beam was fixed in azimuth-elevation coordinates and permitted to drift

TABLE II. Radiometer characteristics.

Mixer noise temperature	3000°K
Image rejection	none
i.f. frequency	35 Mc/sec
i.f. bandwidth, 3 dB	14 Mc/sec
i.f. bandwidth, 1 dB	10 Mc/sec
L. O. frequency	35.2 Gc/sec
Switching frequency	1 kc/sec
Video time constant	5 sec[a]

[a] 1 sec for atmospheric emission temperature observation.

across the planet in right ascension. These drift scans, recorded in analogue form, were converted to digital form at 1-sec intervals and further reduced by digital computer. Since many scans were such that the beam center and the source center were not quite coincident, the slight corrections required in antenna gain and in right-ascension position were applied. Then, before averaging, the individual runs were compared with calibration signals, normalized to a constant range and corrected for atmospheric absorption.

In the second method, Venus was optically tracked with the following sequence: a point approximately four beamwidths away from the planet was tracked for a period of at least 60 sec; then the beam was shifted directly onto Venus for a like period; and finally, the beam again tracked off the source. These on–off tracking data were examined to find the deflection due to emission from Venus, compared with the calibrations, normalized for solid angle, and corrected for atmospheric absorption as before.

The observations of the region of Taurus followed the first method described for Venus except that, of course, no solid-angle normalization was used. Similar techniques were utilized in lunar observation, but the reduction was completed manually.

Path attenuation was determined by observation of the atmospheric emission temperature as a function of zenith angle. Several measurements were made during this period of clear, cold weather and the results extrapolated, using ground-level and radiosonde meteorological data, to cover the experimental period. The zenith-path absorption during these observations varied in the range 0.15 to 0.18 dB.

IV. RESULTS

Venus

The average of 152 drift-scan curves for Venus is shown in Fig. 1. The solid curve is a Gaussian, machine-fitted to the data points by the method of least-squares. The standard deviation of the data is almost a factor of 5 greater than would be anticipated from equipment and data-reduction considerations. The source of this discrepancy is unknown and it raises doubts about the accuracy of the planetary brightness temperature that is derived from the drift scans. After correction for the radiometer time constant, these data yield a value for corrected antenna temperature of 11.5°K. The mean value for the on–off tracking data was found to be 12.5°K with a standard deviation of 0.5°K.

The estimated uncertainty in these values has limits of +19% and −9%, predominantly positive because of the nature of the antenna-pointing errors. A thorough study of the data and uncertainties leads us to believe that the tracking measurements are the more reliable and we have adopted the value for corrected antenna temperature, $T_A = 12.5°\text{K}(+19\%, -9\%)$. This corresponds to a mean brightness temperature for Venus of $380(+72-34)°\text{K}$.

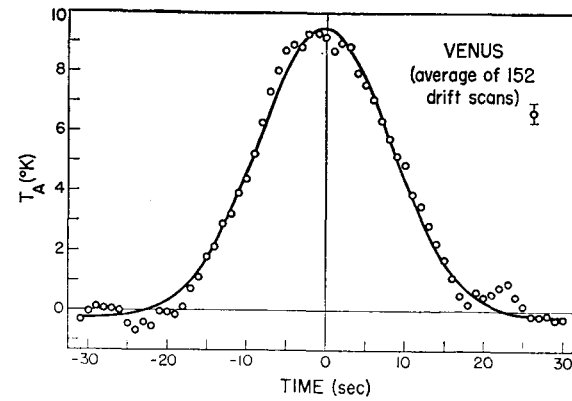

FIG. 1. The average antenna temperature vs time for 152 drift scans of Venus. The antenna-temperature values have been corrected for atmospheric opacity and for small variations in gain when the planet failed to intersect the exact center of the beam. The solid angle of the planet has been normalized to inferior conjunction. The smooth curve represents a fitted Gaussian function. The standard deviation of the data points is indicated in the upper right corner of this figure.

Taurus

Figure 2 shows the averaged response for 18 drift scans through the region of Taurus A. The data point for each second represents the 5-sec average for data centered at that point, this in addition to the time-constant smoothing, to remove fluctuation within one *RC* time constant. The fluctuations found in these averaged data are consistent with the expectations based on equipment and reduction processes. The standard deviation of the data is indicated by the dashed horizontal lines.

The source Taurus A appears at the expected position and, in addition, there is evidence of a second source at the same declination but at a right ascension about 30 sec greater. A similar second source has been reported by Kuz'min and Salomonovich (1961) at a position 36 sec east of Taurus A. A double Gaussian curve has been fitted to the data points by the method of least-squares, assuming that two sources are present. This fit is shown in Fig. 2 as a solid line.

After correction for the receiver time-constant, the peak antenna temperature for Taurus A is found to be 2.2°K. The right-ascension width of Taurus A, assuming that both the source brightness distribution and the antenna pattern can be represented by Gaussian functions, and following the method of Barrett (1961), is determined to be 2.4±0.5 min of arc. The uncertainty was derived by estimating that the width of the fitted curve might be uncertain by about 1 sec of time.

Recently Little (1963) has measured the intensity distribution of Taurus A at a wavelength of 9.1 cm. The source was found to have an elliptical shape with dimensions and orientation such that the central right-ascension half-intensity width was 3.2 min. Our meas-

ured value of 2.4 min is not consistent with this report and the 9.1-cm dimensions are assumed to be invalid at 8.5 mm. For lack of better information as to shape and distribution, it was assumed that the source was circularly symmetric with a Gaussian brightness distribution of half-intensity width, 2.4 min. On this basis, the observed value of Taurus A flux is found to be $[260(+80, -55)]\times 10^{-26}$ W m^{-2} cps^{-1}, where the estimated uncertainty is again predominantly positive because of the nature of the antenna-pointing errors. The uncertainty given does not include consideration of the possible source size and shape. The polarization of the antenna for these measurements was horizontal, corresponding to an electric-vector position angle of 43 deg, measured from north toward east on the celestial sphere.

Evidence of the second Taurus source needs to be evaluated carefully. The Gaussian least-squares fit corresponds to an antenna temperature of 0.55°K with a width between half-maxima of 12.5 sec as compared to the value of 18.6 sec corresponding to a point source at this declination. The antenna temperature, as can be seen in Fig. 2, is a little over twice the estimated standard deviation and the width of the fitted curve is too narrow by 33%. Hence, the data of Fig. 2 must be considered as a probable, but not certain, indication of a second source at nearly the same declination but with about 30 sec (or 7.0 min of arc) separation in right ascension. The Soviet workers (Kuz'min and Salomonovich 1961) reported a second source at about 36 sec greater right ascension and our measurements would seem to lend support to their observations. However, it should be noted that Barrett (1961) at 1.8-cm wavelength failed to find a source at this position even though his antenna had a beamwidth of 3 min and gave an antenna temperature of 6.9±0.2°K on Taurus A. This points to a most unusual spectrum for the second source, a spectrum that very much calls for more accurate measurements at this wavelength and additional measurements at higher frequencies.

Moon

Three drift-scan observations were made through the lunar center approximately one day after full moon (lunar phase 192 deg) with a mean corrected antenna temperature in the central region of 226°K. Numerical integration of the well-defined antenna pattern indicated that 89% of the energy observed originated within a solid angle equal to that subtended by the moon.

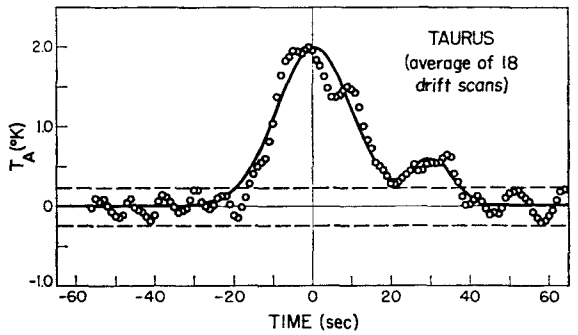

FIG. 2. The average antenna temperature vs time for 18 drift scans of Taurus A. The smooth-fitted curve in this figure includes two Gaussians, one for Taurus A centered at $t=0$ sec and the other corresponding to a probable second source at $t=30$ sec. Dashed lines correspond to deviations from the base line of $\pm\sigma$, the standard deviation of the averaged data points. The same corrections, except for solid angle, have been applied here as in Fig. 1.

With an assumption of uniform brightness of the moon, justified by consideration of the nearly flat response curve at this lunar phase angle and the greater contribution from antenna-pattern weighting near the even more flat central section, the mean central brightness temperature of the nearly full moon was determined to be 254°±20°K.

ACKNOWLEDGMENTS

The authors are indebted to many of their associates at Lincoln Laboratory for assistance with this work. Particular mention should be made of the continued, enthusiastic support and counsel of Jerome Freedman and Dr. J. W. Meyer. Special thanks are also due Herbert Ecklund and Virginia and William Mason for the great assistance rendered in the data-reduction processes.

Many helpful discussions were held with Dr. A. H. Barrett and David Staelin of the MIT Research Laboratory of Electronics and Dr. J. Copeland of the Ewen-Knight Corporation, contributed immeasurably during the instrumentation phase.

REFERENCES

Barrett, A. H. 1961, *Astrophys. J.* **134**, 945.
Fitzgerald, W. D., Lynn, V. L., and Keeping, K. J. 1963, Rept. 46G-4, Lincoln Laboratory, Massachusetts Institute of Technology, Lexington 73, Massachusetts.
Kuz'min, A. D., and Salomonovich, A. Ye. 1961, *Dokl. Akad. Nauk SSSR*, **140**, 81.
Little, A. G., 1963, *Astrophys. J.* **134**, 164.
Lynn, V. L., Meeks, M. L., and Sohigian, M. D. 1963, Tech. Rept. TR 330, Lincoln Laboratory, Massachusetts Institute of Technology, Lexington 73, Massachusetts.

4/9

From the ASTRONOMICAL JOURNAL
69, No. 1, 1964, February—No. 1316
Printed in U. S. A.

Observations of Venus at 2.07 cm

T. P. McCULLOUGH AND J. W. BOLAND
E. O. Hulbert Center for Space Research, U. S. Naval Research Laboratory, Washington, D. C.

Observations of radiation from Venus at 2.07-cm wavelength on four days during the interval 20 February to 25 March 1963 are reported. The average equivalent blackbody temperature for Venus derived from the observations is 500±70°K (p.e.).

MEASUREMENTS of radio emission from Venus have been made by several investigators at wavelengths between 4 mm and 21 cm. Based on the assumption that the radiation is of thermal origin, a blackbody temperature for Venus of about 600°K is obtained for wavelengths between 3 and 21 cm, while wavelengths shorter than 1 cm have indicated lower temperatures, about 350° to 400°K. The results of these observations at 2.07 cm are presented to provide radio data for the spectrum of Venus in the interval between 1 and 3 cm.

Radio emission from Venus at 2.07-cm wavelength was observed on four days during the period 20 February–25 March 1963 using the 50-ft reflector of the Naval Research Laboratory in Washington. This period occured about four months after the inferior conjunction of November 1962 and corresponds to a range of phase angles for Venus of 75 to 61 deg. Unfavorable weather conditions limited these observations and they were terminated because of a limiting signal-to-noise ratio.

The apparatus used for these observations was designed around the Dicke system and is basically the same as has been previously described (Mayer, McCullough, and Sloanaker 1958). The output time constant of the radiometer was about 2 sec and the rms fluctuations in the output record averaged about 0.4°K. The antenna temperatures were calibrated against thermal noise sources using a gas-discharge noise source as an intermediate standard.

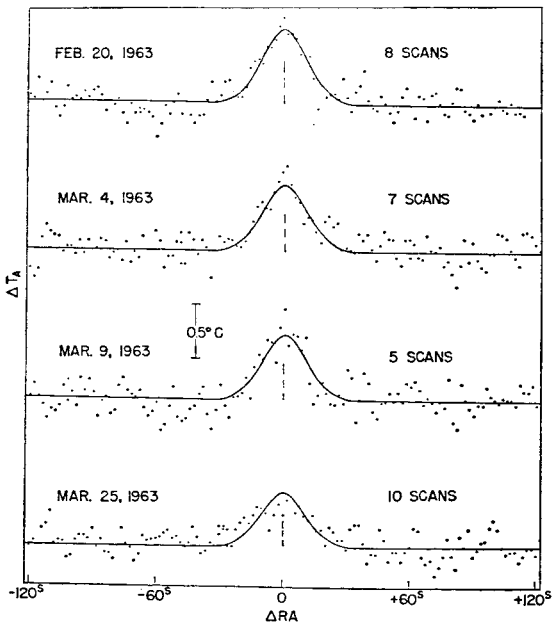

FIG. 1. Average drift scans for each day of observation of Venus at 2.07-cm wavelength with antenna pattern superimposed.

The reception pattern of the antenna was nearly Gaussian in cross section with a half-power diameter of about 5.6 min of arc. The aperture efficiency for the antenna of 56% was estimated from the measured diameters and antenna temperatures of Cas A and Tau A and the published spectra of these sources (Conway, Kellermann, and Long 1963).

A total of 120 right-ascension drift scans were made through or near the planet. The drift scans were made at 2-min-of-arc intervals above, through, and below the predicted declination of Venus. The data were grouped by declinations and averaged to reduce the effect of noise fluctuations. This procedure reduced the data to 16 average drift scans, four for each of the four days of observations. Antenna patterns were fitted to the average curves to obtain antenna temperatures, which were in turn plotted to determine the peak declination and antenna temperature for the day. The average drift scans for each day of observation at the predicted declination of Venus are shown in Fig. 1. Final results have been corrected for atmospheric absorption and uncertainty in pointing the antenna.

Over the observing period, the antenna temperature ranged from 0.70° to 0.54°K. Based on the solid angle of the visible disk of Venus and the weighted antenna temperature for each day, an average equivalent blackbody temperature of 500°±70°K is obtained. On the assumption that the microwave emission for Venus is of thermal origin, and that it originates at or near the surface of the planet, Barrett (1960) has made calculations for attenuation in the atmosphere to show that the reduction in blackbody temperature at millimeter wavelengths may be accounted for by absorption in the atmosphere. The value of 500°K obtained here agrees well with the various model atmospheres proposed by Barrett (1960) for which the atmospheric pressure is between 10–30 terrestrial atm.

REFERENCES

Mayer, C. H., McCullough, T. P., and Sloanaker, R. M. 1958. *Proc. IRE* **46**, 260.
Conway, R. G., Kellermann, K. I., and Long, R. G. 1963, *Monthly Notices Roy. Astron. Soc.* **125**, 261.
Barrett, A. H. 1960, *Astrophys. J.* **133**, 281.

68
370

From the ASTRONOMICAL JOURNAL
69, No. 1, 1964, February—No. 1316
Printed in U. S. A.

Observations of Venus, the Sun, Moon, and Tau A at 1.18-cm Wavelength*

D. H. STAELIN, A. H. BARRETT, AND B. R. KUSSE
Research Laboratory of Electronics, Massachusetts Institute of Technology, Cambridge, Massachusetts

During December 1962 observations were made of Venus, the sun, moon, and Tau A at 1.18-cm wavelength ($f=25.5$ Gc/sec). A 6.0-min beamwidth was obtained by using the paraboloid reflector, of 28-ft diameter, at Lincoln Laboratory, MIT. The radiometer was a Dicke-type superheterodyne with a bandwidth of 8 Mc/sec and a sensitivity of 2.5°K, with a 5-sec integration time.

The average brightness temperature of Venus as determined by 94 drift curves and 42 on–off measurements was 395(+75, −55)°K. Twenty drift curves of Tau A give a flux density of $(295\pm85)\times10^{-26}$ W m^{-2} cps^{-1} when we assume a disk of uniform brightness, 3.6 min in diameter. The brightness temperature of the sun was determined to be 8870±980°K, and the observations of the moon yielded brightness temperatures for the center of the moon of 240±40°K 3.5 days before full moon, 254±30°K 0.3 day before full moon, and 254±30°K 1.8 days after full moon.

The typical zenith attenuation encountered was 0.2 dB, determined by observations of the sun and the sky-brightness temperature. The antenna gain, 64.6±0.5 dB, was determined by scaling the gain measured at 35.2 Gc/sec and by measurements of the beam shape, sidelobe level, and magnitude determined from the solar and lunar data.

DURING December 1962 observations were made of Venus, Tau A, the sun, and the moon at 1.18-cm (25.5 Gc/sec) wavelength. They were made in conjunction with simultaneous 8.5-mm measurements by Lynn, Meeks, and Sohigian at the Lincoln Laboratory of the Massachusetts Institute of Technology. The antenna was the Lincoln Laboratory azimuth-elevation-mounted 28-ft paraboloid located at Lexington, Massachusetts. In these simulaneous observations the same antenna feed and a microwave frequency-separating filter for dividing the signal between the two radiometers were used. One calibration noise tube weakly coupled to the antenna feed line calibrated both radiometers simultaneously. The 8.5-mm observations are described in a companion paper presented in this issue.

The 1.18-cm receiver was a modified Dicke radiometer with a ferrite switch to compare the antenna signal with that from a matched load at room temperature. A 10-dB directional coupler was used to introduce into the antenna feed enough noise signal to balance the antenna temperature with the matched load. The ferrite switch was followed by a balanced mixer incorporating matched 1N26C crystals. The i.f. amplifier had a bandwidth of 8 Mc/sec centered about 30 Mc/sec. The synchronous detector was switched at 94 cps and had a time constant of 5 sec for most observations. The receiver ΔT_{rms} was approximately 2.5°K evaluated at the antenna feed horn.

The calibration noise tube introduced into the antenna feed line a signal equivalent at the feed horn to 15.1±0.27°K. This test source was calibrated by comparison with matched loads immersed in water baths at different temperatures. The observations of the sun and the moon were calibrated by using the balance noise tube. Calibration amplitudes of approximately 1500°K and 150°K, respectively, were used for these sources. This noise tube was calibrated by using matched loads immersed in water and in liquid nitrogen. During these calibrations of the noise tubes, a ferrite isolator inserted between the calibration signals and the radiometer eliminated errors caused by changes in VSWR.

The atmospheric attenuation was determined by using observations of the sun and of sky-brightness temperature as functions of elevation angle. These observations yielded a relation between atmospheric attenuation and ground-level humidity. This relation was then used in conjunction with continuous observations of ground-level humidity to determine the zenith attenuation. Typical measured values for zenith attenuation were 0.15–0.20 dB. The attenuation was low because of the very cold clear weather that prevailed during a great part of the experiment. Ground-level humidity typically was 1.4 g/m^3.

The 67.5±0.5 dB antenna gain at 8.5 mm was obtained by the method described in the companion paper. The antenna gain at 1.18 cm was determined by scaling the gain measured at 8.5 mm, and was checked by using the solar and lunar data. For this check the solar-drift scans were used to determine the beamwidth and relative sidelobe level. The beamwidth was determined by differentiating the solar-drift curves and correcting for the effects of sidelobes and finite thickness, ~0.1 min of the sun's edge at 1.18 cm. This yielded a half-power beamwidth of approximately 6.0 min of arc. The relative sidelobe level was determined by measurements of the amplitudes of the wings of the solar-drift scans.

The values of lunar brightness obtained by other observers at nearby frequencies were averaged to give the estimate of true temperature. The average used was 215°K plus a 37°K sinusoidal variation, with a 40-deg phase lag behind the lunar phase. This temperature was combined with the antenna pattern and the measured lunar temperatures to yield an antenna gain of 64.5 dB. The estimated probable error of this procedure was ±0.5 dB.

The antenna gain determined by scaling the 8.5-mm

* This work was supported in part by the U. S. Army Signal Corps, the Air Force Office of Scientific Research, and the Office of Naval Research; and in part by the National Aeronautics and Space Administration (Contract NaSr-101, and Grant NsG-419).

gain was 64.7±0.5 dB. The gain used for determining the brightness temperatures of Venus and Tau A was 64.6±0.5 dB.

Venus was observed primarily on 11, 12, and 13 December 1962. Two series of observations were made: drift scans and off-on-off measurements. The drift scans

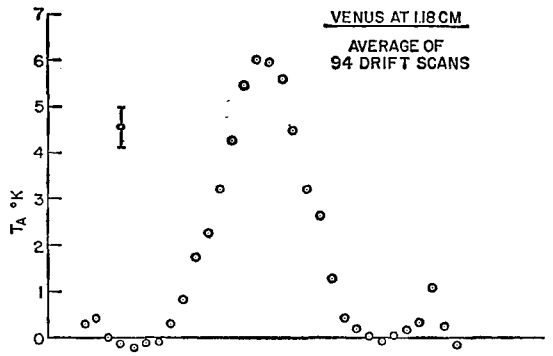

FIG. 1. Average drift curve for Venus.

were taken by placing the antenna beam ahead of the source and holding it stationary while the source drifted past. Samples spaced at 3-sec intervals for 94 drift scans were fed into an IBM 709 computer for averaging. As part of the averaging process, each scan was scaled according to the corresponding atmospheric attenuation, calibration signal amplitude, source solid angle and antenna gain loss resulting from the antenna miss angle. The antenna miss angle is the angle between the source and antenna axis at their closest approach. This angle was measured on a boresighted telescope and usually was ±1 min of arc. The resulting average scan, with the antenna temperature normalized to inferior conjunction, is shown in Fig. 1. After correction for the receiver time constant, this gives an average brightness temperature for Venus of 390°K with +75, −55°K probable error.

Most of the uncertainty is due to the uncertainty of the antenna gain and pointing accuracy. The pointing-accuracy component of the uncertainty, however, is common to both the 8.5-mm and 1.18-cm data. That is, any pointing error would tend to lower the 8.5-mm data more than the 1.18-cm data.

The off-on-off data consisted of positioning the antenna several antenna beamwidths away from the source, on the source, and then off again, each step lasting approximately 2 min. Forty-two observations were averaged to yield a brightness temperature of 400(+75, −55)°K.

The average of these two sets of measurements is 395(+75, −55)°K, which is plotted in Fig. 2, together with the results of several other observers. Many of these other results were obtained during this same inferior conjunction; in particular, Gibson and Corbett's (1963) point at 1.35 cm—the center of a water-vapor resonance. The Mariner 2 spacecraft points reported by Barath *et al.* (1963) are connected by a dotted line. The data are suggestive of a brightness-temperature transition over the small wavelength range 1.18–1.35 cm. Since any spectral features would be very useful in determining the nature of the Cytherean atmosphere, future measurements in this spectral region will be very interesting.

The observations of Tau A were drift scans similar to those taken of Venus, and were processed in the same manner. Twenty drift scans were averaged to obtain an antenna temperature of 2.5°K, which corresponds to an average flux density of $(295\pm85)\times10^{-26}$ W m^{-2} cps^{-1}. The receiver noise dominated the probable error because the signal was quite weak and only a small number of scans were made. The flux value was computed under the assumption that the source was a uniformly bright disk of 3.6-min diameter. If a uniform disk of 5-min diameter is assumed, the result is 325×10^{-26} W m^{-2} cps^{-1}. The observations were made with the polarization 43°±5° from north to east on the celestial sphere.

The sun was observed with 9 drift scans. These yielded a central brightness temperature of 8870°±980°K.

Eight drift scans were made of the moon. These yielded the following central brightness temperatures: 240°±40°K, 3.5 days before full moon; 254°±30°K, 0.3 day before full moon; and 254°±30°K, 1.8 days after full moon.

Both the solar and lunar data were evaluated by assuming uniformly bright disks. The error brackets given for each observation are probable error brackets, and were evaluated by calculating the square root of

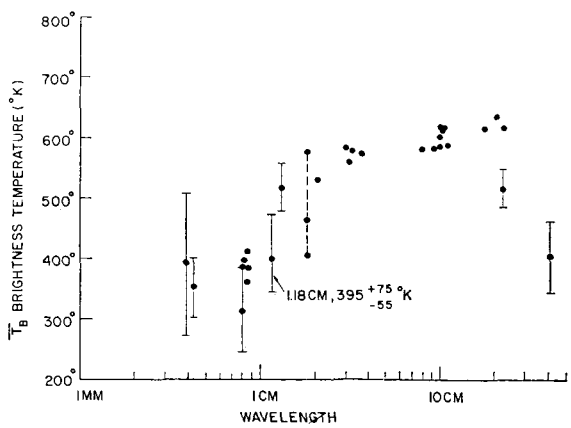

FIG. 2. Experimental spectrum of Venus showing other reported results.

the sum of the mean-square errors for every factor in the final result.

ACKNOWLEDGMENTS

The authors are indebted to many associates for assistance with this experiment and to Lincoln Laboratory,

52

Massachusetts Institute of Technology, for providing many of the facilities. V. L. Lynn and M. D. Sohigian were responsible for the operation of the antenna and for the coordinate calculations. M. L. Meeks cooperated in the data reduction and performed the computer processing of the Venus drift scans. J. W. Meyer assisted greatly in the initial planning of the joint experiment.

REFERENCES

Gibson, J. E., and Corbett, H. H. 1963, *Astron. J.* **68**, 74.
Barath, F. T., Barrett, A. H., Copeland, J., Jones, D. E., and Lilley, A. E. 1963, *Science* **139**, 908.

From the ASTRONOMICAL JOURNAL
69, No. 1, 1964, February—No. 1316
Printed in U. S. A.

Radio Emission from Venus at 8.35 mm*

D. D. THORNTON
Space Sciences Laboratory, University of California, Berkeley

AND

W. J. WELCH
Department of Electrical Engineering and Space Sciences Laboratory, University of California, Berkeley

Observations of the 8.35-mm radio emission from Venus are reported. An average disk temperature of 395°±60°K is obtained for observations during the month prior to the inferior conjunction of November 1962. No fluctuations in excess of 80°K were observed.

I. INTRODUCTION

DURING the month prior to the November 1962 inferior conjunction of Venus, a number of observations of the 8.35-mm emission from the planet were made. The original intent of the program was the investigation of possible variations of the planet's brightness with either phase angle or time. Observations were not continued beyond conjunction because the signal-to-noise ratio in the experiments would not permit measurements to be made over a significantly wide range of phase angles. At the point where the signal-to-noise ratio was greatest, just at conjunction, individual drift scans were compared and found not to be significantly different. An average of all the scans was therefore computed and is presented in this paper.

II. PROCEDURE

The antenna used for these measurements is a 10-ft-diameter aluminum reflector, cast and machined at the U. S. Naval Shipyard in Norfolk, Virginia. A description of the apparatus and calibration procedures used is given in some detail elsewhere (Thornton and Welch 1963), and only a summary of the essential parameters will be included here. The measured antenna gain is 5×10^5 with a probable error of 10%, and the antenna beamwidth is 12.0 min. Accurate pointing of the antenna within 1 min is accomplished by means of an optical sighting telescope. The Dicke-type radiometer has a noise temperature of 2500°K, a bandwidth of 30 Mc/sec, and output fluctuations amounting to about 0.2°K rms with a 5-sec integration time. Gain stability is 0.1% over a 30-min interval. The reference input termination for the Dicke radiometer consists of a small horn of approximately 20 deg beamwidth oriented along the axis of the main antenna beam.

The manner of observation consisted of pointing the antenna west of the planet and allowing the planet to drift through the beam with the antenna stationary. The period for each scan was about 8 min. On any given day, 16 was the maximum number of scans made. The output from the radiometer was recorded in analogue form on strip charts. In order to obtain an average for one day's scans, the individual scan records were combined and averaged in pairs. In addition, the data were transcribed onto IBM cards from the analogue records at 5-sec intervals and reduced by means of a digital computer. The instant of transit of the planet past the cross hair of the sighting telescope was carefully noted so that the individual scans could be aligned within a few seconds of arc.

The atmospheric absorption was inferred from measurements of the antenna temperature as a function of zenith angle. Typical normal optical depths were found to be in the range of 0.05 to 0.06 nepers. In addition to the correction for atmospheric absorption, the effect of the distortion of the drift curves due to the inertia of the integrator was also taken into account. The integrator circuit consists of two simple RC filters in cascade, and with each set for a 5-sec time constant the maxima of the drift curves were reduced by 5% due to this effect.

* Support for this work has been provided by the Office of Naval Research through contract Nonr 222(54) and the Atmospheric Sciences Program of the National Science Foundation, grant NSF G-16741.

54

III. OBSERVATIONS

The result of averaging 16 scans taken on 17 October is shown in Fig. 1, the average obtained by combining the analogue records in pairs. As discussed above, an average was also performed by a digital computer. The peak value was obtained by making a best fit of a Gaussian curve to the data, the Gaussian being a good

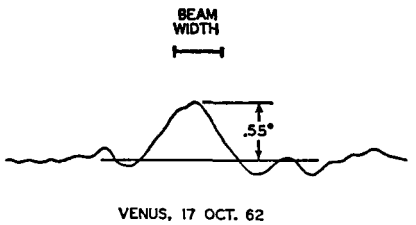

FIG. 1. The average of 16 drift scans of Venus taken on 17 October, 1962, about four weeks before inferior conjunction. The ordinate is antenna temperature.

approximation to the antenna pattern, and, with the corrections discussed above applied, the disk temperature derived from the average is 380°K. The computer also calculated the rms noise in the wings of the average curve yielding a value of 14% of the peak value. Further observations on 6 November and 7 November were treated in the same manner, yielding brightness temperatures of 407 and 417°K, respectively, not significantly different from the 17 October result.

The planetary radiation was apparent on individual drift scans. These scans were compared and no differences between them were found greater than the rms noise calculated for the wings of each drift scan by the computer. Whatever fluctuations are present in the disk temperature at intervals between 8 min and 2 h are therefore less than 80°K. An over-all average for the scans was computed, assuming the disk temperature to be constant. The resulting brightness temperature is 395°K. The probable error is 60°K including both the residual noise on the traces and the systematic errors, the primary source of the latter being the inaccuracy in the antenna gain determination.

IV. CONCLUSION

No variations with time or with respect to phase angle over the small range of about 10 deg which could be accurately investigated were observed in the disk temperature. The over-all average of 395°±60°K is in good agreement with the values of 410(+30, −20)°K obtained by Gibson (1963) and 374°±75°K obtained by Kuz'min and Salomonovich (1963) during the inferior conjunction of 1961. It is also very close to the value of 360°±100°K reported by Copeland (private communication) and the result 380(+72, −34)°K reported by Lynn (private communication) for the November 1962 conjunction. An average of all these results is 384°K, to which one could assign a probable error of about 20°K.

The brightness temperature of 8-mm radiation from Venus near inferior conjunction appears to be fairly accurately established. It remains to confirm the phase variation observed by Kuz'min and Salomonovich (1963). This is especially important since their results indicated that the minimum temperature occurs prior to inferior conjunction at 8 mm, whereas both at 3 cm (Mayer 1961) and at 10 cm (Drake 1962) a minimum after inferior conjunction is indicated. Finally, finding the precise reason for the 8-mm emission temperature being lower than the longer wavelength radiation will require a careful measurement of the brightness temperature over the range from 0.6 to 3.0 cm.

ACKNOWLEDGMENT

It is a pleasure to acknowledge the assistance of W. Caton and the interest and encouragement of Professor S. Silver and Dr. D. Rea.

REFERENCES

Drake, F. 1962, *Publ. Natl. Radio Astron. Obs.* **1**, 165.
Gibson, J. E. 1963, "The Brightness Temperature of Venus at 8.6 mm," *Astrophys. J.* **137**, 611.
Kuz'min, A. D., and Salomonovich, A. E. 1963, "Observations of Radio Emission from Venus and Jupiter at 8 mm Wavelength," *Soviet Astron.—AJ* **6**, 518.
Mayer, C. 1961, *The Solar System, Vol. III, Planets and Satellites*, edited by G. P. Kuiper and B. M. Middlehurst (University of Chicago Press, Chicago), p. 473.
Thornton, D. D., and Welch, W. J. 1963, "8.35 mm Radio Emission from Jupiter" (to be published).

55

From the ASTRONOMICAL JOURNAL
69, No. 1, 1964, February—No. 1316
Printed in U. S. A.

Some Decimeter Observations of Venus During the 1962 Conjunction*

B. G. Clark and C. L. Spencer
Owens Valley Radio Observatory, California Institute of Technology, Pasadena, California

The flux from Venus was measured at various frequencies, giving blackbody disk temperatures of 580 ±60°K at 10.7 cm, 596±100°K at 18 cm and 616±100°K at 21 cm.

An attempt was made to measure the size of the planet at a wavelength of 9.4 cm with an interferometer with a baseline of 5184 wavelengths aligned east–west. Only a very small part of the amplitude-spacing spectrum was observed, but the observations are not what would be expected of a uniform or limb-darkened disk.

I. INTRODUCTION

NEAR the inferior conjunction of Venus in 1962, various measurements were carried out at the Owens Valley Radio Observatory with a variable-spacing interferometer consisting of two 90-ft equatorially mounted paraboloids. These measurements were carried out in conjunction with other programs, and for the most part the telescopes were involved with Venus measurements only when Venus was near culmination.

The measurements fall naturally into two groups. The first is a set of short baseline measurements in September-October of the flux coming from the planet at frequencies of 1420 and 1666 Mc/sec, and several scattered measurements made at 2841 Mc/sec. The second is an attempt to measure the angular diameter of the planet with a baseline of 5180 wavelengths at a frequency of 3184 Mc/sec.

All measurements were made with each antenna having a balanced crystal mixer with each half of the mixer followed by its own i.f. preamplifier, whose outputs were combined in such a phase as to cancel the noise from the klystron local oscillator. The signals from the two antennas are then multiplied together to form the interference fringes. The i.f. bandpass is approximately 4 Mc/sec at 10 Mc/sec.

Table I. Results of Venus flux measurements.

Frequency (Mc/sec)	Date	Spacing (λ)	Disk temp. (°K)
2841	10/29	600	586
2841	12/3	300	574
2841	Average		580
1666	10/10	350	572
1666	10/11	350	622
1666	Average		596
1420	9/26	300	630
1420	9/27	300	908
1420	9/27	300	865
1420	9/27	300	849
1420	9/28	300	343
1420	9/29	300	410
1420	10/1	300	307
1420	Average		616

* This work was supported by the U. S. Office of Naval Research under Contract Nonr 220(19).

II. FLUX MEASUREMENTS

1. At 2841 Mc/sec

At this frequency, Venus near conjunction is a powerful and conspicuous source with the interferometer. It is possible to reduce the uncertainty due to noise below the uncertainty in absolute flux calibration in only a few minutes of observing time. Sometimes the amplitude of the interference fringes was simply read from a chart record, and in other cases an electromechanical integrating system was used (Morris, Clark, and Wilson 1963). The flux from Venus was compared with the flux from the radio source 3C295. The absolute flux of 3C295 was taken to be 10.8×10^{-26} W m^{-2} cps^{-1} at 2841 Mc/sec, as given by Kellermann (1963) from intercomparisons of several sources of similar strength with the flux from Cas A, Tau A, and Cyg A. The accuracy of the absolute calibration is estimated to be better than 10%. This error is larger than noise and indicates the actual uncertainty in the 10.7-cm fluxes given in Table I.

2. At 1420 and 1666 Mc/sec

At these frequencies the limiting factor in the measurements is the confusion from weak sources in the beam at the same time as the planet. Because of the other programs utilizing the interferometer at the same time, the phase of the confusion signal was not determined with sufficient accuracy to subtract the confusion from the measurements, although the amplitudes of the background sources were observed in all the positions after the planet had left. The very high temperature observed on 27 September is probably due to confusion, as a flux corresponding to a Venus disk temperature of about 300°K was found there after the planet had moved on, though Mills (1960) reports no source there. The fluxes for 3C295 used at these frequencies were also obtained or interpolated from Kellermann (1963), and are 20.0×10^{-26} W m^{-2} cps^{-1} at 1420 Mc/sec and 17.3×10^{-26} W m^{-2} cps^{-1} at 1666 Mc/sec. The estimated uncertainty in the average values given in Table I remains about 150°K and results from confusion.

III. SIZE MEASUREMENTS

In an attempt to measure the size of Venus, the telescopes were placed at a baseline of 1600 ft or 5180

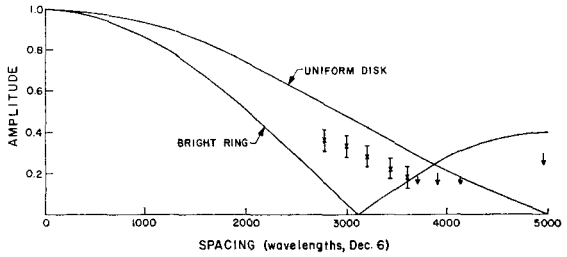

FIG. 1. The observed portion of the amplitude-spacing spectrum of Venus compared with those of a uniform disk and of a thin ring the same diameter as the planet.

wavelengths at 3184 Mc/sec. These measurements were also made with a hybrid mixer-receiver having double sidebands of 4 Mc/sec bandwidth at ± 10 Mc/sec from the center frequency. The antenna was linearly polarized with E vector east–west. The fringe spacing was 40 sec of arc at the meridian, corresponding to slightly less than 3 sec of time. To reduce the fringe period to a convenient value, a phase rotation was introduced into one of the two local oscillators, the rate of which could be adjusted manually to produce a fringe period of about 72 sec. The interferometer output was then run through an RC filter tuned to a 72-sec period, whose bandwidth would correspond to that of a 12-sec time constant. A lumped constant-step variable-delay line and two 1-μsec fixed-cable delay lines, all at i.f., were used to equalize the delay between the two antennas as the hour angle of the source changed (Read 1960). The observing procedure was to set the delay line 25 nsec greater than the setting needed to observe the central fringe of the interferometer, observe the slowed fringes until the central fringe had been observed, and then advance the delay line by 50 nsec. Several small-diameter sources, principally 3C295, were observed to calibrate the sensitivity of the system. Source 3C295 requires about 5% correction for resolution.

Venus was observed at several hour angles to vary the effective baseline. Unfortunately, with the frequency and baseline used, the observations of interest were made at large hour angles, where the behavior of the system is not as well known as at the meridian. The observations were made on 6-9 December and were reduced in both baseline and intensity to December 6.5 UT when the diameter of the planet was 50 sec of arc. The observations are presented in Fig. 1. Also presented are the visibility functions to be expected from a uniform disk and from a thin ring both of 50-sec-of-arc diameter. The error flags indicate the scatter in the observations at a given effective baseline. There are several possibilities for systematic error, especially since the observations of interest were taken at large hour angles and the calibrators were observed rather nearer the meridian. Below are listed some of the possible sources.

(*a*) *An error in the step-delay line.* If the line is not a pure delay, phase coherence is lost and the size of the fringes is decreased. However, these delay lines have previously proved satisfactory for similar baselines and, further, the shape of the amplitude versus delay curve appeared to be about constant at all hour angles, though it was not very carefully observed at large hour angles, indicating that the bandpass of the coherent signal was about constant.

(*b*) *Pointing errors.* There were insufficient strong point sources to adequately calibrate the pointing of the antennas, and the pointing-error corrections on one antenna were made by surveying the antenna base-frame to the same orientation it had at the previous spacing, and using the same correction curves, a procedure which seemed justified by measurements on 3C295 and Cyg A, both far north of Venus. Subsequent measurements at much shorter baselines, where one may calibrate on larger sources than are visible at 5000 wavelengths baseline, indicate that this calibration was adequate and that even at large hour angles the pointing was probably within 2.5 min, where the beam is down by only 5%.

(*c*) *Seeing.* It is well known that the seeing disk can sometimes exceed 40 sec of arc in diameter, and that the desert in daytime has notoriously bad seeing. However, one would expect seeing to affect the calibrating point sources nearly as much as the planet and, further, the observations at large negative hour angles, taken just before or during sunrise, should show much less effect than those taken at large positive hour angles at about noon. The observations of the planet taken in both positions show little or no difference, and from this result we have assumed that the effect of seeing is negligible.

The two-dimensional amplitude-spacing spectrum is the Fourier transform of the brightness distribution of the planet (Moffet 1962). With the baseline fixed at 1600 ft east–west and the hour angle changing, the effective baseline traces a curve in the spacing plane, which for objects near the equator is approximately a straight line aligned east–west. If this be the case, the visibility along this line is the Fourier transform of the fan-beam scan of the planet. Observations with sufficient sensitivity along the amplitude-spacing spectrum thus yield uniquely the strip-scan brightness distribution. However, the present measurements essentially constitute only a small part of the amplitude-spacing spectrum, so, rather than inverting the transform directly, we must fit reasonable models to the data. Several models can be fitted because the data occupy such a small part of the amplitude-spacing spectrum. The data might, for instance, be interpreted as representing a uniform disk 15% larger than the visible planet, or as a thin ring containing $\frac{1}{4}$ the flux from the planet at the limb of the uniform disk. It is not possible to explain the observations by a strong pole-darkening due to polar cooling, though this will tend to lower the transform.

In summary, these measurements tend to indicate

that all of the flux from Venus at 9.5 cm does not arise from a uniform or limb-darkened disk.

ACKNOWLEDGMENT

We are indebted to the director of the observatory, Gordon Stanley, for suggesting these experiments, and for his constant encouragement. We would also like to thank C. H. Mayer for several helpful discussions.

REFERENCES

Kellermann, K. I. 1963, Ph.D. thesis, California Institute of Technology, Pasadena.
Korol'kov, D. V., Pariĭskiĭ, Yu. N., Timofeyeva, G. M., and Khaĭkin, S. E. 1963, *Dokl. Akad. Nauk SSSR* **149**, 65.
Mills, B. Y., Slee, O. B., and Hill, E. R. 1960, *Australian J. Phys.* **13**, 676.
Moffet, A. T. 1962, *Astrophys. J. Suppl.* **67**, 7, 93.
Morris, D., Clark, B. G., and Wilson, R. B. 1963, *Obs. Calif. Inst. Tech. Radio Obs.* 5.
Read, R. B. 1960, *IRE Trans.* **AP-9**, 31.

From the ASTRONOMICAL JOURNAL
69, No. 1, 1964, February—No. 1316
Printed in U. S. A.

Study of Venus by CW Radar*

R. L. CARPENTER
Jet Propulsion Laboratory, California Institute of Technology, Pasadena, California

Between 1 October and 17 December 1962, when Venus was closest to the earth, radar observations were made on a nearly daily basis at the NASA/JPL Deep Space Instrumentation Facility at Goldstone, California. During these observations, several different experiments were performed. One of these was to obtain high-resolution spectra of the reflection from Venus of a CW signal. These spectra show a detail that appeared to move slowly from day to day. If the detail is the result of an actual surface feature on Venus, then its motion would be due to the planet's rotation. Assuming this to be the case, the motion of the detail corresponds to an angular velocity of about half of that expected if Venus were rotating synchronously. The angular velocity leads to a sidereal rotation period of either 1200 days forward or 230 days retrograde. Measurements of the base bandwidth of the signal versus date are incompatible with both synchronous and the 1200-day forward rotation. They lead to a retrograde period of 266 days. An analysis of the base bandwidth measurements for both the 1961 and 1962 inferior conjunctions appears to preclude the possibility that the axis of Venus lies near the plane of its orbit. It is concluded that the most consistent interpretation of the data is that Venus rotates retrograde with a sidereal period of about 250 days and that its axis is approximately perpendicular to its orbit. Estimates of the opacity of Venus' atmosphere to the radar's wavelength (12.5 cm) indicate that the absorption is small. A backscattering function is derived from a CW spectrum that suggests that Venus is significantly smoother than the moon. The reflectivity and dielectric constant were found to be 9.75% and 3.75, respectively, suggesting that Venus has a dry, sandy, or rocky surface. An attempt is made to estimate the rms slope of the surface. The results obtained from an analysis of the backscattering function and the autocorrelation function of the signal suggest that the rms slope is between 4 and 7 deg.

I. INTRODUCTION

RADAR observations furnish a unique opportunity for the investigation of the planet Venus. Microwave radiation can traverse its cloud layer and be reflected by its surface. A study of these reflections can give information about the physical characteristics of Venus' surface as well as the planet's elusive period of rotation.

Between 1 October and 17 December 1962, when Venus was closest to the earth, radar observations were made on a nearly daily basis at the NASA/JPL Deep Space Instrumentation Facility at Goldstone, California. During these observations several different experiments were performed. One of these was to obtain high-resolution spectra of the reflection from Venus of a pure unmodulated signal (usually referred to as a CW or continuous wave signal). Due to the Doppler effect caused by the planet's rotation, the reflected signal is no longer a sharp spectral line as it was when transmitted, but is more or less broadened depending on the planet's angular velocity and surface roughness. The interpretation of these broadened CW spectra is the subject of this paper.

II. RADAR SYSTEM AND METHOD OF OBSERVATION

The radar system operated at a frequency of 2388 Mc/sec ($\lambda = 12.5$ cm) with an average transmitter power of 13 kW. The antenna, used for both transmission and reception, was an 85-ft parabolic dish with circularly polarized feeds. The receiving system contained a low-noise maser and parametric amplifier as its first stages. The over-all system noise temperature, including sky noise, averaged between 40° and 45°K.

The experimental procedure consisted of transmitting

* This paper presents the results of one phase of research carried out at the Jet Propulsion Laboratory, California Institute of Technology, under Contract NAS 7-100, sponsored by the National Aeronautics and Space Administration.

59

the unmodulated or CW carrier for a duration equaling the signal's round trip time to Venus (about 5 min). The radar was then switched to its receive mode for the same duration to receive the reflected signal. Special bandpass and low-pass filters were incorporated in the receiver so that only that part of the spectrum within ± 77 cps of the signal was received. The net result was that the signal was very accurately heterodyned down to an audio frequency of exactly 97.5 cps with a spectrum extending from about 20 to 175 cps. This signal was recorded on magnetic tape for processing at a later time. Recordings were made on an almost daily basis throughout the experiment.

Between each complete transmit-receive cycle a noise run was recorded with the radar in its receive mode, but with no signal present. These runs determined the spectral distortion of the entire system, and were used to remove it from the signal spectra.

The changing reception frequency of the reflected signal, resulting from the Doppler effect caused by the relative motion between the radar and Venus, was removed by an ephemeris-controlled subsystem which is part of the receiver. It kept the signal's frequency constant to within $\pm \frac{1}{2}$ cps.

To process the recorded signal, the tapes were played back and sampled at 375 samples per second by an analogue-to-digital (A/D) converter; this converter generated a second tape in the correct format, to be read into an IBM 7090 computer on which the spectrum was calculated.

A special program was used to compute the spectrum of the signal. It was designed to compute the spectrum, based on either the full 16-bit amplitude resolution of the A/D converter or 4-bit or binary resolution. The binary resolution case was used for all spectral computations in this paper; however, both the 16-bit and the 4-bit resolutions were tried as a check on the accuracy of the computed spectra. The only difference between the binary and the 4- and 16-bit cases was that in the binary case the fluctuations on the spectrum were more exaggerated. Even though more data are needed in the binary case than otherwise for spectra of comparable smoothness, the saving in computer time generally justifies the binary calculation. (The running time required in the binary case is $\frac{1}{8}$ the time for the full-resolution case even though $2\frac{1}{2}$ times more data must be used.) The true spectrum of the signal can be obtained using only binary resolution if the amplitude probability distribution of the signal is Gaussian (Lawson and Uhlenbeck 1950; Price 1958), which is the case for Venus' radar echo. The signal and noise spectra were computed with a frequency resolution of 1 and 2 cps, respectively. Resolution is defined here as the width at the half-power point of the spectrum of a pure sinusoidal waveform, i.e., an infinitely narrow spectral line. The noise spectra were computed with coarser resolution (and consequently were smoother) so as not to introduce noise into the signal spectra when they were corrected for the distortion caused by the receiving system.

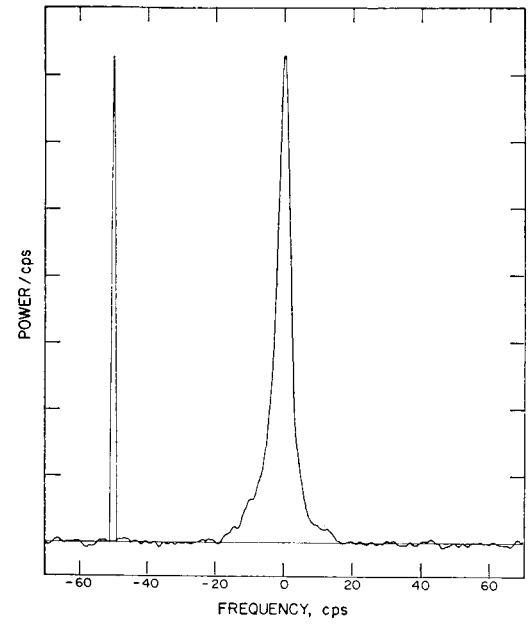

FIG. 1. CW radar spectrum of Venus for 13 November 1962. The frequency scale is relative to 97.5 cps. Spectral resolution is shown by the spike on the left.

III. CW SPECTRA

Figure 1 shows the spectrum obtained on 13 November 1962, when Venus was at its closest. It was computed from about an hour of recorded signal. The ordinate is relative signal power (per unit bandwidth) and the abscissa is frequency. The 1-cps resolution of the spectrum is shown by the spike on the left. The plot can be interpreted equally well as signal power versus radial velocity relative to the center of the planet. A frequency shift of 1 cps corresponds to a difference in radial velocity of 6.3 cm/sec.

On a rotating planet, regions of constant radial velocity (and hence Doppler frequency) consist of lines across its disk that are parallel to the axis of rotation. The center line, along the planet's axis, has zero radial velocity because the radial velocity due to the motion of the whole planet relative to the radar station is removed by the ephemeris-controlled receiver. This center line corresponds to the peak of the spectrum. Lines farther removed from the center line have greater radial velocities (of either sign) until the limbs of the planet are reached. The difference in the frequency between these maximumly separated lines is called the limb-to-limb bandwidth, and marks the maximum possible width of the spectrum. In this connection, note the abruptness with which the spectrum disappears into the background noise. Whether or not this disappearance marks the limbs of Venus is discussed later.

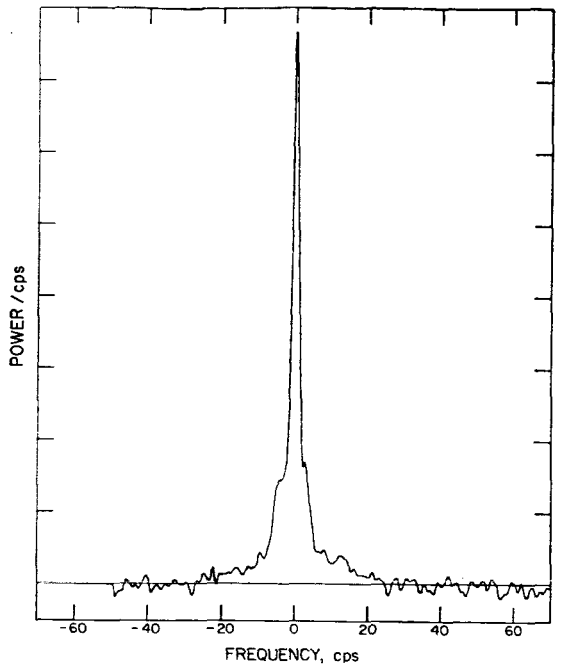

FIG. 2. CW radar spectrum of Venus for 22 October 1962.

One of the most remarkable of the spectra obtained during the experiment occurred on 22 October; it is shown in Fig. 2. Note the needlelike central peak. This spectrum has the narrowest half-power bandwidth of all those obtained. Its value is 2.3 cps. The next day the spike had disappeared, and as far as could be determined the radar system was operating equally well on both days. The half-power bandwidth for the spectrum on 23 October was 5.4 cps. Less spectacular changes occurred several times during the experiment. The cause of these changes is unknown—perhaps they represent the passage of different types of surface features through or near the sub-earth on Venus.

IV. SURFACE FEATURES AND ROTATION

If a large surface feature is present on the planet that scatters back to the radar more energy than the surrounding areas, it will show up as an irregularity or detail on the spectrum. Most of the irregularities are random fluctuations produced by noise. However, on close examination one irregularity was found to persist from day to day and to change its position slowly. Figure 3 shows the lower portions of six spectra obtained during the week preceding conjunction. The spectra have been positioned horizontally so that their peaks line up. Note the detail on the lower left side of each. It is about 1 dB above the adjacent parts of the spectrum and approximately 5 dB above the average peak background noise. At least a suggestion of a similar detail was found on most of the spectra obtained in the month preceding conjunction. Note also that the detail appears to have moved slightly to the left during the week. This motion is toward the low-frequency side of the spectra and corresponds to the receding part of the planet.

Figure 4 shows the position of the detail relative to the peak of the spectrum. The ordinate is the date of the observation and the abscissa is the frequency difference between the peak and detail in cps. The width of the boxes corresponds to the approximate width of the detail. The filled boxes are considered good identifications, while the unfilled and dotted ones are fair and poor, respectively.

The relative permanence of the detail strongly suggests that it was caused by an actual physiographic feature on the surface of Venus and that its motion was the result of the planet's rotation. The true nature of the feature can only be guessed at; however, it is not unreasonable to assume that it is a particularly rough region of rather large extent. This roughness does not necessarily imply mountains; it merely indicates that the region is rough to a scale of the 12.5-cm radar wavelength.

If the spectral detail is indeed the result of a surface feature on Venus, then the rate at which it moves may be used to estimate the planet's rotation period. The relation between the detail's motion and the planet's component of angular velocity perpendicular to the

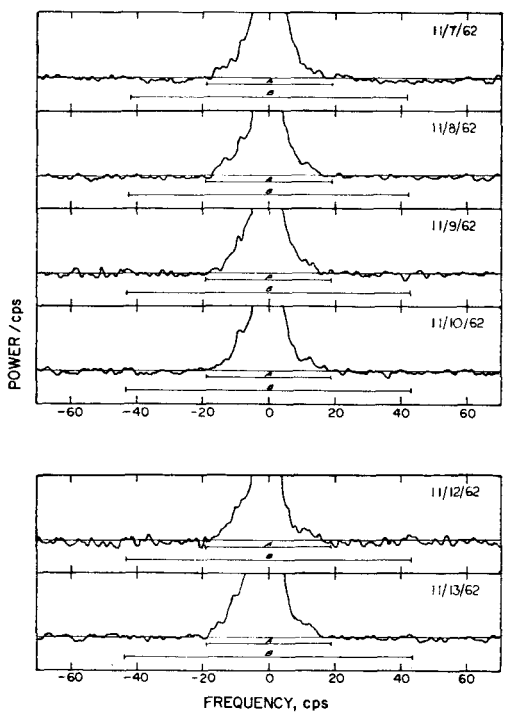

FIG. 3. Lower portion of the spectra obtained during the week preceding conjunction. Note persistent detail on the left side of each spectrum. Bars A and B are the computed limb-to-limb bandwidths for 250-day retrograde and synchronous rotation, respectively.

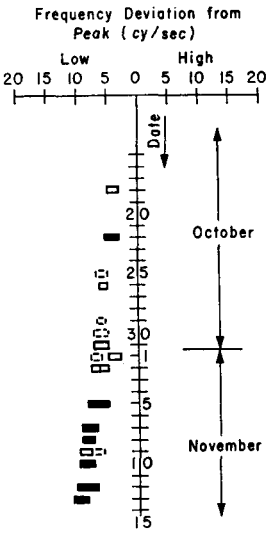

FIG. 4. Position of the spectral detail versus date.

line of sight, is

$$\dot{\theta}=\left(\frac{\lambda}{2R}\sec\phi\,\sec\theta\dot{f}\right)^{\frac{1}{2}}, \qquad (1)$$

where $\dot{\theta}$ is the apparent angular velocity of the planet; θ is the longitude of feature; ϕ is the latitude of feature; $\dot{f}$ is the rate at which feature moves across spectrum; λ is the signal wavelength; and R is the radius of Venus. To obtain the angular velocity, the latitude and longitude of the feature relative to the center of the planet's disk must be known. By measuring the position of the detail, relative to the maximum observable half-width of the spectrum's base, its longitude may be estimated. This assumes that the spectrum extends to the limb of the planet. If this is not the case, the longitude will be overestimated which will result in overestimating the angular velocity. Fortunately, the angular velocity varies as the square root of the secant of the latitude and longitude; hence, it is insensitive to the detail's position if it is within 45 deg of the center of the disk.

Using the best spectra obtained near conjunction, the estimated longitude of the detail was about 23 deg. Its latitude cannot be found from the current data, and was assumed also equal to 23 deg. Based on Fig. 4, the estimated motion of the detail across the spectrum for the week prior to conjunction was 0.28 (+0.30, −0.10) cycles per day. This corresponds to an apparent angular velocity of 2.0 (+0.87, −0.41)$\times10^{-7}$ rad/sec. Synchronous (225 days forward) rotation would have given about 4.3×10^{-7} rad/sec. If it is assumed that the axis of Venus is perpendicular to its orbit, then the angular velocity corresponds to a sidereal rotation period of approximately 1200 days forward or 230 (+40, −50) days retrograde. These are underestimates of the period because of the uncertainty in longitude and latitude of the detail.

V. BANDWIDTH AND ROTATION

A second and independent method of measuring the angular velocity of Venus is to estimate the limb-to-limb bandwidth from the base bandwidth (the width of the base of the spectra). This method assumes that reflections were received from near the limbs as well as from the center of the disk.

The apparent angular velocity of Venus as seen from the earth consists of the projection onto a plane perpendicular to the line of sight of the sum of two components: (1) a component due to the rotation of Venus on its own axis and (2) a component due to an apparent rotation caused by Venus passing the earth in space. If Venus were rotating forward on its axis, which is the case for synchronous rotation, the two components would add, giving a maximum bandwidth near conjunction. If Venus were rotating backwards, the two components would subtract, giving a minimum bandwidth near conjunction.

Figure 5 shows the measured base bandwidths versus

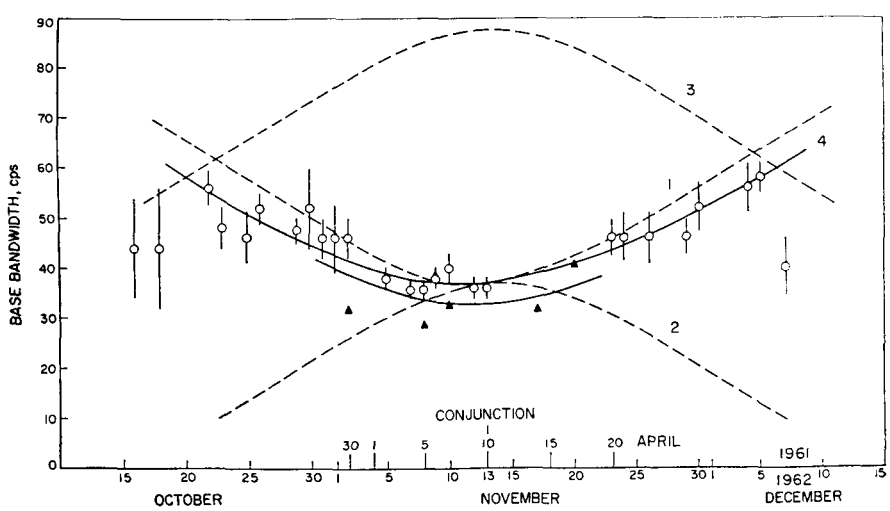

FIG. 5. Measured base bandwidth versus date. Circles and triangles are the 1962 and 1961 measurements, respectively. Curves 1 and 4 are the theoretical limb-to-limb bandwidths for 230-day and 266-day retrograde rotation, respectively. Curves 2 and 3 are for 1200 days forward and synchronous rotation, respectively.

62

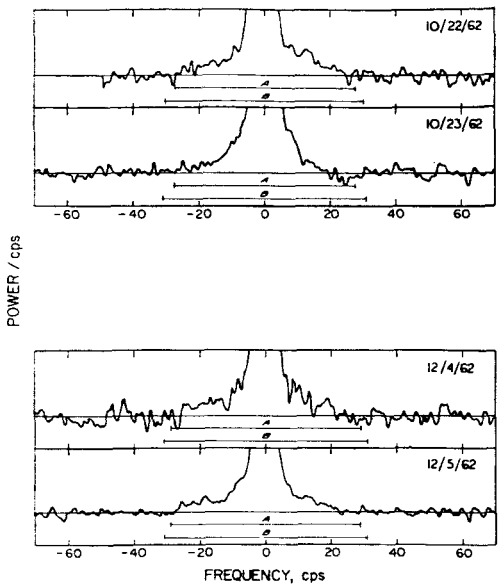

FIG. 6. Lower portion of the spectra obtained three weeks before and after conjunction. Bars A and B are the computed limb-to-limb bandwidths for 250-day retrograde and synchronous rotation, respectively.

date. On most of the spectra the base extended farther from the peak on the low-frequency side than on the high-frequency side. The most plausible explanation of this phenomenon is that there was an actual asymmetry in the backscattering behavior of the surface near the two limbs. At any rate, since it is impossible to obtain reflections from beyond the limb, and since the effects of noise would tend to make the limbs less apparent, the greater spectral widths on the low-frequency side were used to estimate the base bandwidths. The error flags are estimates of the accuracy with which the disappearance of spectra into the noise could be measured. Curves 1, 2, and 3 show the limb-to-limb bandwidths computed assuming that the axis of Venus was perpendicular to its orbit for sidereal periods of 230 days retrograde, 1200 days forward, and for synchronous rotation, respectively. Except for the anomalous points obtained early and late in the program, the base bandwidths are in closest agreement with the 230-day retrograde case. The anomalous points are believed caused by the greater noise on their spectra. This was a consequence of Venus' greater distance from the earth and relatively short signal-integration times. As the noise on the spectra increases, the weaker reflections from the limbs become less discernable and, therefore, the measured base bandwidth would underestimate the limb-to-limb bandwidth.

If it is assumed that the base bandwidth corresponds to the limb-to-limb bandwidth, then the former may be used to compute the rotation and axis orientation of Venus. To perform this analysis, a program was written for the IBM 7094 computer that solves for the period and axis direction by a nonlinear least-squares method using the ephemeris of the earth and Venus and the base bandwidth measurements. Curve 4 in Fig. 5 shows the best fit limb-to-limb bandwidth curve to the date after excluding the anomalous end points. It corresponds to a sidereal period of 266 days with the axis directed toward right ascension 41 deg and declination -69 deg.

Kuiper (1954) has published a period and axis orientation based on optical observations of Venus. He reported a period of 14 days with the axis directed toward right ascension $52\frac{1}{2}$ deg and declination 81 deg. Aside from the obvious disagreement in period and direction of rotation, it is interesting that the right ascensions are within 12 deg of each other.

Because of the nonlinear nature of the least-squares program, more than one solution fitted the 1962 data. However, when the 1962 data are combined with the base bandwidth measurements of the best spectra obtained during the 1961 radar experiment (Victor, Stevens, and Golomb 1961), only the solution given above was possible. This is important because it appears to preclude the possibility that the axis of Venus lies near the plane of its orbit. The 1961 measurements are represented by the triangles in Fig. 5. The error flags, all approximately ± 7 cps, were omitted from the diagram so that the other results would not be confused. The lower solid line is the fit for the 1961 data. It is an extension of the 1962 limb-to-limb bandwidth curve back to the 1961 conjunction.

The agreement between the periods obtained by tracking the motion of the spectral detail and the fit to the base bandwidth measurements is very satisfactory considering the differences in these methods. Taken together the results strongly suggest that the sidereal rotation period of Venus is not synchronous, but rather 250 days$\pm$40 days retrograde, and that its axis is approximately perpendicular to its orbit. (It should be noted that this period corresponds to a synodic period of about 118 days.)

The fact that the base bandwidths are a minimum near conjunction argues strongly against synchronous rotation. To show this, two pairs of spectra, obtained three weeks before and after conjunction, are compared with those obtained near conjunction. Figure 6 shows the lower portion of the two pairs of spectra taken three weeks before and after conjunction. The bars A and B below each spectrum are the computed limb-to-limb bandwidths for 250 days retrograde and synchronous rotation, respectively. In Fig. 3, which shows the spectra obtained near conjunction, A and B again correspond to retrograde and synchronous rotation, respectively. Clearly, these spectra are incompatible with synchronous rotation.

VI. DEPOLARIZED SPECTRUM

When a circularly polarized wave is reflected from a smooth surface, the sense of polarization is reversed.

The receiving antenna must be matched to this polarization or no echo will be received. When the surface becomes rough, the reflected wave will be partly depolarized and will contain both right and left circularly polarized components. If the receiving antenna is in its mismatched polarization mode, a depolarized spectrum of the echo is obtained. Terrestrial backscattering measurements (Peake 1962) indicate that the backscattering function $P(\phi)$ (the power scattered back to the radar per unit area of the surface as a function of the angle of incidence ϕ) of the depolarized component tends to follow a cosine power law of low order, i.e., $P(\phi) \approx \cos^2\phi$. Evans and Pettengill (1963) find similar results for the moon. Their depolarized backscattering function follows $\cos^1\phi$.

From the foregoing discussion, it appears that if a depolarized spectrum is obtained for Venus, it will have an approximate $\cos^2\phi$ backscattering function. Figure 7 shows the depolarized spectrum obtained on 11 November 1962. The ordinate is expressed in decibels. The smooth curves are the expected theoretical spectra, assuming a $\cos^2\phi$ or Lambert backscattering function; curve A is for 250-day retrograde rotation and B for synchronous rotation. Again we see fair agreement with the retrograde case and lack of agreement with the synchronous case.

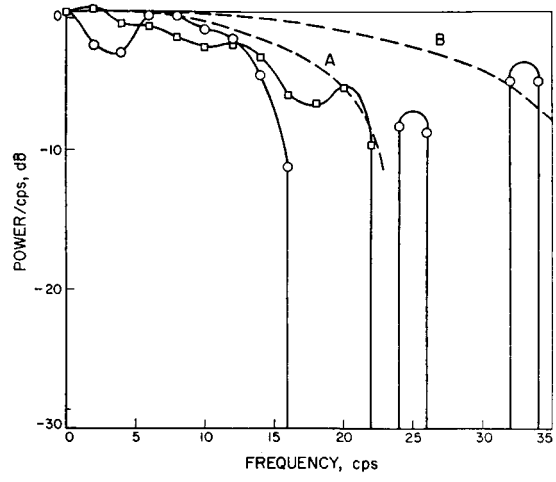

FIG. 7. Depolarization spectrum obtained 1 November 1962 plotted as log power versus frequency. Circles are for the upper-frequency side, and squares for the lower-frequency side. Curves A and B are the theoretical depolarized spectra, assuming a $\cos^2\phi$ law, for 250-day retrograde and synchronous rotation, respectively.

VII. ATMOSPHERIC OPACITY

The accuracy with which the base bandwidth equals the limb-to-limb bandwidth depends not only on the backscattering characteristics of the surface at steep inclinations, but also on the opacity of the atmosphere of Venus. At first glance this may appear negligible; however, because the radar signal must traverse the atmosphere twice, and near the limbs, particularly, the air mass is increased many times, appreciable absorption may result. For an incidence angle of 70 deg the signal must traverse approximately 6 air masses on its two-way path through the atmosphere. An incidence angle of 70 deg corresponds to energy being reflected from regions 9/10 of the way to the limb. When the very high surface pressures currently being proposed are considered (10–100 atm), the opacity of the atmosphere may become significant.

To explore this possibility the opacity of several model atmospheres was investigated. Barrett (1961) has studied the opacity of Venus' atmosphere, assuming a composition of 75% CO_2, 24% N_2 and 1% water vapor. Using his results for a surface pressure of 10 atm, the two-way absorption at an incidence angle of 70 deg is 7% at 12.5 cm, a small but not insignificant amount. For a pressure of 20 atm the absorption increases to 26%, which would begin to reduce the base bandwidth measurements.

Some authors (Cameron 1963) are suggesting pressures of the order of 100 atm. Fortunately, such high pressures are arrived at by assuming a considerably lower percentage of CO_2 and water vapor, and consequently the opacity is not changed markedly. Spinrad (1962) has recently made a careful analysis of the optical spectrum of Venus and concludes that its atmosphere probably contains not more than one part in 10^5 of water and 4% of CO_2 by mass. If the balance of the atmosphere is N_2, then CO_2 is the only important source of opacity in the microwave region.

A rough estimate of the opacity may be obtained by assuming an isothermal atmosphere with a composition of 95% N_2 and 5% CO_2. Under these conditions the absorption produced for a double traversal through the atmosphere at an incidence angle of 70 deg is about 5%. This result is based on a preliminary value for the microwave absorption coefficient for the above composition by Thaddeus (1963). An absorption of 5% would not adversely affect the base bandwidth measurement.

The above analysis is very approximate and is intended to indicate whether or not the atmospheric absorption has any effect on the radar results. It appears from these calculations that the absorption may have a detectable effect and that the base bandwidth measurements may be somewhat smaller than otherwise. At any rate, because of the crudeness of the analysis and poor knowledge of the reflecting characteristics of Venus' surface, correcting the base bandwidth measurements is unwarranted. It is interesting to note that if the rotation of Venus can be established, the study of the reflections from the limbs may lead to a measurement of the microwave opacity of the atmosphere and thus a better understanding of its structure.

VIII. BACKSCATTERING FUNCTION OF THE SURFACE

An important parameter that describes the radar properties of a surface is its backscattering function

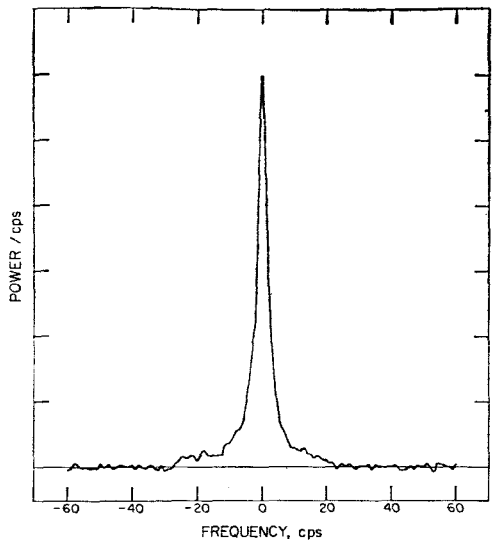

FIG. 8. CW radar spectrum of Venus for 5 December 1962. This spectrum was used to complete the backscattering function.

$P(\phi)$. As mentioned previously, it is a measure of the relative power scattered back to the radar by a unit area of the surface as a function of the angle of incidence ϕ. It is unity for $\phi=0$, and usually decreases more or less rapidly as ϕ increases. The character of this decrease depends on the statistical properties of the surface; the smoother the surface, the more rapidly does $P(\phi)$ decrease with ϕ. For a surface that scatters according to Lambert's law, $P(\phi)=\cos^2\phi$ and for Lommel–Seeliger scattering, $P(\phi)=\cos\phi$. For a perfectly reflecting surface $P(\phi)=1$ at $\phi=0$ and is zero for $\phi\neq 0$.

The relation between the CW spectrum and the backscattering function is given by

$$P_s(f) \propto \pm \int_0^{(f_0^2-f^2)^{\frac{1}{2}}} \frac{P(\phi)}{(f_0^2-f^2-y^2)^{\frac{1}{2}}} dy, \qquad (2)$$

where

$$\phi=\sin^{-1}[(f^2+y^2)^{\frac{1}{2}}/f_0],$$

f is the frequency, and f_0 is the center-to-limb bandwidth, i.e., half the limb-to-limb bandwidth. The CW spectra give $P_s(f)$ and $P(\phi)$ is to be determined. Fortunately, $P_s(f)$ can be transformed into Abel's integral equation whose inverse is well known. The result is

$$P(\phi) \propto \cos\phi \int_{f_0 \sin\phi}^{f_0} \frac{P_s'(f)}{(f^2-f_0^2\sin^2\phi)^{\frac{1}{2}}} df. \qquad (3)$$

Using this equation, the backscattering function for the spectrum of 5 December was computed. This spectrum was chosen for several reasons. First, it has a low noise level and is fairly representative of the other spectra. Second, it should be less affected by the distortion introduced by the one cycle frequency resolution of the computations. The spectrum is about $1\frac{1}{2}$ times broader than those obtained near conjunction, hence more resolution increments are contained in its spectrum. This was an important consideration in its choice because "instrumental" broadening of the spectrum will distort the backscattering function. Third, f_0, the center-to-limb bandwidth, is approximately the same whether the retrograde period found above or a synchronous period is assumed. This arises because the limb-to-limb bandwidth for retrograde and synchronous rotation cross near 5th December (see Fig. 5).

In order to obtain the best possible spectrum on which to compute the backscattering function, the spectrum for 5th December was recomputed using eight levels of amplitude resolution rather than the binary resolution described earlier. It is shown in Fig. 8. Careful examination of this spectrum indicates that the rms noise level is more than 23 dB below its peak.

The backscattering function, computed from Eq. (3), for 5-deg intervals, is shown by the points in Fig. 9. The circles are based on the upper-frequency side of the spectrum and the squares on the low-frequency side; this accounts for having two points per interval. Some points are missing because the result was negative. The center-to-limb bandwidth was assumed to be 28 cps.

The computed backscattering function for Venus looks similar to the moon's, which is remarkable, considering the completely different environments of their surfaces. It has a steep quasi-specular component for incidence angles under 25 deg which merges into a diffuse component for larger angles. The diffuse component appears to follow a Lambert ($\cos^2\phi$) law. The

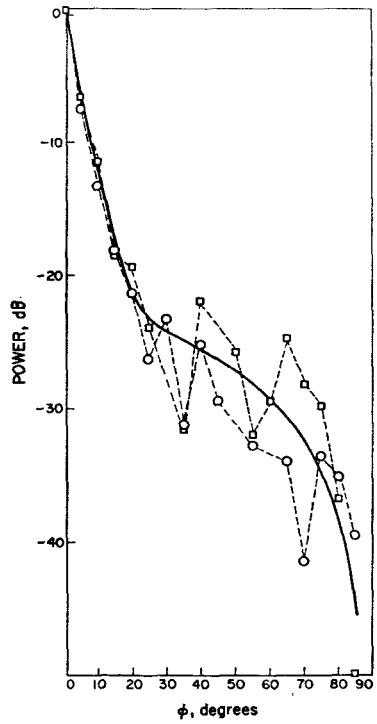

FIG. 9. Computed backscattering function using spectrum shown in Fig. 8. Circles are for the upper-frequency side and squares for the lower-frequency side. Curve shows the theoretical backscattering function.

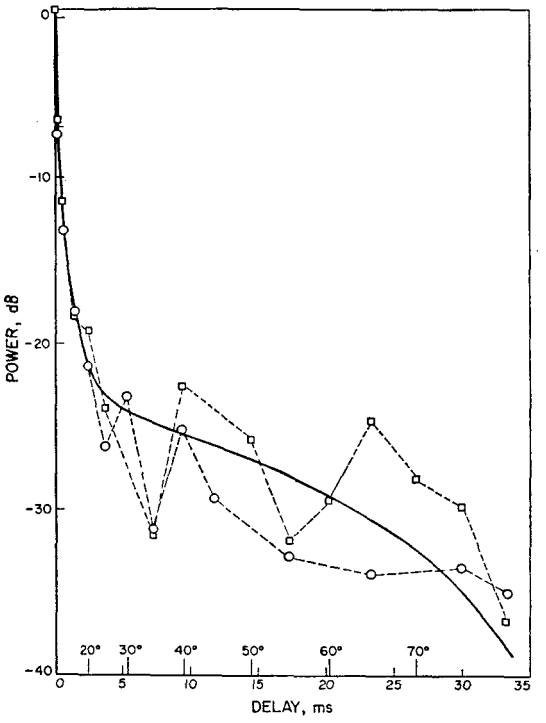

FIG. 10. Same backscattering function as in Fig. 9, but showing response to a pulse-type radar. Abscissa is delay in milliseconds. Limb is at about 40 msec.

curve in Fig. 9 corresponds to

$$\sigma(\phi)=\frac{208}{209}e^{-16.5\sin\phi}+\frac{1}{209}\cos^2\phi, \tag{4}$$

which has the same functional form as that given by Evans and Pettengill (1963) for the backscattering function of the moon. It matches the data reasonably well considering the scatter of the data. By integrating the quasi-specular and diffuse components of this equation separately, it is found that about 28% of the total reflected power is in the diffuse component. The corresponding value for the moon is approximately 20% (Evans and Pettengill 1963).

Hughes (1961) has studied the backscattering function of the moon at 10 cm and finds that it is closely represented by

$$P(\phi)=e^{-10.2\phi} \tag{5}$$

for angles between 4 and 13 deg. Apparently Venus is significantly smoother than the moon, at least for the part of the surface that produces the quasi-specular component.

Figure 10 shows the computed response of Venus to a pulse-type radar. It was derived from the backscattering function by transforming the ϕ coordinate to a time delay

$$t=(2R/c)(1-\cos\phi), \tag{6}$$

where c is the velocity of light. Note the extremely sharp decay produced by the quasi-specular component and the low-lying diffuse component. The latter is about 23 dB below the peak and apparently accounts for its lack of detection by Pettengill *et al.* (1962) during their 1961 radar study of Venus.

IX. REFLECTIVITY

The ratio of the areas of the signal and the noise spectra is a measure of the received signal-to-noise ratio. This ratio may be used to determine the power of the returned signal. The radar cross section σ of the planet may be determined from the observed signal power by use of the radar equation:

$$\sigma=(4\pi)^3d^4P_r/G_tG_r\lambda^2P_t, \tag{7}$$

where d is the distance to Venus; P_r is the received power; G_r is the gain of the receiving antenna (54.2 $\pm$1 dB); G_t is the gain of the transmitting antenna (54.1$\pm$1 dB); and P_t is the transmitter power. The value for P_r is obtained from the measured signal-to-noise ratio and system noise temperature

$$P_r=(s/n)kT, \tag{8}$$

where (s/n) is the signal-to-noise ratio per cycle of bandwidth; k is Boltzmann's constant; and T is the system noise temperature.

The radar cross section of a planet is given by

$$\sigma=\pi R^2g\rho, \tag{9}$$

where ρ is the power reflectivity of the surface material at normal incidence, and g is the directivity, i.e., the ratio of the power scattered back toward the receiver to the average power scattered in all directions. The directivity is dependent on the scale of the planet's surface roughness; it is unity for both a smooth and rough sphere if the roughness is due to undulations that are greater than a half-wavelength (Feinstein 1954). It is 8/3 for a Lambert scattering sphere (Greig, Metzger, and Waer 1948).

Equation (9) shows that the reflectivity of the surface cannot be obtained directly from a measurement of the radar cross section, only the product $g\rho$. The weighted mean value obtained throughout the experiment is

$$g\rho=0.0975\ (+0.026,\ -0.020).$$

The dielectric constant k of the reflecting surface, assuming zero conductivity, is given by

$$k=\left(\frac{1+\rho^{\frac{1}{2}}}{1-\rho^{\frac{1}{2}}}\right)^2. \tag{10}$$

Assuming $g=1.0$, k is found to be 3.75 (+0.55, −0.25). It suggests that Venus has a dry, sandy, or rocky surface.

If it is assumed that the backscattering function consists of a quasi-specular and a diffuse component,

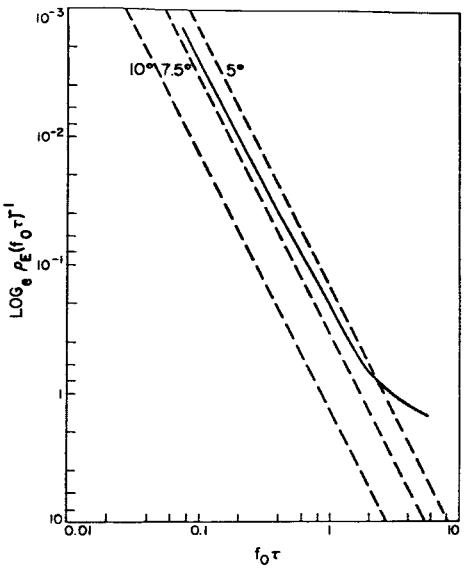

FIG. 11. Observed envelope of the autocorrelation function of the signal after removing the Lambert scattering term. The straight lines are the theoretically expected values for the given rms slopes.

then the computation of the dielectric constant is more involved and account must be taken of their directivities. As mentioned earlier, the directivities of the quasi-specular and diffuse components (assuming Lambert) are one and 8/3, respectively. The accuracy of the reflectivity measurements hardly justifies this more refined analysis. However, when the directivities are taken into account, the dielectric constant is reduced slightly to 3.6. The analysis also indicated that the diffuse component results from about $12\frac{1}{2}\%$ of the surface being rough to 12.5 cm.

X. VENUS SURFACE ROUGHNESS

There are essentially two different approaches to the statistical description of a surface that are used to interpret the radar observations. One is to assume that the surface can be approximated by a series of facets of varying size and inclination. The backscattering function of the surface is then determined by the relative number of facets of different sizes that are oriented perpendicular to the line of sight. The other approach is to assume that the surface fluctuates randomly in elevation as a function of position. The surface is then specified by giving the probability distribution of elevation around some mean elevation, and the spatial correlation function of the surface. The latter function is the correlation between the elevations of a pair of points on the surface as a function of their horizontal separation.

The latter approach assumes that the radiation is scattered from an irregular surface by diffraction. As such, the methods of physical optics are used. The problem has been studied by several authors (Davies 1954; Feinstein 1954; Daniels 1961, 1963; Hayre and Moore 1961; Bramley 1962; Hughes 1961). Daniels' analysis is followed here.

Under the assumptions of physical optics, and assuming that the surface has a Gaussian probability distribution in elevation around some mean value (this assumption appears to hold for a wide variety of terrains on the earth: Hayre and Moore 1961), then Daniels shows that the envelope of the autocorrelation function of the received signal $\rho_E(f_0\tau)$ is approximately related to the spatial correlation function of the surface $\rho(2s/\lambda)$ by

$$\rho_E(f_0\tau) \approx \exp\{-\alpha[1-\rho(2s/\lambda)]\}, \tag{11}$$

where

$$\alpha = 16\pi^2(\sigma/\lambda)^2, \tag{12}$$

s is the horizontal distance along the surface, σ is the standard deviation of the elevation about its mean, and τ is the time lag in the computation of the signal's autocorrelation function. The product $f_0\tau$ is a convenient dimensionless argument for the autocorrelation function.

At first glance it would appear that since $\rho_E(f_0\tau)$ is measurable, both the spatial correlation of the surface $\rho(2s/\lambda)$ and the standard deviation of the elevation σ averaged over the surface of Venus could be found. The latter follows from Eq. (11) because for large distances on the surface, $\rho(2s/\lambda)$ would approach zero leaving α as the asymptotic value of $\rho_E(f_0\tau)$ for large $f_0\tau$. Then σ could be found from α through Eq. (12). Unfortunately, even for an improbably small value of σ of 12.5 cm, $\alpha = 158$ and, consequently, $\rho_E(f_0\tau)$ will be too small to measure accurately before $\rho(2s/\lambda)$ has departed appreciably from unity. Therefore, α and $\rho(2s/\lambda)$ cannot be found until $\rho_E(f_0\tau)$ can be measured with extremely high precision.

However, Daniels (1963a) has devised a means for finding the rms slope. He has shown that if the slope of the autocorrelation function of the signal is zero at the origin, then for sufficiently small values of $f_0\tau$ the autocorrelation function becomes Gaussian with the rms slope m as a parameter:

$$\rho_E(f_0\tau) = \exp[-2\pi^2 m^2 (f_0\tau)^2]. \tag{13}$$

An analysis of the autocorrelation function has shown that its slope at the origin is indeed zero; consequently, it may be compared with Eq. (13) to find the rms slope of the surface.

Before making this comparison, however, Daniels (1963b) points out that it is necessary to remove the diffuse component from the data. Equation (11) was derived based on an undulating surface for which Huygen's principle is applicable. It is not applicable to surfaces that have scatterers much smaller than a wavelength and which appear to account for the diffuse component (Winter 1962). The diffuse component was

assumed to follow Lambert's law and its autocorrelation function was subtracted from the autocorrelation function of the signal (the autocorrelation functions may be subtracted because it is assumed that the quasi-specular and diffuse components are additive). The result was then renormalized to unity at the origin. Figure 11 shows the comparison of the corrected autocorrelation function with Eq. (13) for three values of the rms slope. The plot was constructed so that Gaussian curves follow straight lines. The three theoretical lines are for slopes of 5, 7.5, and 10 deg, respectively. The data are asymptotic to an rms slope of 6.2 deg. This figure is quite tentative because it depends on the magnitude of the diffuse component, which is difficult to establish. If the strength of the diffuse component has been underestimated, then the rms slope would be still smaller, and vice versa.

The interpretation of the rms slope in terms of surface relief is not possible at present because of the lack of knowledge of slopes on the earth. However, Daniels (1963b) finds an rms slope for the moon of about 6.5 deg, which again indicates, as was found by comparing the backscattering functions, that Venus is smoother than the moon.

As indicated at the beginning of this section, an alternate description of the surface is the assumption that it consists of facets of varying size and inclination. If the areas of facets are independent of their slope, then the backscattering function defines the slope angle's probability distribution (after normalization); consequently, the rms value of the slope angles is given by

$$\left(\int_0^{\frac{1}{2}\pi} \phi^2 P(\phi) d\phi\right)^{\frac{1}{2}}. \qquad (14)$$

Using the quasi-specular component only, the rms inclination is 4.8 deg. For the moon the corresponding result is about 8 deg. The interpretation of these results in terms of the general appearance of the surface of Venus must await backscattering studies of a wide variety of surface configurations.

ACKNOWLEDGMENTS

I should like to thank William Thomas for his many contributions in constructing the spectral analysis program, Gerald S. Levy for the depolarized spectrum, Dr. H. C. Rumsey, who inverted the integral equation giving the backscattering function, and Dr. W. F. Gillmore, Jr., for his suggestions on writing the program to compute the backscattering function. I am also grateful to Dr. R. Goldstein for many useful discussions and for the use of his program to determine the axis orientation of Venus from the base bandwidth measurements, and W. K. Victor and Robertson Stevens, who were in charge of the over-all radar program.

REFERENCES

Barrett, A. H. 1961, *Astrophys. J.* **133**, 281.
Bramley, E. N. 1962, *Proc. Phys. Soc.* (*London*) **80**, 1128.
Cameron, A. G. W. 1963, *The Origin of the Atmospheres of Venus and the Earth* (Goddard Institute for Space Studies, NASA, New York).
Daniels, F. B. 1961, *J. Geophys. Res.* **66**, 1781.
——. 1963a, *ibid.* **68**, 449.
——. 1963b, *ibid.* **68**, 2864.
Davies, H. 1954, *Proc. IEE* (IV) **101**, 208.
Evans, J. V., and Pettengill, G. H. 1963, *J. Geophys. Res.* **68**, 423.
Feinstein, J. 1954, *IRE Trans.* **AP-2**, 23.
Greig, D. P., Metzger, S., and Waer, R. 1948, *Proc. IRE* **36**, 652.
Hayre, H. S., and More, R. K. 1961, *J. Res. Natl. Bur. Stds.* **65D**, 427.
Hughes, V. A. 1961, *Proc. Phys. Soc.* (*London*) **78**, 988.
Kuiper, G. P. 1954, *Astrophys. J.* **120**, 603.
Lawson, J. L., and Uhlenbeck, G. E. 1950, *Threshold Signals* (McGraw-Hill Book Company, Inc., New York), pp. 56–63.
Peake, W. H. 1962 (private communication).
Pettengill, G. H. *et al.* 1962, *Astron. J.* **67**, 181.
Price, R. 1958, *IRE Trans.* **IT-4**, 69.
Spinrad, H. 1962, *Icarus* **1**, 266.
Thaddeus, P. 1963, reported by Cameron in his paper listed above.
Victor, W. K., Stevens, R., and Golomb, S. W. (Editors) 1961, *Radar Exploration of Venus*; *Goldstone Observatory Report for March–May* 1961. Tech. Rept. No. 32–132, Jet Propulsion Laboratory, Pasadena, California.
Winter, D. F. 1962, *J. Res. Natl. Bur. Stds.* **66D**, 215.

From the ASTRONOMICAL JOURNAL
69, No. 1, 1964, February—No. 1316
Printed in U. S. A.

Venus Characteristics by Earth-Based Radar*

R. M. GOLDSTEIN
Jet Propulsion Laboratory, California Institute of Technology, Pasadena, California

This paper describes three types of radar experiments which were performed upon Venus during the inferior conjunction of November 1962.

In the first, only the total echo power was measured, while in the second, this power was analyzed into its frequency components. The third type divided the echo power into range zones and then subdivided these into frequency components.

The resulting data indicate the following characteristics: an average radar cross section for Venus of 10%; the cross section fluctuates from day to day; a roughness characteristic, or scattering law, which also fluctuates; and the surprising result that Venus rotates retrograde with a period of about 250 days and with its axis nearly perpendicular to its orbit.

I. INTRODUCTION

IN the design of a radar experiment, one may control both the form of the transmitted signal and the type of processing applied to the echo. This possibility gives radar its unique potential for gathering characteristic facts about Venus, as the planet may be expected to interact differently with different incident waveforms. The design problem is to select a suitable waveform–receiver combination to extract the desired information from Venus. As usual, the overwhelming difficulty in this problem is caused by the extremely feeble power contained in the echo, which is immersed in relatively strong background noise. Thus every step of signal processing must be carefully considered so as to conserve signal-to-noise ratio.

The experiments to be described were performed at the NASA/JPL Deep Space Instrumentation Facility at Goldstone, located in a radio-quiet area deep within the Mojave Desert of California. Ten kW of 12.5-cm rf power were beamed at Venus from an 85-ft paraboloidal antenna. The same antenna was used alternately for both transmission and reception. After its 55-million-mile round trip, the signal was attenuated to a power level of only 10^{-21} W. It would be impossible to make use of this feeble signal were it not for the extraordinary quality of the receiver—the total noise temperature being, typically, 37°K.

One Venusian feature of great interest is its radar cross section (the fraction of the power returned, compared to that from a perfect reflector). Radio astronomers have developed a technique to detect and measure such weak signals. Called a switched, or Dicke, radiometer, the receiver alternately listens to the signal (with the noise) and then to noise only. It detects the small resulting change in output and is thus free (to first order) of drifts and gain changes. Switching the input of a receiver brings about some formidable engineering problems that can be avoided altogether in the radar case by switching the transmitter off and on. Thus, an appropriate transmitted signal is a slow modulation, on and off, of the carrier; the corresponding receiver is a switched radiometer; and the information gathered is the radar cross section of Venus. How the cross section varies with time, with matched and crossed circular polarization, and matched and rotated linear polarization is discussed subsequently.

The transmission of a pure sinusoid, coupled with spectral analysis at the receiver, has proved to be a fruitful combination to study surface roughness and rotation characteristics of Venus. This is so because angular velocity imparts to each element of Venusian territory a specified line-of-sight velocity which manifests itself as a Doppler shift of frequency in the received spectrogram. The magnitude of the shift depends on both the position of the reflecting element and the rotation of Venus, while the strength of the echo depends upon the elements and ability to reflect at the specified inclination to the line of sight (the backscatter function).

Thus, in principle, both the component of rotation perpendicular to the line of sight, and the backscatter function can be determined from a spectrogram. Although the backscatter function cannot tell precisely what the Venusian surface is made of, it may give insight into the problem, and it can be used as a criterion to test hypotheses and so to eliminate some possibilities. However, small errors in estimating the perpendicular component of rotation from a spectrogram yield important errors in the corresponding backscatter function.

A transmitter–receiver pair exists which can specifically extract the rotation component from Venus. It is a combination of a range gate and a spectrometer. A range gate is a device that accepts signals from a selected distance and rejects those from closer of farther ranges. This is accomplished by modulating the transmitter with a wide-band waveform and using the waveform's inverse (delayed by just the time of flight) to remove the modulation at the receiver. In this manner, echoes from the proper distance pass through the system unaltered, while those from other ranges remain wide-band and may be removed by filtering.

Spectral analysis of the output of the range gate then reveals the line of sight velocity of a specified portion of Venus. From this, the rotation component can be cal-

* This paper presents the results of one phase of research carried out at the Jet Propulsion Laboratory, California Institute of Technology, under Contract No. NAS 7-100, sponsored by the National Aeronautics and Space Administration.

culated independently of the scattering law. Such information, combined with the spectrograms mentioned above, produce an unambiguous backscatter function. In addition, observation of the component of rotation for several months, as Venus swings by us in her orbit, provides enough information to infer the complete rotation vector of Venus.

II. RADIOMETER

The radiometer is essentially a power-measuring device. This is normally done by squaring the received signal and then averaging the result. However, in the Venus radar case, by far the largest source of power is the thermal noise of the antenna and the receiver. In order to eliminate that large component, the transmitter is switched on and off and the change of receiver power is noted.

The block diagram of Fig. 1 illustrates this method. The keying period is about 2 sec. The signal is converted to a final i.f. of 1 kc/sec before being squared. The bandwidth, determined by a plug-in filter, was chosen to be as narrow as possible to eliminate the most noise, but wide enough to let all of the signal power through. During the experiment, 100- and 50-cps filters proved to be the most convenient.

The average output of the square-law device is proportional to the total power of its input, but the instantaneous value fluctuates widely about this average because of noise in the input. This signal is then smoothed by one of two accumulators (integrators) depending upon whether the signal contains the echo power from Venus, or just the noise. Thus the receiver switch of Fig. 1 must be delayed from the transmitter switch by precisely the time of flight. The proper delay is computed from the Venus and earth ephemerides.

After smoothing for about 2 sec the contents of the noise-only accumulator is subtracted from that of the signal-plus-noise accumulator. The result, proportional to the signal power, is filtered by a simple RC circuit and displayed on a strip-chart recorder. Because of the low signal-to-noise ratio, a long time constant of 60 sec was used.

All of the operations, from the receiver output on, were performed on a small general-purpose computer (Packard–Bell Pb 250). The receiver output was envelope-detected and then sampled at a rate of 300 samples per second (an ample rate for the 100-cps bandwidth) by an analogue-to-digital converter and then fed directly to the computer. The use of a digital computer provides many advantages other than the usual ones of freedom from drifts and gain changes, etc. For example, the computer simulates a square-law device with high accuracy. Hence, the output is truly linear in power, which is a great convenience. Also, the long time constant of the RC filter is realized by a simple recursion formula in the computer, without the problem of charge leaking off of a capacitor during the

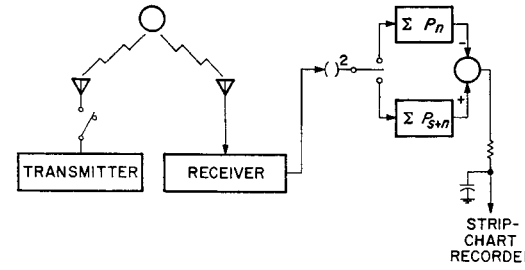

FIG. 1. Radiometer block diagram.

alternate 5 min when the transmitter is on and the receiver off.

At the end of a 5-min receive cycle, the computer types out the signal power, the noise power, and their ratio. Additional runs can either be computed cumulatively or successively.

At the end of an observation period of, say, several hours, the grand average of the ratio of the signal power to noise power (SNR) is typed out by the computer. This number has, of course, fluctuations about its mean value which are caused by the stochastic nature of both the signal and the noise. Detailed calculations show that the standard deviation of these fluctuations, σ_{SNR}, is

$$\sigma_{\mathrm{SNR}}=\frac{P_{s+n}}{P_n}\frac{2}{(BT)^{\frac{1}{2}}},$$

where P_{s+n} is the total signal plus noise power, P_n is the noise power, T is the total observation time, and B is the predetection bandwidth.

The average value of SNR is, of course, P_s/P_n. Therefore, the signal-to-noise ratio of the radiometer (or postdetection signal-to-noise ratio) is

$$\mathrm{SNR(radiometer)}=\frac{P_s}{2N}\left(\frac{T}{B}\right)^{\frac{1}{2}}$$

when P_s is small compared to P_n. The noise density is represented by N. This is the standard switched-radiometer formula, and it shows that the sampling process does not cost anything in basic signal detectability.

The equations were tested experimentally by measuring the fluctuations when only noise was applied, and also by injecting known amounts of signal. The agreement is excellent.

The signal power can be calibrated by keying in a known amount of power from a separate source. It can also be calibrated by multiplying the signal-to-noise ratio by kTB. The second method was used for the Venus experiment, as it is insensitive to time-varying system gain; and the temperature measurement was quite stable and accurate.

A plot of how the radar cross section of Venus changed during the course of the experiment is given in Fig. 2. This figure shows a phenomenon that can be called,

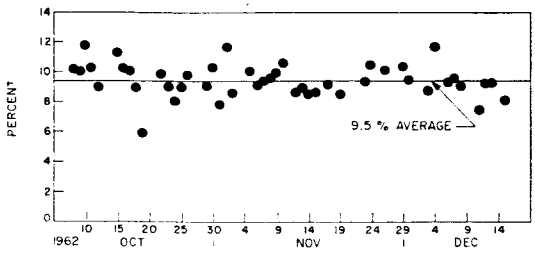

FIG. 2. Radar cross section of venus.

appropriately, "Venus-induced" noise. The fluctuations from day to day are far greater than can be accounted for by thermal noise or experimented procedure. This scatter must then be caused by some changing characteristic or aspect of Venus herself.

A typical sample of a strip-chart record, showing signal power (through a 60-sec time constant) as a function of time, is given in Fig. 3. Another advantage of digital techniques is apparent in Fig. 3—instead of going off scale at the top, the reading just starts over again from the bottom.

III. SPECTRAL ANALYSIS

It is always desirable to have more information than that which is given by total power measurements. When the strength of an echo is sufficient to provide an extra margin over the requirements of detection, it becomes possible to measure the frequency distribution of the power.

A sine wave of high spectral purity is transmitted to Venus, but the echo's spectrum is broadened because of the effective rotation of Venus, acting through the Doppler effect.

Because of the geometry of a sphere, the contours of constant Doppler shift are seen as parallel lines, projected on the planet's disk. Thus spectral analysis of the echo power is equivalent to scanning the disk of Venus with a fine fan-beam antenna. Each point on the spectrogram gives the total power reflected from one thin strip across the planet.

Upon calculating what shape spectrum $P(f)$ to expect, one finds that it is a function of the effective rotation rate and the backscatter function $F(\theta)$ (the ability of a surface element to reflect at various angles of incidence). The relation is (Goldstein 1962a)

$$P(f)=\int_{\sin^{-1}f/a}^{\frac{1}{2}\pi}\frac{F(\theta)\sin\theta d\theta}{(a^2\sin^2\theta-f^2)^{\frac{1}{2}}}, \qquad (1)$$

where a is the rotation constant. This formula is based on the assumption that all surface elements have the same backscatter function. This integral has been inverted to yield

$$F(\theta)=-\frac{2a^2\cos\theta}{\pi}\int_{a\sin\theta}^{a}\frac{P'(f)df}{(f^2-a^2\sin^2\theta)^{\frac{1}{2}}}. \qquad (2)$$

Note that it is necessary to have the constant a before this formula can be used.

Many spectrograms were taken during the three months of the Venus 1962 experiment, and Eq. (2) was applied to the best ones. The constant a was found by considerations to be discussed subsequently.

The correlation approach was used to find the power spectrum of the echo. That is, the autocorrelation function of the signal was measured and the spectrum then calculated by Fourier transformation. The theory behind spectral measurement and the correlation approach is well covered by Blackman and Tukey (1959). They have shown that increased spectral resolution can be obtained only at the cost of increased fluctuations, and that in any case, accurate spectrograms inherently require great amounts of input data. High accuracy is quite necessary in this application, since the Venus echo is only a perturbation of the thermal background noise. Some of the spectrograms required the processing of up to 4 h of signal.

A block diagram of the spectrum analyzer is given in Fig. 4. There, the entire maser, paramp, programmed local oscillator, several stages of conversion and i.f. amplification, etc., have all been reduced to one block labeled "bandpass filter." The center frequency is 1 kc/sec and the width is controlled by a plug-in filter. As in the case of the radiometer, 100 and 50 cps proved most convenient. The output of the filter is sampled at the Nyquist rate for the bandwidth used. The spectrum of the sampler output is thus periodic, the signal appearing in the frequency intervals of 0 to B cps (Fig. 4), and B to $2B$, $2B$ to $3B$, ... Because of this effect, the signal does not have to be heterodyned down to the desired range of 0 to B cps.

The limiter is used as an analogue-to-digital converter, quantizing to only two levels. This is the major feature of our method. The digital correlator computes the autocorrelation function of the signal at y (Fig. 4) by forming the sums

$$R_k=\sum_{n=1}^{N}y_n y_{n+k}, \qquad k=0, 1, \cdots, 44,$$

where y_n is the nth sample of the signal at y. Because of the limiter, values of y_n are always either plus one or minus one, so that the correlator can calculate the terms in the equation above at a rate of 3 million per second. The correlator is a special-purpose machine

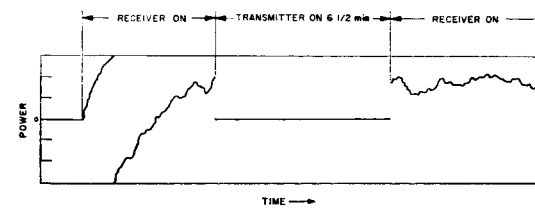

FIG. 3. Strip-chart recording.

which computes 45 points on the autocorrelation function, at a maximum sampling rate of $66\frac{2}{3}$ kc/sec, and can integrate (at that rate) for weeks without an overflow (described in detail in Space Programs Summary, No. 37–14, Vol. I, p. 111, Jet Propulsion Laboratory, Pasadena, California).

It is the correlation function at x (Fig. 4) which is desired, but that at y which is measured. One might think that the action of the limiter may alter the spectrum at x beyond recovery. Fortunately, this is not so, and a simple correction formula (Davenport and Root 1958) applied to the autocorrelation function at y suffices. The correction and the Fourier transformation are performed on the same general-purpose computer (Pb 250) used for the radiometer.

The spectrum produced is the sum of the desired signal and the ubiquitous noise. To provide meaningful results, the noise-only spectrum is computed separately and subtracted from the total spectrum. It must be measured to the same accuracy as the total spectrum, however, so the same technique used in the radiometer is applied. The transmitter is continuously keyed, 1 sec on and 1 sec off, and the two resulting spectra are subtracted. The action of the limiter complicates this procedure somewhat, since the limiter output has a constant power regardless of whether the signal is present or not in the noise. This is accounted for by using the output of the radiometer to determine the magnitude of the noise spectrum to be subtracted.

Detailed analysis shows (Goldstein 1962b) that the postdetection signal-to-noise ratio of the device is

$$\mathrm{SNR(spectrometer)} = \frac{2}{\pi}\frac{P_s}{2N}\left(\frac{T}{B}\right)^{\frac{1}{2}},$$

where P_s is the signal power, T is the observation time, N is the noise power density, and B is the bandwidth in which P_s is contained. The signal power is again assumed small, compared to the noise power.

Once again we have the switched radiometer formula, except for the constant $2/\pi$. This factor is the direct result of the clipping technique and represents the cost of that considerable simplification.

The radiometer and spectrometer experiments are run simultaneously. During the receiving cycle the Pb 250 acts as the radiometer and the special-purpose machine measures the autocorrelation function. During the transmitting cycle, the Pb 250 corrects and transforms the autocorrelation function and displays the

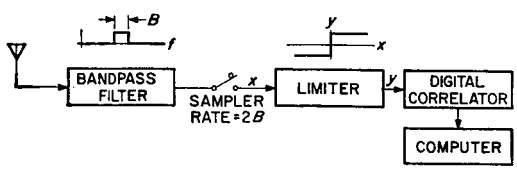

FIG. 4. Spectrometer block diagram.

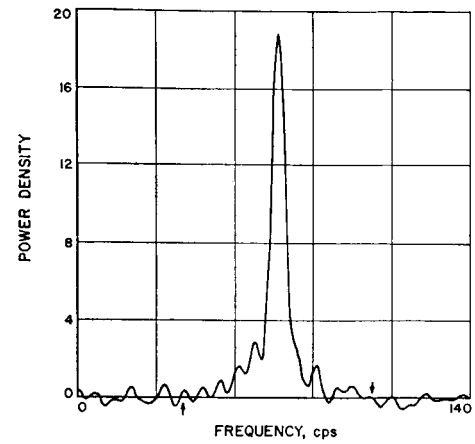

FIG. 5. Venus spectrogram, 15 October.

resulting spectrum on an $x-y$ plotter. Permanent records are kept via the computer's typewriter.

Figures 5 through 11 are representative Venus spectrograms, spaced throughout the experiment. As in the signal-strength measurements, there are significant changes in the spectra from day to day, particularly in the division of power between the central "spike" and the wider-band "shoulders." This change is strongly correlated with signal strength, the echo being stronger when power is concentrated into the spike.

Variable amounts of asymmetry are also apparent in these spectrograms. This violates the assumption of uniformity, made in the derivation of the backscatter formula; hence the backscatter function derived from these spectra must be considered as an average.

A very pronounced trend may be seen in these spectrograms: a narrowing of the base bandwidth (maximum frequency spread of the echo) as conjunction is approached (November 12) and a subsequent widening again as the planet recedes. Note that Fig. 8 has a different frequency scale from the others. This change is tied to the relation between the spin axis and the orbit of Venus. The Doppler spread is caused by the effective rotation, which is the vector sum of two components. One is the actual spin vector of the planet and the other is due to the motion of the center of Venus relative to the radar station. The spectral narrowing thus indicates retrograde rotation, since at conjunction the spin component and the orbital component counteract each other.

The arrows marked on the abscissas of the spectrograms show the frequencies of echoes reflected from the limbs of Venus. The positions were determined by a method to be discussed subsequently. We conclude from examining these marks that echoes up to the limbs are, in fact, detected.

Figure 12 presents the backscatter function $F(\theta)$, averaged over the days of closest approach. Recall that $F(\theta)$ is defined as the radar cross section of a unit

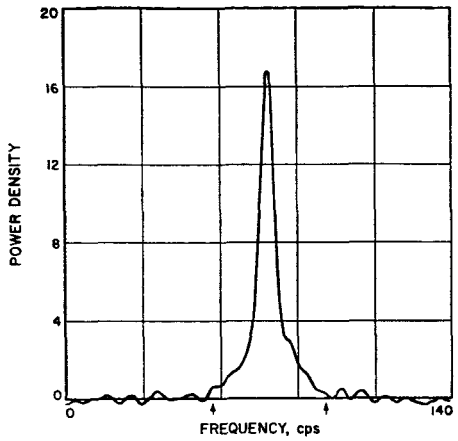

FIG. 6. Venus spectrogram, 25 October.

square, taken as a function of the angle of incidence. There was considerable variation in this function from day to day.

The backscatter function has been distorted by the instrument which measured the spectrum. The spectrograms have a limited resolution, i.e., the ability to distinguish fine detail. Theory shows (Blackman and Tukey 1959) that resolution must be limited if meaningful results are to be obtained in a high-noise environment. The effect of this limit is a broadening, or smearing, of fine detail in the spectrograms. Of course, the backscatter function must reflect this broadening. To demonstrate the extent of this effect, the spectrum that

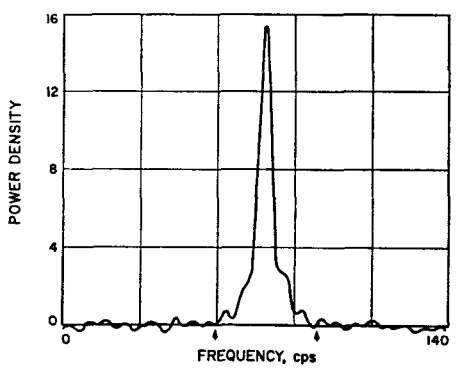

FIG. 7. Venus spectrogram, 5 November.

would result from a plane mirror surface $[F(\theta)=\delta(\theta)]$ was calculated. The result of placing this spectrum into Eq. (2) is shown dotted in Fig. 12.

As can be seen, Venus is a rather smooth object for 12.5-cm radiation. The edge of Venus ($\theta=90$ deg) is quite dark, which illustrates a fact that can be proved analytically: the limbs are much more accurately identified on a spectrogram than on a backscatter function.

IV. RANGE-GATED SPECTRA

When the echo power is strong enough to permit good resolution in the spectrograms, it is possible to add another dimension, that of time delay, to the analysis. This is done by a range gate, which is a device that accepts echoes from a specified distance and rejects echoes from closer or farther distances. Thus the target is divided into concentric rings of points equidistant from the radar. The echo from a given ring is isolated from the total by the range gate. This echo is then analyzed for its frequency content by the method described above. The result is a two-dimensional radar map of the target, the target being divided into parallel strips by the spectrometer and into concentric rings by the range gate.

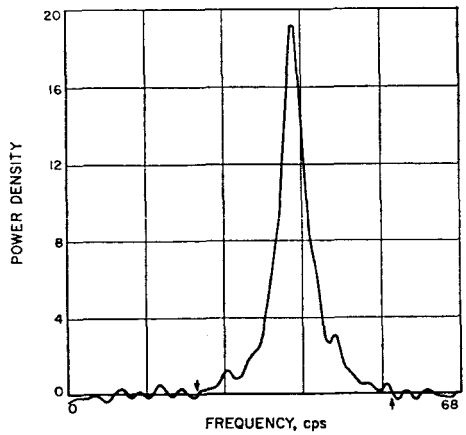

FIG. 8. Venus spectrogram, 10 November.

The narrow bandwidths of the spectrograms in Figs. 5 to 11 pose a question: does Venus have a rough surface, allowing echoes to be heard all the way to the limbs, and rotate very slowly; or is the surface shiny and the rotation much faster? Since the range gate selects signals reflected from known positions on Venus, that device enables the question to be answered.

The method of range gating so that a given range zone may be isolated from the others (without destroying its spectral composition) is diagrammed in Fig. 13.

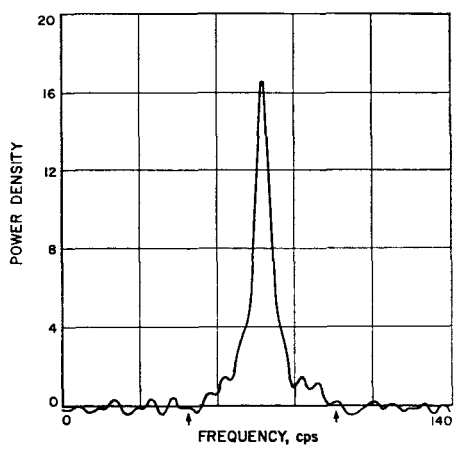

FIG. 9. Venus spectrogram, 23 November.

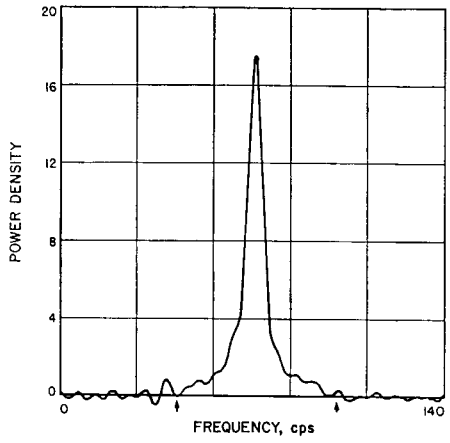

FIG. 10. Venus spectrogram, 4 December.

The transmitted carrier is multiplied by a binary code. The code chosen for the Venus experiment is a pseudo-random (Golomb 1955) square wave, generated by a 5-section shift register. The clock frequency is variable, but 800 cps was convenient to use, producing zone depths on Venus of 178 km. The transmitted signal is thus wide band.

At the receiver, the signal is multiplied by a very carefully delayed version of the same pseudo-random wave, thereby canceling out the modulation impressed at the transmitter and leaving the signal narrow band.

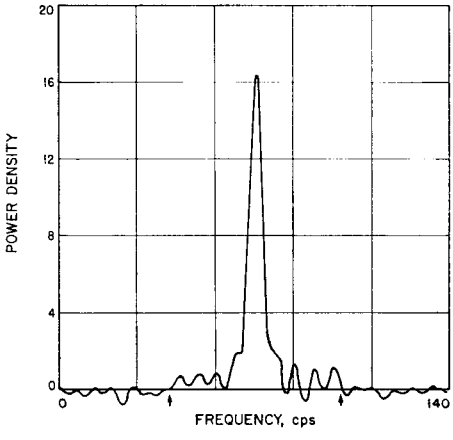

FIG. 11. Venus spectrogram, 6 December.

If the echo originates from the center of the range zone, the timing is perfect and the cancellation complete. If the echo occurs in the zone, but away from the center, cancellation is only partial. Hence part of the signal power remains narrow band and part wide band. The magnitude of the narrow-band component can be shown to be the autocorrelation function, for the appropriate delay, of the code waveform. The two-level autocorrelation function of the pseudo-random square wave is thus ideal for our use. "Crosstalk" between zones is virtually eliminated. Power from all of the "wrong" zones is completely wide band and appears as noise to the spectrometer, where it is negligible as compared to the thermal noise already present.

During some of these experiments, the signal was recorded on tape (before being multiplied), along with the code, so that the same signal could be examined for the content of each range zone. It was an advantage to have a high-speed correlator, since hours of signal were processed in a matter of minutes.

A sample range-gated set of spectra is reproduced in Fig. 14. It is the result of 3 h (for each zone) of signal integration. The large "spike" is the reflection from the front cap of Venus (Zone 1). It contains most of the

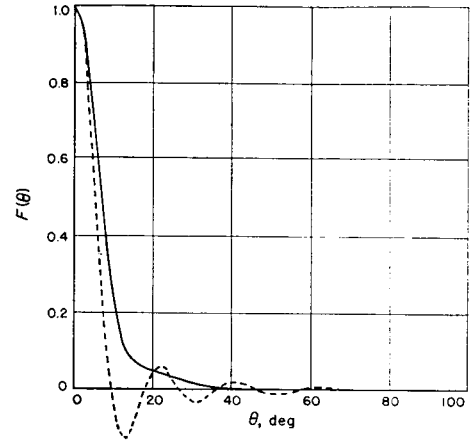

FIG. 12. Average Venus backscatter function.

power and has a very narrow bandwidth. The next 178-km slice of Venus (Zone 2) shows the characteristic double hump and increased Doppler broadening. Zone 0 is just ahead of the planet. Normally, there would be no power reflected from this zone. However, the range gate was misaligned slightly to allow the position of the range gate to be calibrated from the amount of power in Zone 0.

The maximum spread of each range-gated spectrum gives the line-of-sight velocity at the known edge of that range zone. Thus, spectra sets such as Fig. 14 give directly the component of rotation which is perpendicular to the line of sight, and they do so quite independently of surface roughness. Moreover, the rotation

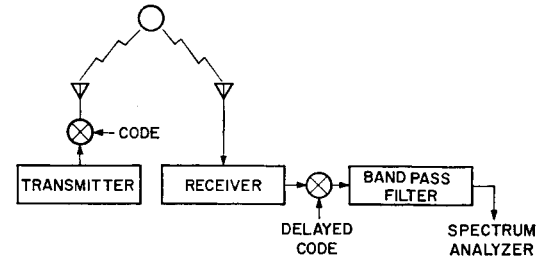

FIG. 13. Range-gate block diagram.

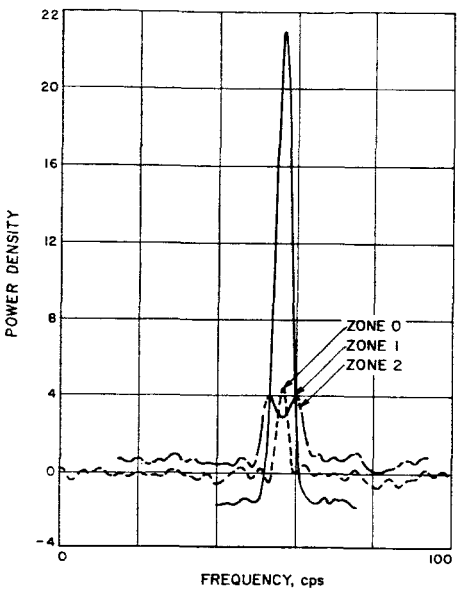

FIG. 14. Range-gated Venus spectra, 14 November.

component is overdetermined, since the width of several of the spectra may be measured.

V. ROTATION

Spectrograms of the types presented previously enable all three components of the rotation vector of Venus to be found. The important data from the spectrograms are their base bandwidths (frequency-spreads that correspond to echoes from the limbs of Venus).

The base bandwidths are measured directly from the range-gated spectra. These results are used to remove the shiny–rough ambiguity from the base bandwidths estimated from the normal spectrograms. The result is a set of about 30 bandwidths, both range-gated and normal, spaced over the three months of the 1962 Venus experiment. These reduced data are shown in Fig. 15.

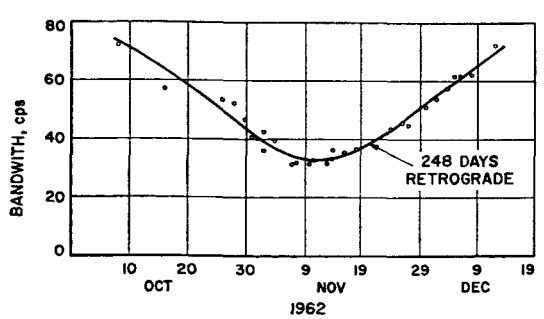

FIG. 15. Venus base-bandwidths.

Theoretical bandwidths B may be calculated from the formula

$$B^2 = |\mathbf{w}_T|^2 - \frac{(\mathbf{R}\cdot\mathbf{w}_T)^2}{|\mathbf{R}|^2},$$

where $\mathbf{w}_T$ is the total rotation vector and $\mathbf{R}$ is the vector joining the centers of earth and Venus.

The total rotation is composed of two parts:

$$\mathbf{w}_T = \mathbf{w}_0 + \mathbf{w}_s,$$

where $\mathbf{w}_0$ is caused by relative motion between Venus and earth, and $\mathbf{w}_s$ is the true spin vector which is to be found.

The orbital part may be calculated from the Venus–earth ephemeris:

$$\mathbf{w}_0 = \dot{\mathbf{R}} \times \mathbf{R}/|\mathbf{R}|^2,$$

where $\dot{\mathbf{R}}$ is the time derivative of $\mathbf{R}$.

A computer program was written to find that spin vector $\mathbf{w}_s$ which minimized the sum of the squares of the theoretical bandwidths minus the measured ones. Five bandwidth measurements from the Jet Propulsion Laboratory's 1961 Venus experiment were included. The resulting theoretical curve is shown as the solid line in Fig. 15. The corresponding spin vector shows the surprising result that the rotation period of Venus is approximately 248 days retrograde and the coordinates of the axis of Venus are 119 deg right ascension and −78 deg declination.

It is difficult to assess the accuracy of these numbers. However, running the same program with the bandwidths altered by reasonable amounts indicates that the period is accurate to well within ±15%. The coordinates of the axis are probably accurate to within a solid angle of ±15 deg.

Experiments planned for the Venus conjunction of June, 1964 should refine the accuracy of these numbers considerably.

ACKNOWLEDGMENT

The author gratefully acknowledges the work of Dr. H. C. Rumsey, who inverted the integral of Eq. (2), and Dr. W. F. Gillmore, Jr., who programmed this integral for the spectral data.

REFERENCES

Blackman, R. B., and Tukey, J. W. 1959, *The Measurement of Power Spectra* (Dover Publications, Inc., New York).

Davenport, W. B., and Root, W. L. 1958, *Random Signals and Noise* (McGraw-Hill Book Company, Inc., New York), p. 107.

Goldstein, R. 1962a, *Radar Exploration of Venus*, Tech. Rept. No. 32-280, Jet Propulsion Laboratory, Pasadena, California.

——. 1962b, "A Technique for the Measurement of the Power Spectra of Very Weak Signals," *IRE Trans.* **PGSET 8**, 2.

Golomb, S. W. 1955, *Sequences with Randomness Properties*, Terminal Prog. Rept. Glenn L. Martin Company, Baltimore, Maryland, June.